# GRADING LIGHT

Utilizing plastic deformation to functionally
grade ceramic light screens

by
Isabel Ochoa

## AUTHOR'S DECLARATION

This thesis consists of material all of which I authored or co-authored: see Statement of Contributions included in the thesis. This is a true copy of the thesis, including any required final revisions, as accepted by my examiners. I understand that my thesis may be made electronically available to the public.

## STATEMENT OF CONTRIBUTIONS

Isabel Ochoa was the sole author of Part 1 (Preface) and Part 5 (Conclusion) which were written under the supervision of Assistant Professor David Correa. No portion of this document was written for publication. Exceptions to sole authorship of material are as follows:

Part 2 (Light and Ceramic Material Performance) was co-authored by Isabel Ochoa and James Clarke-Hicks under the supervision of Assistant Professor David Correa. Isabel Ochoa was the lead author and drafted the manuscript. James Clarke-Hicks provided intellectual input on manuscript drafts.

Part 3 (Digitally Fabricated Ceramics) was co-authored by Isabel Ochoa and James Clarke-Hicks under the supervision of Assistant Professor David Correa. James Clarke-Hicks was the lead author and drafted the manuscript. Isabel Ochoa provided intellectual input on manuscript drafts.

Part 4 (Methodology) was co-authored by Isabel Ochoa and James Clarke-Hicks under the supervision of Assistant Professor David Correa. Isabel Ochoa was the primary investigator and lead author for the 'S' and 'XL' Typology subsections. James Clarke-Hicks was the primary investigator and lead author for the 'M' and 'L' Typology subsections.

All final diagrams and photo documentation are co-authored by Isabel Ochoa and James Clarke-Hicks.

# ABSTRACT

When interacting with light, surface geometries and clay bodies can work together to heighten the perception of depth and alter illumination. This thesis investigates how clay 3D printing can generate materially responsive engagements between ceramics and light. A computational methodology is developed to produce texture and sculptural relief in ceramic surfaces. Liquid Deposition Modeling is used to study the plastic deformation of clay during wet-processing. Most 3D printing technologies are currently conceived as end-stage production processes characterized by high-fidelity between digital models and physical outputs. Stoneware and porcelain have a wide variety of working properties and ceramic traits that demand new approaches to digital tooling. By making the study of material behaviour essential to the design process, clay 3D printing enables non-linear design-to-production systems. The research outputs are a series of stoneware and porcelain screens that vary in brightness and illumination based on how light may be obstructed, reflected or transmitted across their surfaces. Prototypes are developed at full scale to understand the relationship between sensory engagement and material properties.

The scope, context and research methods are divided into three parts:

**Light and Ceramic Material Performance**– Explains stoneware and porcelain's performance capabilities in the context of Functionally Graded Additive Manufacturing.

**Ceramics and Digital Fabrication**– Explains the tools by which the research methods are produced in the context of how tool path design is being leveraged in the practice of digitally crafted ceramics.

**Methodology**– Outlines the methods involved in making qualitative changes to alter light-scattering behaviour in 3D printed clay screens. The research is structured around a series of four light screen typologies. Each typology utilizes unique digital and physical tooling methods, harnesses plastic deformation, structural capabilities, and light scattering behaviour in porcelain and stoneware structures.

## ACKNOWLEDGMENTS

# TABLE OF CONTENTS

# LIST OF FIGURES

# PART 1

## INTRODUCTION

## 1.1 REIMAGINING DESIGN-TO-PRODUCTION SYSTEMS

Additive manufacturing can act as a catalyst for process redesign in contemporary high-fired ceramic practices. From studio pottery to industrial-scale manufacturing, formative methods of making are the most widely used modes of ceramic production. Their pervasiveness is attributed to clay's plasticity in its working state. In efforts to limit plastic deformation during wet-processing, formative manufacturing employs casts or moulds to shape clay. In architectural ceramics, formwork yields outputs characterized by symmetry and redundancy, intended to function as units aggregated to build large composite structures. As a result, architectural ceramics are primarily conceived as "aesthetic boundary layers for buildings,"[1] fixed as cladding to supporting walls. This conception of materiality supports persistent gaps in the structuring of the architectural discipline where light and materials are implemented as fixtures and finishes, making them supplementary and interchangeable. Working drawings are used to describe form, but light and materials are communicated using language, relegated to notes and specifications.[2]

This research proposes that material behaviour itself can be a means to compute form and act as a creative source for innovation. Rather than utilizing formwork to limit the plastic deformation of clay, additive manufacturing enables the fine-tune control of material deposition during the wet-processing of ceramics. In this research, plastic deformation becomes a tool to harness light-scattering

---

1. Bechthold et al., *Ceramic Material Systems,* 8.
2. Lloyd Thomas, "Architecture and Material Practice," 3.
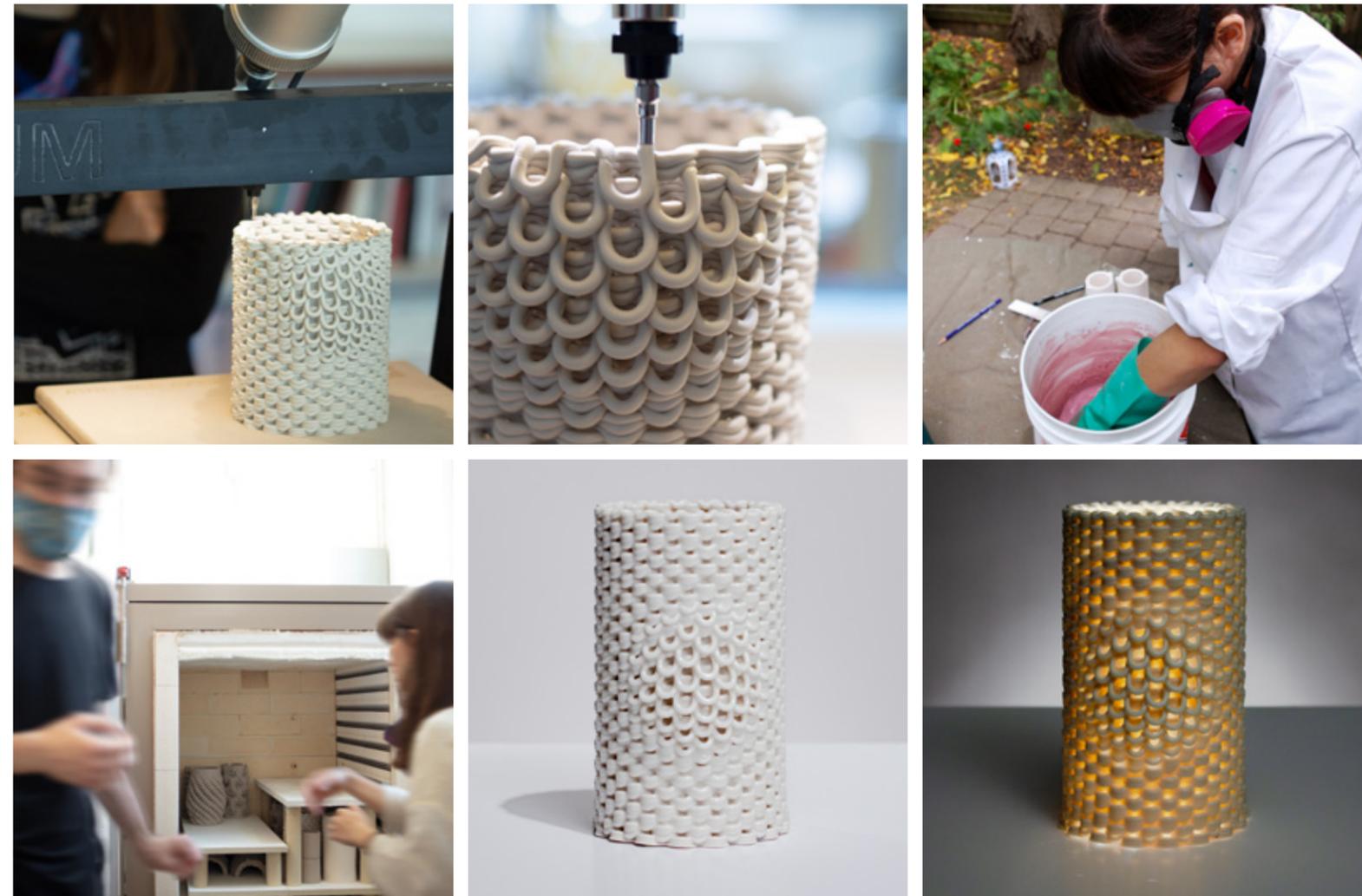


**Figure 1.1.1** Design-to-production process.

behaviour. By making material computation essential to ceramic craft, 3D printing can enrich the practice of architecture by creating a direct connection between conceptualization and production.

## 1.2 COLLABORATIVE PROJECT DEVELOPMENT

The joint development of this work emerged out of shared interests with James Clarke-Hicks to design processes (rather than products) and to work through design problems by making physical artifacts. Our design-by-making approach to research benefited from collaborative work. The physical labour required to execute fabrication tasks often required more than a single individual. Our research focused on designing artifacts as well as suite of material computation tools. Having the opportunity to solve these computational problems jointly became critical to the success of this project. Design conceptualization and execution in all prototypes were carried out with input from both team members. Having dual input on all physical prototypes and digital development strengthened the research by giving it a more objective lens. This was particularly useful when studying tacit/implicit modes of material performance. Evaluating the success of interactions between ceramics and light involves perception and is, therefore, highly subjective. The collaborative pursuit of this work evolved into shared enthusiasm for researching the relationship between material behaviour and sensory experiences. Research interests diverged regarding the development of material computation. This is reflected in the breakdown of Parts 2, 3 and 4 of this document:

**Part 2: Light and Ceramic Material Performance**– Focuses on examining the physical nature of clay, its working properties and ceramic traits and how these attributes can be computationally manipulated to harness light scattering effects.

**Part 3: Ceramics and Digital Fabrication**– Focuses on examining the tools by which the material is processed and situates the research in relationship to ornamental, formative and performative uses for the technology.

**Part 4: Methodology**– Brings together both authors' respective research on material computation to develop a joint suite of tools to manipulate texture, relief and light scattering effects in ceramic surfaces.

## 1.3 MATERIAL COMPUTATION

My interest in developing this work was to examine how designers could have more agency over design-to-production systems. In our research methods, we aimed to establish a design framework that supports the development of ceramic material computation. Material computation integrates material behaviour and materialization through computational design thinking.[3] By recognizing that materials are active agents,[4] computational design becomes an exchange between maker and ceramic in the shaping of matter and light. If architectural practice is to support new

---

3.  Menges, "Computational Material Culture," 78.
4.  DeLanda, "The New Materiality," 17.

morphological and tectonic possibilities, the study of materials cannot be conceived of as scale models or orthographic representations. Instead, material studies must reflect the qualitative changes that transform material behaviour over time.[5] Prototyping at 1:1 scale was essential in harnessing structural stability, plastic deformation, and light scattering behaviour in porcelain and stoneware structures. These clay bodies have distinct working properties and ceramic traits. As a result, material computation was vastly different when working with these two mediums- requiring different preparation methods, digital parameters, and digital and physical tools to be processed effectively. Performance characteristics were subject to changes across all phases of materialization, including material preparation, wet-processing, drying and firing. Therefore, photographically documenting transformations in these attributes became an essential tool in both the design process and communicating the research outcomes in this document. Documentation also became the most effective way of understanding the relationship between material deposition during the wet-processing of clay and light scattering behaviour in its ceramic counterparts.

Thinking sectionally about how changes in material deposition impact light scattering behaviour became an indispensable mode of inquiry. Due to the fluidity of the material post-wet-processing, we were able to retroactively cut physical sections through prototypes to better understand plastic deformation. Clay 3D printing enabled rapid adaptations to emergent material behaviour, resulting in non-linear relationships between computation and materialization processes.

---

5.  Menges, "Fusing the Computational," 10.



**Figure 1.3.1** Terracotta undergoing plastic deformation and subsequent delamination during 3D printing.

**PART 2**

---

LIGHT AND
CERAMIC MATERIAL
PERFORMANCE

## 2.1 MATERIAL PERFORMANCE

This section of the thesis document examines the relationship between light and two types of high-fired clay bodies: stoneware and porcelain. Fired ceramics, considered the first human-engineered material, are built from clay bodies in their 'wet' or 'plastic' state and subsequently fired into fixed ceramic forms.[1] Each clay body contains a unique variety of primary and secondary clays and other mineral substances combined to produce distinct working properties and ceramic traits. The transformation of clay's malleable physical make-up into hard, heat-resistant, waterproof vessels generally coincides with the development of agrarian culture.[2] The emergence of fired ceramic objects designed for specific domestic and agricultural uses reflected a shifting human need to harness ceramic material performance. The thesis investigates two distinct types of performance attributes:

1. **Working properties.**
2. **Fired ceramic traits.**

The firing process gives ceramics their characteristic impermeability, translucency, heat resistance, and the capacity to take on a variety of finish appearances. These material performance characteristics have given fired ceramics an enduring place in our material history. Since the invention of fired brick and ceramic tiles, fired ceramics have also become ingrained in the history of our built environment. However, clay's working properties allow us to mould

---

1. Violatti, "Pottery in Antiquity."

2. Violatti, "Pottery in Antiquity."



**Figure 2.1.1** Stoneware light screen detail.

**Figure 2.1.2** Examples of clay's working properties- plasticity and the ability of the material to retain its given shape.
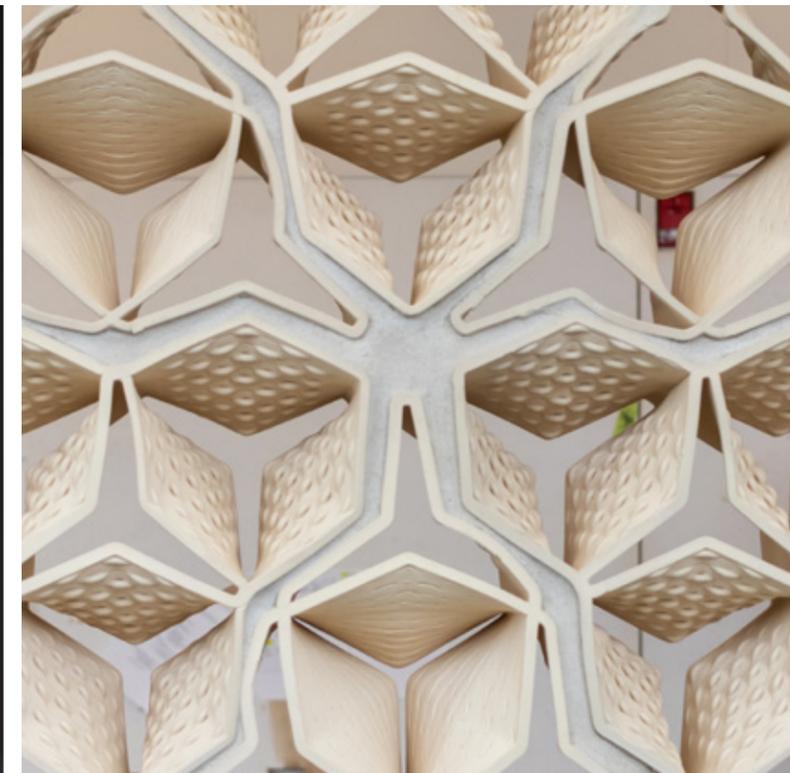
**Figure 2.1.3** Examples of ceramic traits- transluscency and compressive strength.

soft lumps of mud into vessels, ovens, musical instruments and building envelope components. Working properties, such as plasticity and tensile strength, are distinguished from fired ceramic traits in that they allow unfired clay bodies to support highly contoured surfaces and complex forms. This thesis utilizes 3D printing as a tool to harness stoneware and porcelain's respective material performance attributes.

## 2.2 WET-PROCESSING

Clay can be shaped in a wide range of states, "from dry powders to near-liquid slip, and in its plastic state can be formed without heat under relatively low pressure."[3] Unfired clay, commonly referred to as 'raw' clay, is easily modelled when saturated with moisture. Throughout history, raw clay's working properties have made wet-processing methods of craft highly pervasive.

Wet-processing is an umbrella term for various techniques for shaping clay, both analogue or machined. Clay 3D printing is distinguished from other types of wet-processing methodologies by its lack of formwork: the practice relies on the structural capabilities of the material to produce self-supporting forms. Mechanisms for machining clay such as extrusion, slump-moulding, die-cutting, plastic pressing, and slip casting have been developed to control performance attributes that result in formal inconsistencies and structural instability. These fabrication methodologies are known as

---

3. Bechthold et al., *Ceramic Material Systems,* 26.



**Figure 2.2.1** Traditional coil potting by Sylvie Enjalbert.

**Figure 2.2.2** Inlaid slip casting moulds by Kelly Justice.

'formative' manufacturing. Formwork, such as casting moulds, plastic presses, and extrusion dies, are often costly to manufacture. The production of thousands of components is typically required to offset the cost of designing and making formwork.[4] Processing multiple components through the same mould promotes economy and ease of fabrication. As a result, clay's elastic and structural limitations have steered modes of ceramic production to favour symmetry and redundancy. In the field of architecture, ceramic material systems predominantly consist of aggregate arrangements of repeating bricks or tiles. Within contemporary applications for the material, the desire for customization is often at odds with the need for component redundancy. 3D printing offers an alternative approach to wet-processing that promotes component variability and rapid prototyping.

## 2.3 FUNCTIONALLY GRADED CERAMIC SYSTEMS

In the current paradigm of ceramic material systems, sectional consistency conflicts with the desire for graded material performance. From wheel-thrown vessels to slip-cast tiles, uniform wall thicknesses ensure minimized deformation during wet-processing, drying, and firing ceramics. In order to conform to building systems, formal consistency across components aims to regulate material performance. This thesis experiments with the notion that material performance precedes form. The research outputs capitalize on highly customized ways of altering light scattering behaviour, not easily reproduced

---

4.   Bechthold et al., *Ceramic Material Systems,* 28.



**Figure 2.3.1** Slump moulded building system at Villa Nurbs by CLOUD 9.



**Figure 2.3.2** Plastic pressed building system at Badalona Apartments by Lagula Architects.



**Figure 2.3.3** Slip cast building system at Saint Rupert Church by Meck Arkitecten.

through alternative production processes. The scope of work focuses on harnessing two types of 3D printed, high-fired ceramic traits:

1. **In porcelain structures–** light transmission and scattering as a function of extrusion variability.
2. **In stoneware structures–** the direction of incident light through porous, multi-layered component sections.

Variable performance characteristics can be achieved by:

1. **Altering a material's physical and chemical make-up.**
2. **Formal optimization.**

Formal optimization results in 'functionally graded' or 'intensive' materials.[5] These terms refer to substances with changing properties across their volume, such as heat, density, colour, and elasticity.[6] Synthetic functionally graded materials emerged in the 1980s when Japanese material scientists in the aerospace industry designed a composite material having the ability to withstand high-temperature differences across its volume.[7] While the practice of designing customized clay bodies is common to both production pottery and the field of architectural ceramics, it is essential to note that clay body optimizations falls outside the scope of this investigation. Commercially available stonewares and porcelains were selected based on pre-determined attributes. The thesis instead takes a formal approach to designing 'intensive' sectional qualities for ceramic components via the controlled deposition of material (Figures 2.3.5-2.3.8).

5.  Mahamood and Akinlabi, "Introduction," 1-8; Reiser and Umemoto, "Intensive and Extensive," 72.

6.  Mahamood and Akinlabi, "Introduction," 1.

7.  Reiser and Umemoto, "Intensive and Extensive," 72.
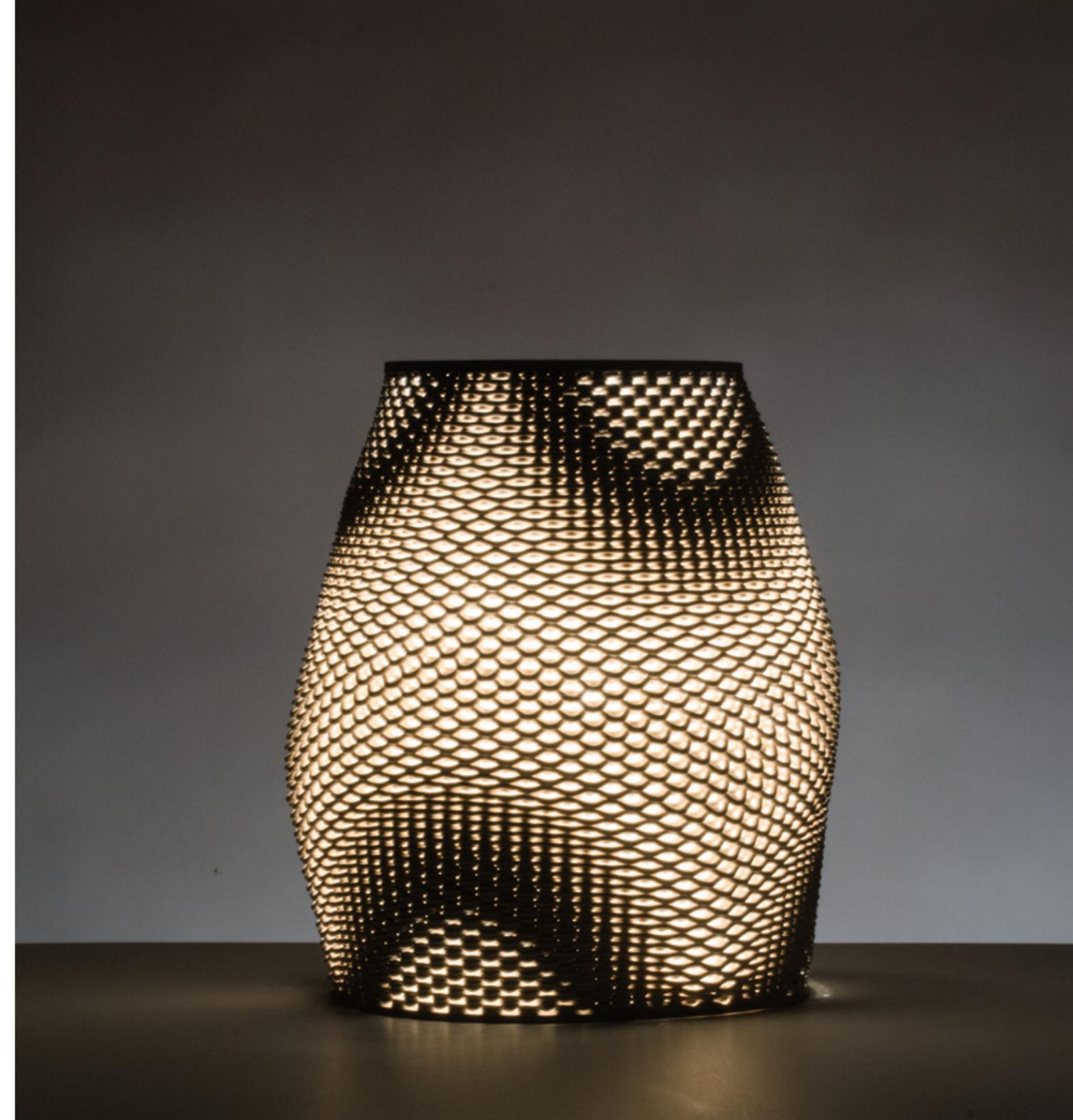
**Figure 2.3.4** Stoneware light screen showing functionally graded brightness levels across its surface (320mm x 320mm x 400mm).

# FOUR FUNCTIONALLY GRADED LIGHT SCREEN TYPOLOGIES
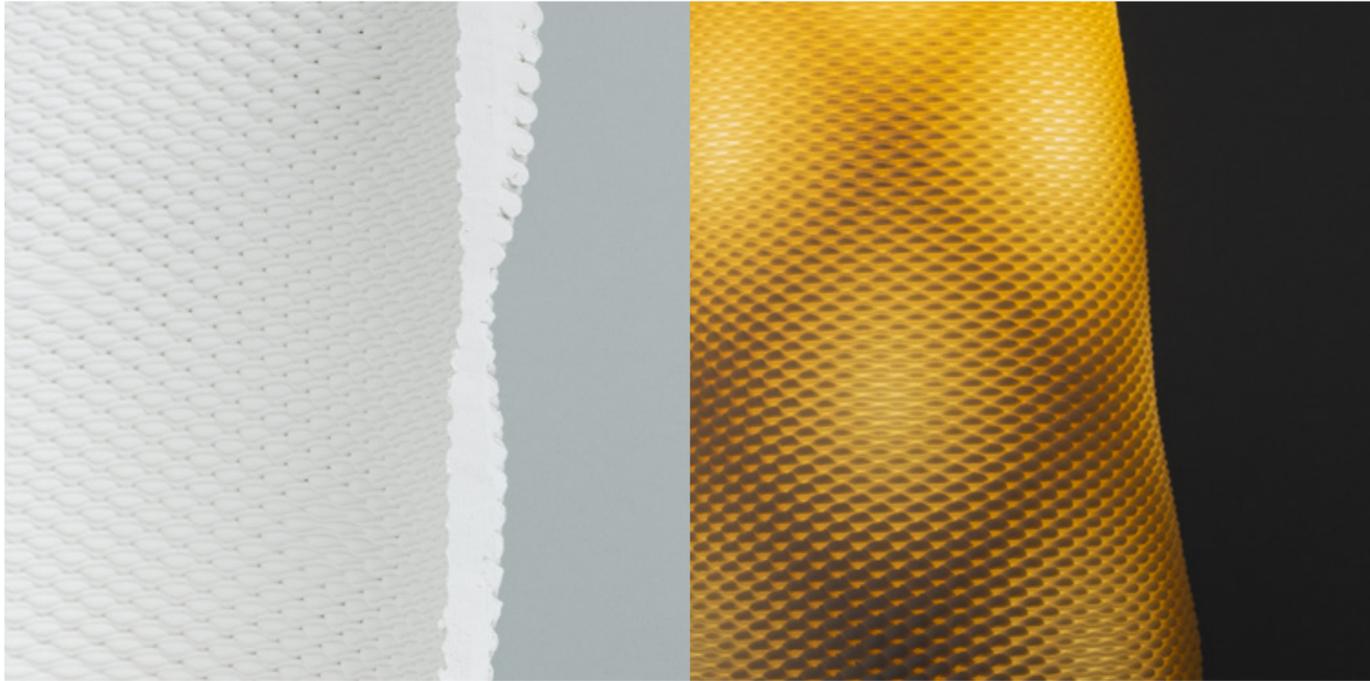


**Figure 2.3.5** 'S' light screen typology.



**Figure 2.3.6** 'M' light screen typology.



**Figure 2.3.7** 'L' light screen typology.



**Figure 2.3.8** 'XL' light screen typology.

Within the field of computational design, this methodological approach is described as Functionally Graded Rapid Prototyping (FGRP) or Functionally Graded Additive Manufacturing (FGAM).[8] These terms refer to a 3D printing process where material deposition is organized and graded across an object by "mapping performance requirements and allocating material properties throughout 3D space."[9] This research utilizes a Functionally Graded Additive Manufacturing approach to map the relationship between deformation in 3D printed clay structures to the resulting light-scattering properties in their fired ceramic counterparts. This relationship operates sectionally: variable aperture size and material thickness (Figures 2.3.5-2.3.8) directly correspond to brightness levels in ceramic light screens.

## 2.4 OPENWORK CERAMICS

Porous sectional conditions can be described as 'openwork.' In ceramic practice, openwork is the technique of creating gaps that completely penetrate the surface of a solid material.[10] Openwork can be achieved using several fabrication methods, including carving, slip casting and hand-building. In architectural ceramics, this technique has historically functioned to produce ornament as well as filter light. Notable examples of these applications date back to early Indo-Islamic construction, such as the Alhambra Palace (800-1400 CE).[11] Architectural elements such as porous 'muqarnas' (vaulting) and 'jali' walls are used within the Alhambra to filter daylight. These building

---

8.  Oxman et al., "Functionally Graded," 483; Pei et al., "A Study of 4D Printing," 147.

9.  Pei et al., "A Study of 4D Printing," 147.

10.  Ward, "Openwork."

11.  Grabar, "The Archeological," 25.
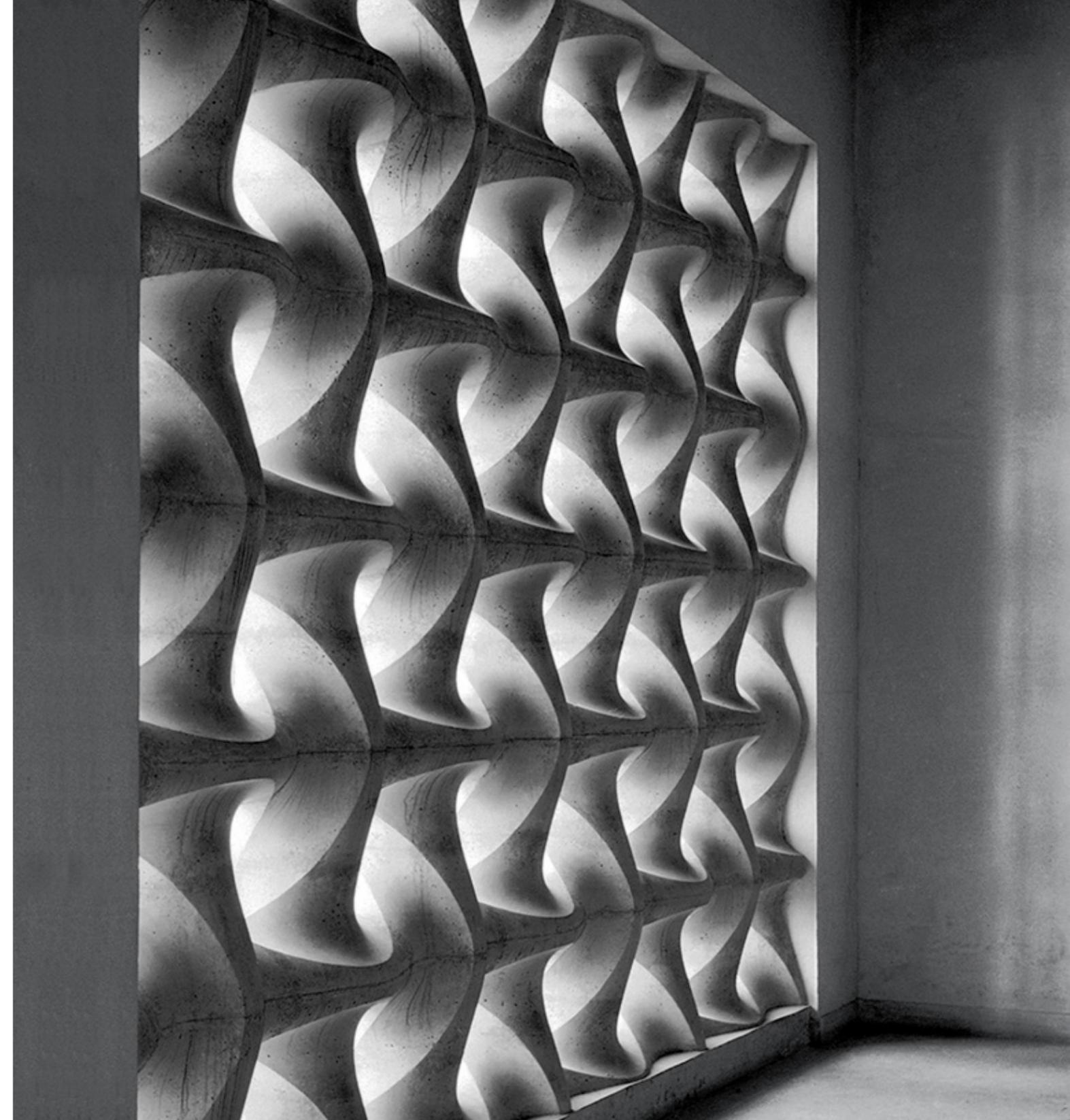
**Figure 2.4.1** 'Continua' Screen, 'Design 2' by Erwin Hauer. Cast Hydrostone. Pfarre Liesing Church, Austria, 1951.

components consist of complex three-dimensional geometric tessellations incorporated as surface decoration.[12] A tessellation is defined as the covering of a plane with a series of congruent or non-congruent shapes.[13] Although contemporary uses of the word predominantly pertain to the field of mathematics, the verb 'to tessellate' originates from the ancient world of building construction and design. Its Latin root term 'tesserae,' meaning mosaic tiles, were early examples of ceramic material systems.[14] Fabrication methods used to produce ceramic tessellations can substantially impact their resulting geometric expressions. The openwork elements at the Alhambra are carved from solid blocks of stone. Subtractive working methodologies, such as carving, yield continuous openings. Additive manufacturing methodologies can create multi-layered sectional conditions. The works of sculptor Erwin Hauer are examples of cast light screens that expand the traditional conception of tiled surfaces into complex three-dimensional tessellations. Hauer's works were initially produced in the 1950s, using traditional formworks for curing concrete, limestone and hydrostone.[15] Hauer's 'Continua' screens consist of identical ceramic units aggregated to form porous wall systems. Although there is sectional variation within individual units, their redundancy produces uniform light scattering effects across the entire volume of an installation. 3D printing allows for grading complex sectional tessellations, otherwise not possible through alternative fabrication methods. Without the need for formwork, the economy of fabrication is no longer contingent on component redundancy. With the emergence of computational design in contemporary architecture, there has been renewed interest

and engagement in complex geometries.[16] This thesis develops a computational methodology for grading brightness and light scattering via tool path tessellations. Parametric modelling enables rapid responses to emergent tool path deviations that occur due to clay's working properties during wet-processing.

## 2.5 WORKING PROPERTIES

### Clay Body Composition

For this research, three commercially available clays are utilized. Ingredients are provided by the manufacturer, shrinkage rates are observed by authors and measured from digital file dimensions to cone 6 firing.

1. **PSH 516 (516)**– stoneware.[17] Shrinkage rate: 12%.
   Quartz 18.1-24.4
   Kaolin Clay >30
   Feldspar 7-13
   Nepheline Syenite 10-30
   Titanium Dioxide 0.3-1.4

2. **Laguna Frost (LF)**– porcelain.[18] Shrinkage rate: 20%
   Quartz 10-25
   Halloysite 25-65
   Nepheline Syenite 25-65

12. Bechthold et al., *Ceramic Material Systems,* 86.

13. Clampham, "Tessellation."

14. Bechthold et al., *Ceramic Material Systems,* 86.

15. Hauer, *Continua*, 8-9.

16. Bechthold et al., *Ceramic Material Systems,* 87.

17. "Clay PSH 516."

18. "Clay Laguna Frost."

Bentonite <5

**3. Polar Ice (PI)** – porcelain.[19] Shrinkage rate: 15%
   Quartz 20
   Kaolinite 42
   Feldspar 35

The plasticity of each clay body is attributed to grain size and shape. Particles cling to one another when lubricated with water, resulting in a whole mass' ability to retain its given form.[20] Clay is classified into two broad divisions that speak to its particle make-up and working properties: primary and secondary clays. Primary clays such as kaolin are retrieved from their original deposits and have not been water-borne.[21] LF and PI clay bodies have high percentages of kaolin content. Since there has been little opportunity for sorting, grinding and mineral and organic contamination, primary clays are pure in colour (whiteness), are typically coarse-grained and relatively non-plastic.[22] In contrast, 516 is mainly composed of secondary clays. Figure 2.5.1 illustrates stoneware's high degree of plasticity in its 'wet' state. These substances have been transported by water through new sites, containing material from various sources and have been ground down to fine particles.[23] The proportion of primary clays, secondary clays, and moisture content in a clay body impact:

1. Plasticity and ability to hold shapes during wet-processing.
2. Warping, cracking or deformation due to drying.
3. Warping, cracking or deformation due to firing.

---

19. "Polar Ice."
20. Rhodes, *Clay and Glazes*, 10.
21. Rhodes, *Clay and Glazes*, 11-12.
22. Rhodes, *Clay and Glazes*, 11.
23. Rhodes, *Clay and Glazes*, 12.

**Figure 2.5.1** Wet processing a stoneware light screen (320mm x 320mm x 400mm).

**Figure 2.5.2** Tool path variability across a stoneware clay body (100mm x 100mm x 200mm).

**Figure 2.5.3** Tool path variability across a porcelain clay body (100mm x 100mm x 200mm).

To enhance formal precision and dimensional tolerances, controlling plastic deformation requires the selection or design of clay bodies. In this research, changes in clay body composition are limited to moisture control. Clay requires a minimum of 35 parts weight in water for every 100 parts of clay to become plastic enough to model.[24] This amount increases significantly depending on the plasticity and density of the clay. Figures 2.5.2 and 2.5.3 represent the same tool path 3D printed with stoneware and porcelain, respectively. Both pieces are printed with identical parameters using the Potterbot XLS-1. The amount of added water required to extrude the porcelain clay body resulted in a paste-like consistency. In contrast, the stoneware was able to hold its shape during preparation. The resulting physical outputs demonstrate how each material's moisture content and plasticity impact tool path variability during wet-processing. Although both clay bodies sag away from the original location where they were deposited, the porcelain deforms more significantly. As a result, the overall height of the porcelain print was reduced by twenty-seven percent relative to the stoneware. This behaviour presented significant challenges during wet-processing and drying. While too little moisture will impede extrusion, over-saturation will result in buckling and eventual collapse (see Figure 2.5.5).

24.    Rhodes, *Clay and Glazes*, 9-11.



**Figure 2.5.4** Delaminated stoneware light screen (100mm x 100mm x 150mm).

**Figure 2.5.5** Over-saturated clay body resulting in structural collapse (300mm x 300mm x 500mm).

## Sectional Limitations

Filtering light through clay bodies requires distinct sectional qualities to suit their respective material properties. While porcelain's ability to transmit light increases when wall sections are minimized, stoneware openwork benefits from the structural stability provided by robust supporting walls. Figures 2.5.9 and 2.5.10 illustrate the difference in wall thickness at which these two mediums operate within the scope of this research. In clay 3D printing, sectional depth is determined by nozzle size. A printer's ability to deposit material through a given nozzle diameter is dependent on clay body consistency and the strength of its extrusion system. Two 3D printers were utilized to attune the fabrication process to the working properties of each material:

1. **Lutum 4**– for porcelain.
   Nozzle Diameter: 0.5mm to 7mm.
   Cartidge Capacity: 1400cc

2. **Potterbot XLS-1**– for stoneware.
   Nozzle Diameter: 3.5mm to 10mm.
   Cartridge Capacity: 3600cc

Transmitting light through porcelain requires a very fine nozzle. Figures 5.5.2 and 5.5.3 were extruded using the same 5mm nozzle on the Potterbot XLS-1. The Potterbot's limited motor strength and high cartridge capacity made it difficult to extrude the
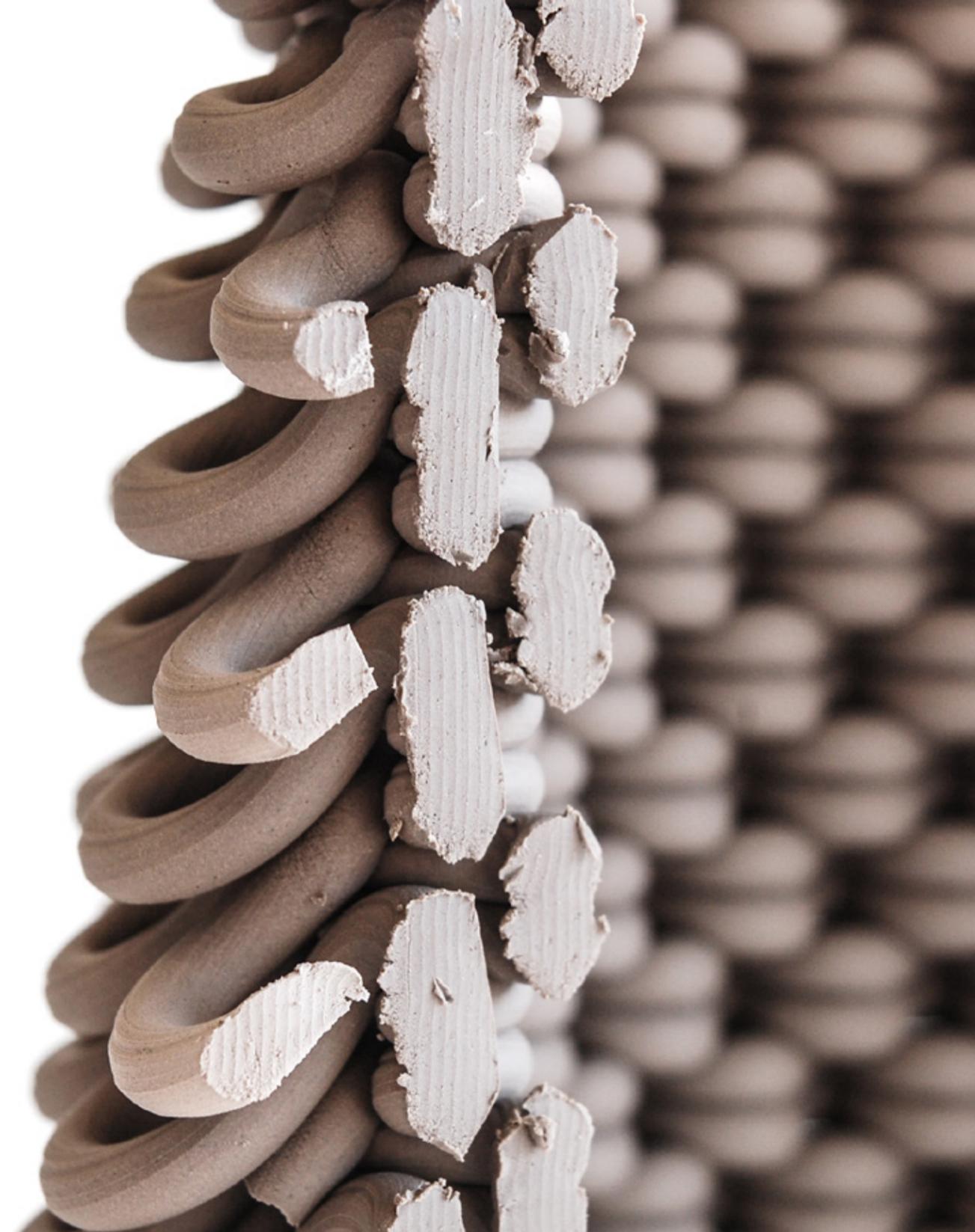
**Figure 2.5.6** Section cut through an openwork light shade (100mm x 100mm x 200mm).

# FIGURE 2.5.7 WET-PROCESSING 3D PRINTED HIGH-FIRED CERAMICS

**01.** Material Preparation

**02.** Machine Set-up



**02.** Machine Set-up (Continued)
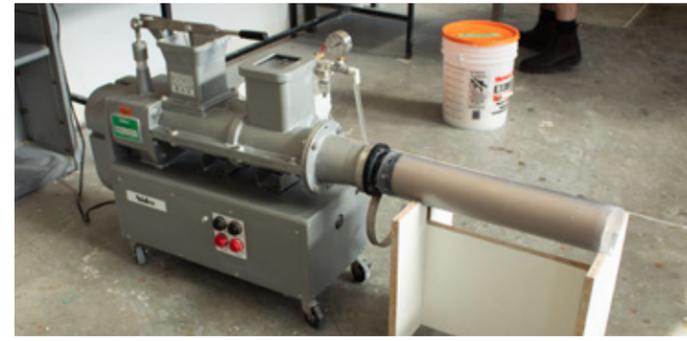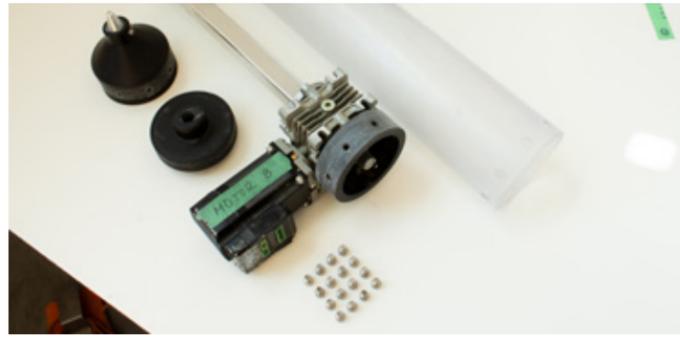
**03.** Printing



**04.** Reclaim
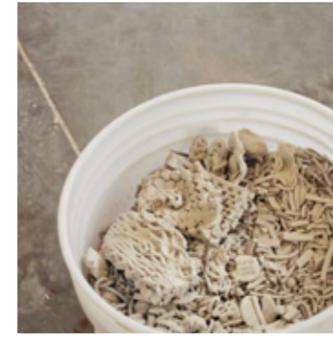
**05.** Drying

**06.** Bisque Firing
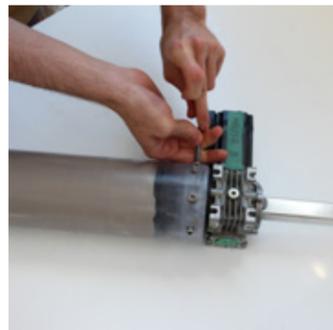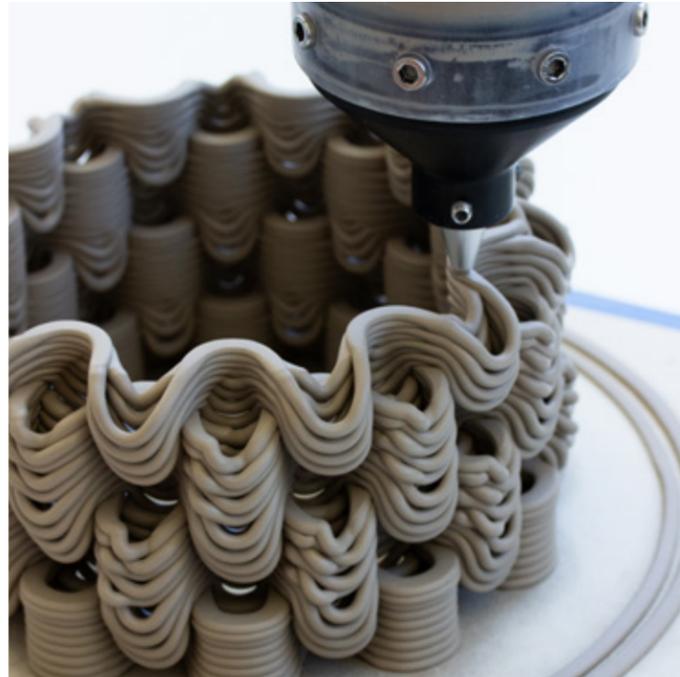


**07.** Glaze Application

**07.** Glaze Firing
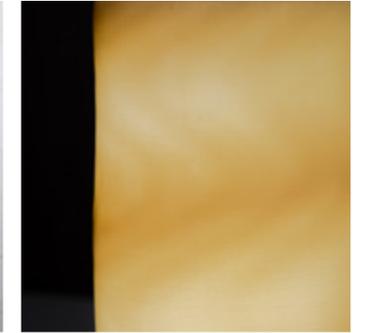
dense, non-plastic porcelain clay body through a small opening. To compensate for these tooling limitations, the clay body was super-saturated with water until soft enough to print. Figure 5.5.3 underwent a significant amount of plastic deformation during processing and did not allow for visible light transmission. When decreasing the nozzle size to reduce wall thickness, motor failure occurred. To yield thinner walls and less plastic deformation, all subsequent research on porcelain was conducted using the Lutum 4. The machine's auger and compressed air system make it possible to extrude relatively dense clays through nozzles as thin as 0.5mm. Although the Lutum can extrude heavily moisture-saturated material, its compressed air system increases the chances of introducing air bubbles into the clay. In thin porcelain sections, the smallest air bubbles result in print failure. Air bubbles can be mitigated by de-airing the clay and loading the Lutum print cartridges as compactly as possible.

Sectional depth limits overall print size as well as the capacity of clay bodies to support highly contoured surfaces. The stoneware light screen in Figure 2.5.8 is made possible by the structural stability of a thick wall section. The geometry of these 'light shelves' is reliant on controlled deformation. Robust coils allow the material to deform evenly across large voids in the geometry. Thin coils required to transmit light through porcelain limit the material's ability to hold its shape during wet-processing.



**Figure 2.5.8** Stoneware light screen (70mm x 70mm x 150mm), extruded using the Potterbot XLS using a 5mm nozzle.

**Figure 2.5.9** 1mm porcelain wall detail (100mm x 100mm x 200mm), extruded using the Lutum 4.



**Figure 2.5.10** 5mm stoneware wall detail (100mm x 100mm x 200mm), extruded using the Potterbot XLS-1.

## 2.6 FIRED CERAMIC TRAITS

Four key characteristics of light are investigated in relation to tool path development. These include: brightness/reflectance, shadow, transmission, and scattering.

### Brightness

Brightness is the perceived interaction between illumination levels and the quantity of light transmitted through and reflected off a given material.[25] Colour plays a significant role in altering brightness: dark colours absorb light while light colours have greater reflectance. Stonewares are distinguished by their high degree of plasticity and wide range of colours ranging from buff, tan, grey and light to dark brown at maturation. Figure 2.5.10 shows 516 fired to full temperature. To maximize brightness, the material was sourced because it was the lightest commercially and locally available stoneware. Since light transmission is of no consideration across the clay body itself, stoneware can take on an indefinite number of glazes. Glazes are distinguished as matte (low reflectance) or gloss glazes (high reflectance). These effects are largely dependent on the transformation of the glaze that occurs during firing. If the mixture does not wholly melt at maximum temperature, it results in a 'rougher,' and therefore, more matte surface.[26] Opacity and matteness are therefore related- the roughness that results in a matte surface prohibits transparency- meaning a matte glaze would limit light

transmission through a porcelain body. The impacts of glaze effects on brightness and reflectance were briefly investigated (see Part 4: Methodology).

Brightness levels in stoneware light screens are dependent upon porosity. Within the scope of research, porosity refers to visible apertures in a clay body that facilitate the passage of light. Additive manufacturing offers the opportunity to layer openwork structures to alter a luminaire's angle of incidence- "the angle at which rays of light emitted from a light source strike an object or surface before reflection."[27] Openwork light screens can be designed to direct incident light in one or multiple directions. Tool path design is used to control aperture size and placement, and subsequently, fine-tune brightness. Figure 2.6.1 illustrates how maximizing aperture size can increase brightness. However, as apertures become larger, there is less material to adhere to across print layers. Material instability is aggravated when gaps widen significantly in the X-Y axis, causing layers to be displaced down the Z-axis. The final study in the series shown in Figure 2.6.1 illustrates how excess displaced material can diminish brightness. Brightness in relationship to a porcelain clay body is simply related to the material's thickness, allowing for higher or lower levels of light transmission. Colour differences in LF and PI at full maturation are subtle while unlit. However, when illuminated, LF has a significantly warmer glow than PI when housing the same luminaire.

---

25.   Winchip, *Fundamentals of Lighting*, 39.

26.   Rhodes, *Clay and Glazes*, 203.

27.   Winchip, *Fundamentals of Lighting*, 343.
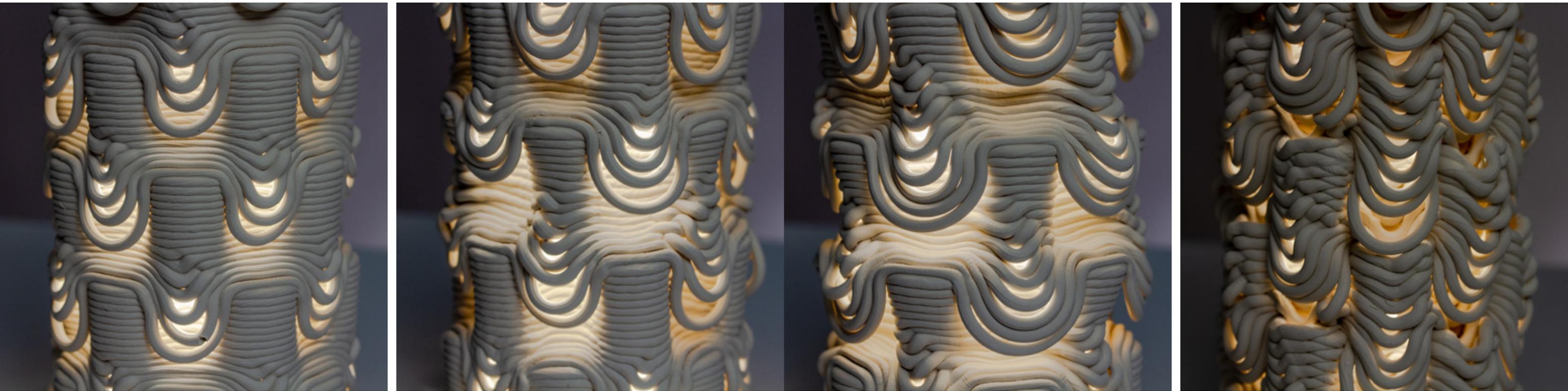
**Figure 2.6.1** Relationship between aperture size and brightness in stoneware light screens (100mm x 100mm x 200mm).

## Shadow

Aperture placement, shape and size also produce various forms of shadow. Since stoneware clay bodies are entirely opaque, shadows can be cast by juxtaposing apertures with solid surfaces. Experiments in Figure 2.6.2 direct incident light downwards through apertures of varying sectional qualities. Tool paths are graded in the X-Y axis, resulting in apertures that open and close with solid surfaces for stability in between. Scattered light is projected across the ground-creating variegated patches of shadow in between.
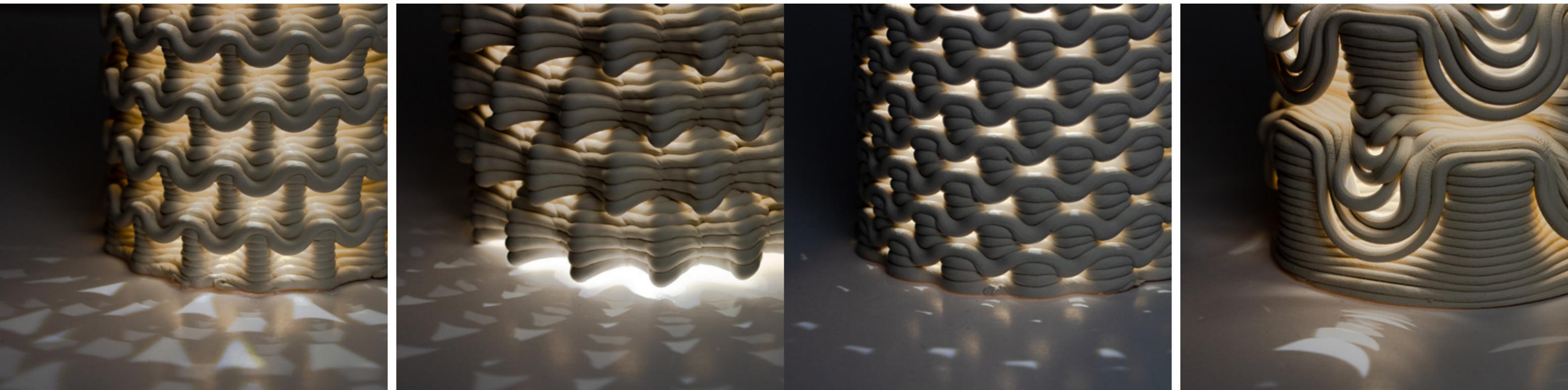


**Figure 2.6.2** Stoneware light screen shadow studies (100mm x 100mm x 200mm).

## Light Transmission

Light transmission (or translucency) describes the movement of light through a material. Light transmission can be achieved within a clay body by combining feldspar and kaolin and firing to the point where the clay body is on the verge of vitrification.[28] Kaolin gives porcelain its translucency and its lack of plasticity, making the material challenging to manipulate. Porcelain is only capable of diffuse transmission- causing light to be partially reflected and absorbed, and partially diffused through its surface. Porcelain's diffuse transmission differs from clear plastics or glass that allow direct transmission where most light can penetrate the material's surface. Testing light transmission required printing porcelain tubes of identical sizes and shapes with varying wall thicknesses (Figure 2.6.3). Tests ranged from 1.2mm to 15mm. With LF, diffuse transmission was visible at thicknesses less than 10mm. However, lumen levels exceeding 100lm are only visible at thickness less than 4mm. Although the thinnest tests were the most translucent, they were also the most unstable. Traces of this are evident in the variability of the tool mark. Significant deformation can also be perceived across the overall form of the cylinders when surface depth is minimized, suggesting more significant tendencies to slump during the firing process.

---

28.    Rhodes, *Clay and Glazes*, 25.
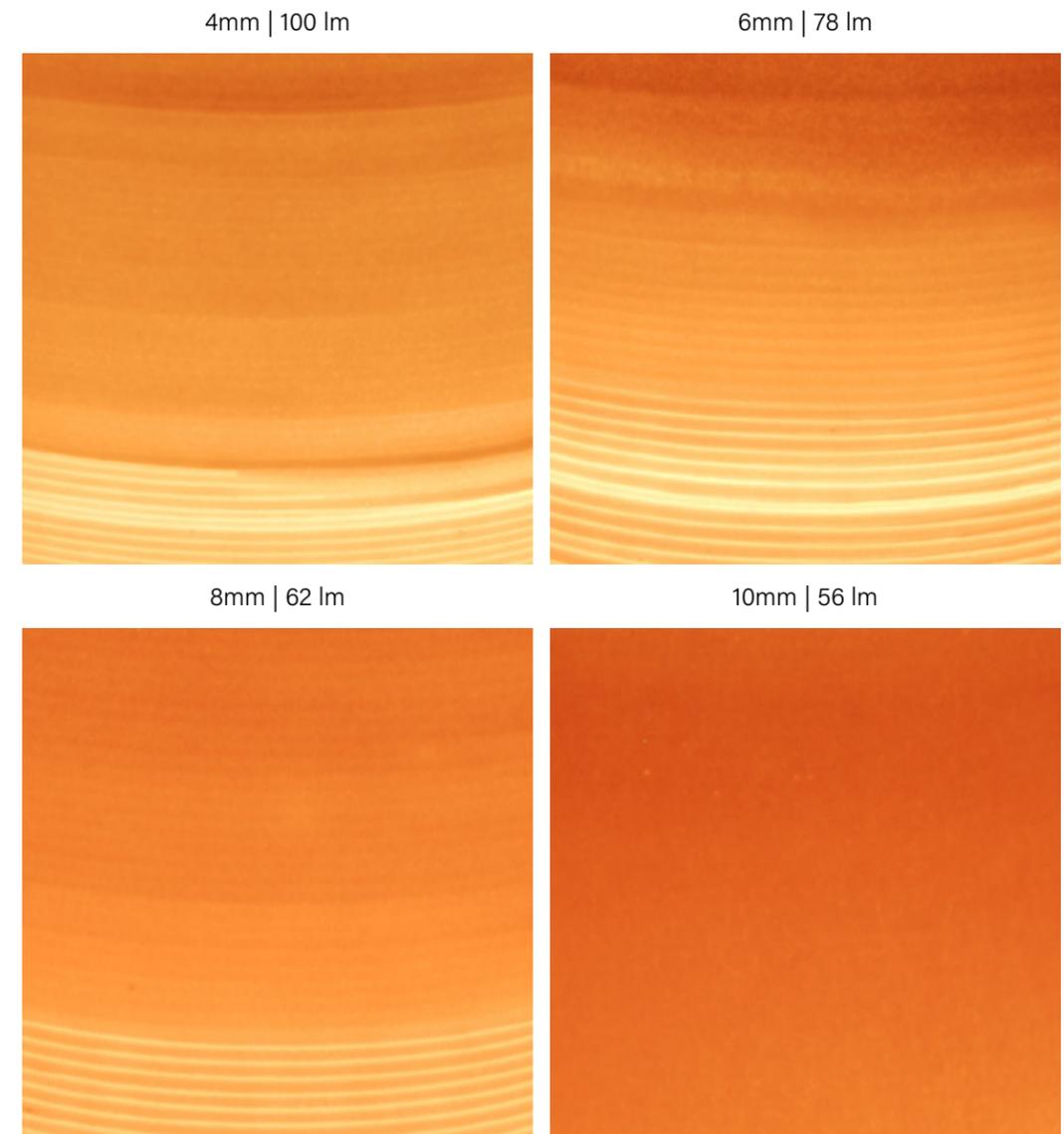


**Figure 2.6.3** LF light transmission tests.

## Light Scattering and Reflectance

Sectional layering within an openwork light fixture facilitates the control of incident light as it scatters across a space. Since illumination does not require a direct path of travel, both direct and indirect glare can be mitigated. Glare is the product of excessive brightness- it occurs "when the eye has to adjust to contrasting light levels, there is a loss of visual acuity and a potential for eye fatigue and strain, resulting in negative subjective reaction."[29] Many forms of contemporary lighting design fail to address glare. Exposed Edison bulbs have become increasingly popular within residential and commercial applications. Since small light apertures are generally more problematic in terms of glare than light dispersed over large areas, mitigating glare within openwork light screens is reliant on sectionally overlapping layers of material. The light screens in Figures 2.6.4 and 2.6.5 were printed with identical apertures and fired to full temperature. While neither screen allows a direct relationship between the light source and the viewer, added light transmission across the PI creates excess reflectance and glare. When examining the individual print coil, light is obstructed at its center and is increasingly transmitted as the cross-section of the coil becomes thinner at its edges. This condition not only enhances transmission but also increases interreflection. Light is contained within the multi-layered light screen and is continuously reflected from its porcelain surfaces. The contrast between opaque areas and areas of light transmission becomes too great, causing glare to occur.

---

29.   Winchip, *Fundamentals of Lighting*, 41-42.
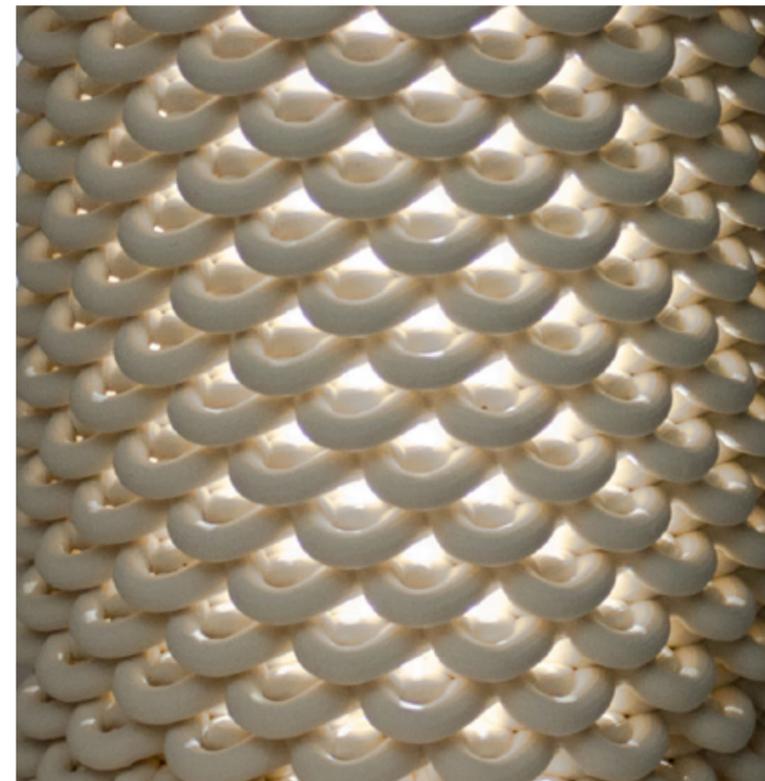


**Figure 2.6.4** Stoneware aperture study.
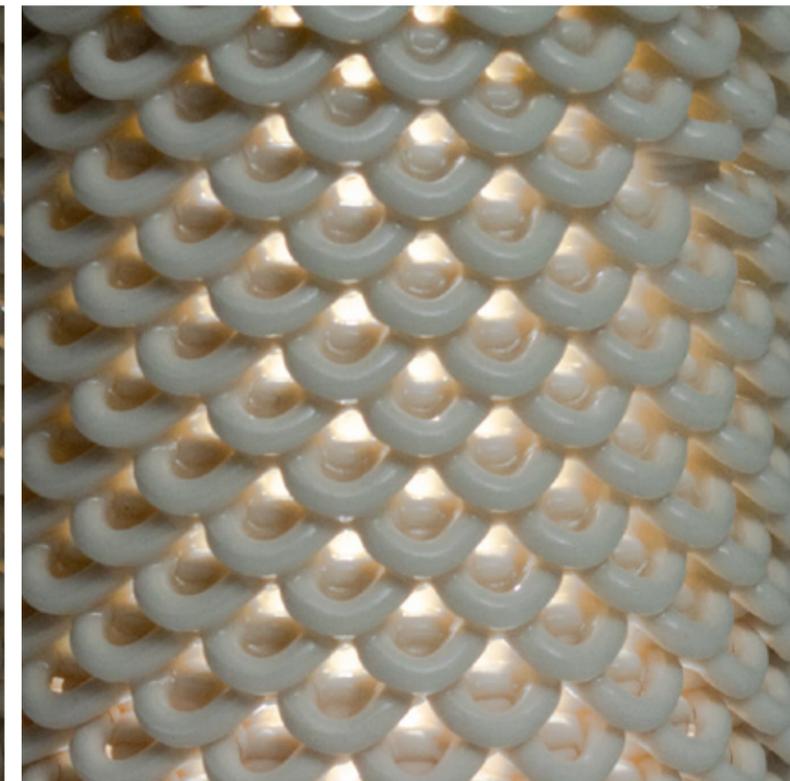
**Figure 2.6.5** Porcelain aperture study.

Figures 2.6.6 and 2.6.8 best illustrate the relationship between contrast or glare and porcelain coil size. The piece in Figures 2.5.9 and 2.6.6 was printed with a 1mm nozzle and has substantially less material cross-sectionally than Figures 2.6.7 and 2.6.8. Although light transmission is significantly increased, contrast remains high. Therefore, minimizing coil thickness is essential in minimizing interreflection. In porcelain fixtures, print coils are most effectively used at high densities with less than 1.6mm diameter, as seen in Figure 2.6.6. These small coils are often more decorative than performative.



**Figure 2.6.6** Porcelain light screen (100mm x 100mm x 200mm), extruded using the Lutum 4.5 using a 1mm diameter nozzle.

**Figure 2.6.7** Porcelain light screen detail (100mm x 100mm x 200mm), extruded using the Lutum 4 using a 3mm diameter nozzle.

**Figure 2.6.8** Porcelain light screen (100mm x 100mm x 200mm), extruded using the Lutum 4 using a 3mm diameter nozzle.

# PART 3

## DIGITALLY FABRICATED CERAMICS

## 3.1 LIQUID DEPOSITION MODELING

Ceramic is a broad term that encompasses many materials and composites. In additive manufacturing, a variety of material properties associated with ceramics are utilized by specialized technologies. Technical or engineering ceramics are used in Nanoparticle Jetting to produce durable medical implants. Ceramic composites are being utilized in concrete printing to create the first inhabitable 3D printed homes. There are many forms of ceramic printing, but none are as widely adopted and versatile as Liquid Deposition Modeling (LDM). LDM printers utilize common ceramics to produce masonry units, pottery, crockery, and other artifacts.[1] There are several contributing factors to the widespread adoption of LDM in the production of ceramic artifacts. As previously stated, LDM utilizes common clay bodies such as earthenware and stoneware. These clay bodies are cheap, abundant and have a deep historical continuity that spans 26,000 years of documented production.

LDM printers represent the majority of custom-built and commercially available desktop ceramic printers in use today.[2] Compared to other additive manufacturing technologies, LDM printer components are relatively simple to manufacture and widely available, granting this technology popularity with DYI communities and open-source maker platforms.[3] Across all ceramic additive manufacturing technologies, LDM has the most comprehensive influence among different parties. This technology is utilized by hobbyists, artists, academics and industry practitioners. LDM printers

---

1. Carlota, "Ceramic 3D Printing."

2. Carlota, "Ceramic 3D Printing."

3. Gürsoy, "From Control to Uncertainty," 23.
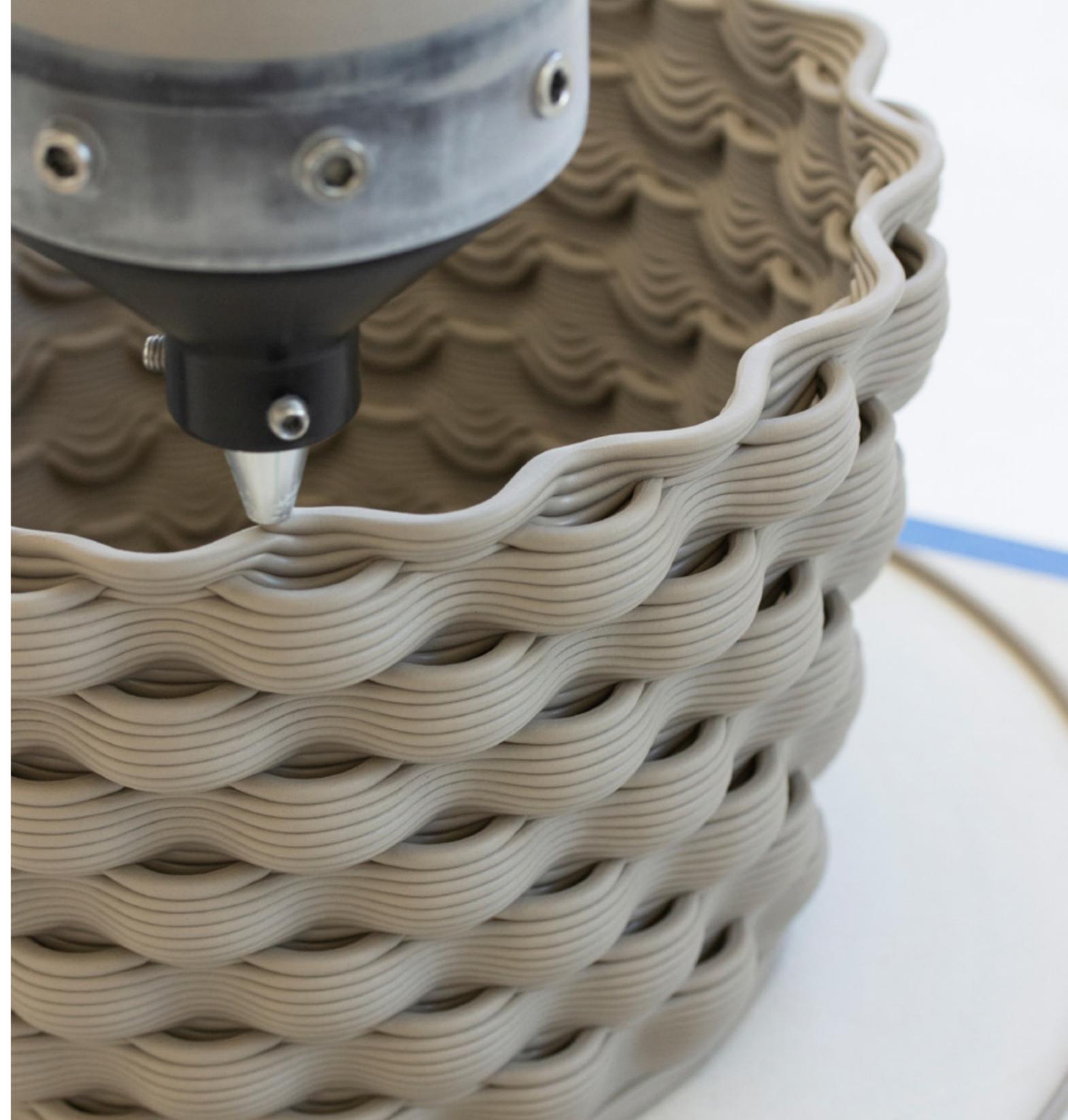


**Figure 3.1.1** 'L' prototype print in progress.

have become commercialized with the introduction of manufacturers like Potterbot, Lutum and DetlaWasp. The research presented in this thesis was conducted using two commercially available LDM clay printers: the Potterbot XLS-1 and the Lutum 4.

## Fabrication Advantages and Limitations

The Potterbot XLS-1 is a SCARA printer that can rotate 360 degrees with a maximum arm extension of 900mm. A 3600cc vertical acrylic cartridge is clipped to the end of the printer arm. The cartridge is loaded with clay using a pugmill. A rubber puck drives clay through a nozzle in a continuous bead, similar to a syringe. The puck is driven through the tube by a threaded rod attached to a high torque stepper motor. Extensive rotational reach paired with robust extruder components makes this printer ideal for rapid prototyping large ceramic forms.[4] Depending on the print speed and extrusion rate, a full 3600cc cartridge of clay empties in 80 to 110 minutes of printing. The Potterbot XLS-1 is one of the largest-capacity commercially available clay printers. All stoneware prototypes within this body of research are printed with the Potterbot XLS-1. The final stoneware prototypes are designed to leverage the speed and cartridge capacity of the Potterbot XLS-1.

The Potterbot XLS-1 utilizes fast, large-scale printing at the expense of precision. There are many drawbacks to employing a high-volume syringe-type extruder system. Within this body of

4.    "Potterbot XLS-1."



**Figure 3.1.2** M prototype in terracotta, delaminating during printing.

research, the most significant obstacles that informed the design and fabrication of stoneware apertures were:

1. **Minimum extrusion tolerances** – Printing translucent porcelain requires a level of precision that transgresses the minimum extrusion capabilities of the Potterbot XLS-1. Employing low extrusion modifiers causes the high torque stepper motor to seize.
2. **Minimum nozzle tolerances**– The Potterbot XLS-1 prints most efficiently with 4-8 mm nozzles, whereas 1-3mm nozzles are required to achieve ideal translucencies in fired porcelain.
3. **Shuddering effect**– The Potterbot XLS-1 can stop instantaneously and pivot directions, but the high-capacity tube and large arch of the print arm introduce shuddering when navigating sharp turns. Any vibration of the nozzle translates to unintended ripples in the printed form. Due to this shuddering effect, high tool path resolution and the elimination of sharp angles are critical to achieving clean prints.
4. **Lack of pausing function**– The Potterbot XLS-1 does not have pause capabilities. Although the digital interface allows the print to be paused, the pressure build-up in the acrylic cartridge required to extrude clay translates to a ten-second delay in extrusion.

The Lutum 4 is a gantry printer with a two-part extruder system attached to an x-axis armature. The two-part extruder system consists of a pressurized clay cartridge and an auger. Clay is loaded in a 700cc or 1400cc acrylic tube, which sheathe into a steel cartridge. The cartridge is sealed and pressurized to 3-6 Bar via an air compressor.
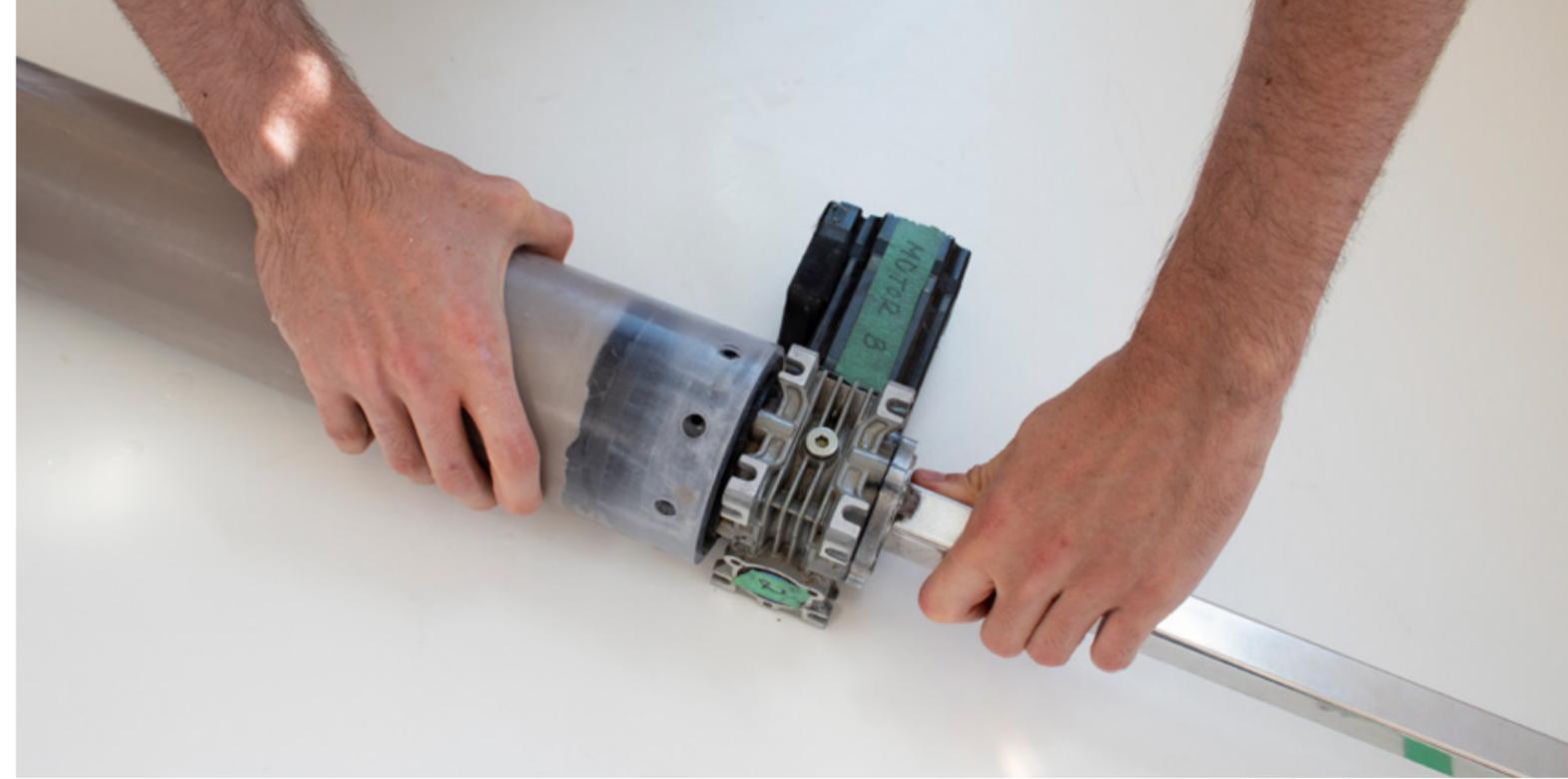


**Figure 3.1.3** The acrylic cartridge of the Potterbot XLS-1 is attached to the stepper motor by eight hex screws.



**Figure 3.1.4** Attaching a loaded cartridge to the printer armature.

Cartridge pressurization forces a puck in the tube to push clay into the auger housing. The auger can extrude clay out nozzles as small as 0.5mm, making this printer ideal for testing extrusion variability with porcelain clay bodies. The Lutum 4 has a higher print resolution than this thesis's research agenda, as porcelain prototypes in this thesis utilize 1-3mm nozzles. The compact frame of the printer allows for the navigation of sharp geometry without shuddering. The auger and compressor system eliminates extrusion delay, allowing extrusion variation to become a tool for creating ornament.

The Lutum 4 dual auger and pressurized cartridge extruder system offers a high degree of precision but introduces unique complications to the printing process. The main printer limitations that had to be addressed in order to utilize the light transmission properties of porcelain effectively were:

1. **Nozzle clogging–** Extra time and effort are required to prepare porcelain for printing to ensure a consistent clay body. A small dry scrap of clay is enough to clog the nozzle and force a complete print restart.

2. **Consistent cartridge pressure–** Insufficient pressure can lead to delamination in printing, while excessive pressure can cause an airway to open through the clay in the cartridge, resulting in a print blowout. Cartridge pressurization needs to be recalibrated with each new batch of clay.

3. **Print preparation–** Inconsistencies that lead to print failures equate to heavier research setbacks as a 1400cc cartridge takes upwards of 4 hours to load by hand and up to 8 hours to print.
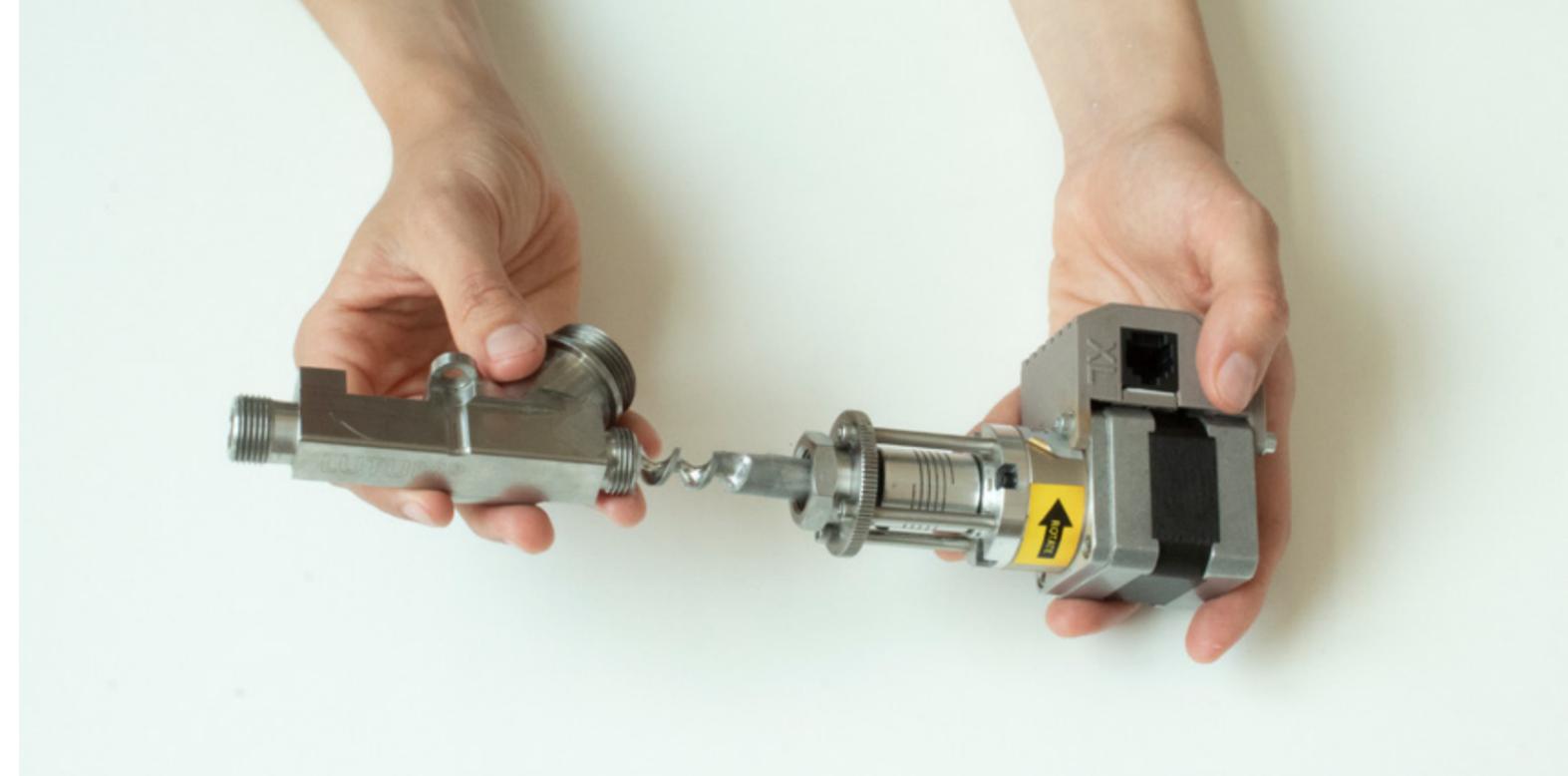


**Figure 3.1.5** Threading the auger housing to the stepper motor.



**Figure 3.1.6** Prepping the clay cartridge for pressurization via. compressed air.

## 3.2 PRINT LAYER RESOLUTION

LDM functions similarly to Fused Deposition Modelling (FDM). Both additive manufacturing technologies operate on the same principles but differ significantly in how they bond material layers. In both cases, planar layers are extruded from a nozzle in a continuous bead. FDM printing utilizes rapid heating and cooling of filament to fuse deposited layers, whereas LDM printing with clay has no external heating or fusing mechanisms. Clay remains plastic and heavily moisture saturated during the printing process, allowing the extruded clay to bond to former layers of plastic material. FDM is one of the most common desktop 3D printing technologies.[5] Thermoplastics used for 3D printing, such as ABS or PLA, are low-cost and readily available. These are two of the most desirable material traits when translating digital geometry to a physical form. FDM and LDM leave a visible tool mark in the form of striations that envelops prints. The concept of 'resolution' in 3D printing becomes an essential driver in addressing visible tool marks left by the printing process. The success of a 3D print is often measured by how closely the physical print resembles its digital origin.[6] Just as screens, cameras, and printer advancements have been driven by offering consumers higher resolution outputs, so has 3D printing.[7] Many additive manufacturing technologies strive to erase any visible tool marks by increasing resolution capabilities.[8] Material behaviour results in vastly different print layer scales among deposition modelling technologies. Current consumer-grade plastic and resin printers offer print layer resolutions between 25 and 300 microns. The clay printers used

---

5. Kluska et al., "The Accuracy," 70.
6. Gourdoukis, "Digital Craftsmanship," 50.
7. "What does Resolution."
8. Rosenwasser et al., "Clay Non-Wovens," 502.
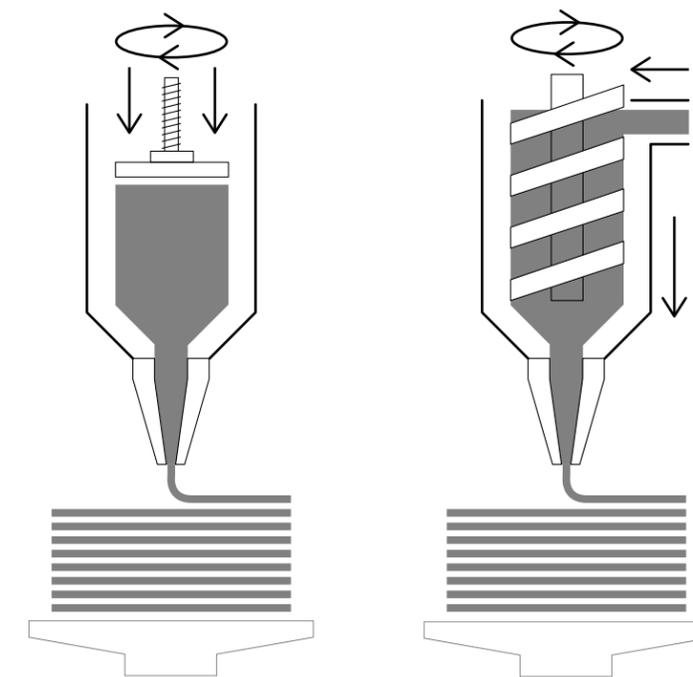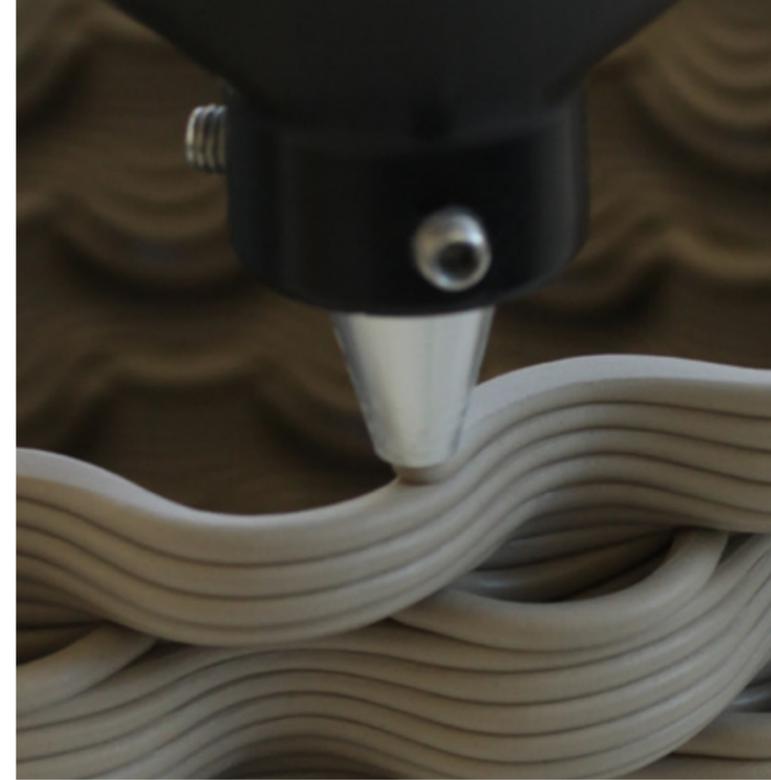


**Figure 3.2.1** LDM print in progress (left) and sectional diagram of printing mechanism (right).
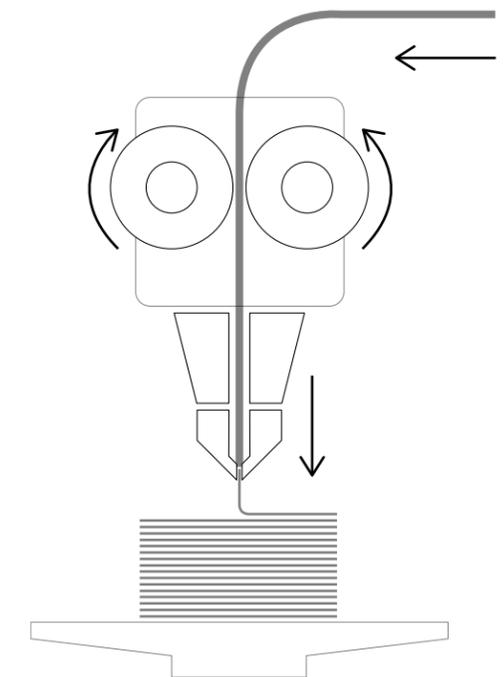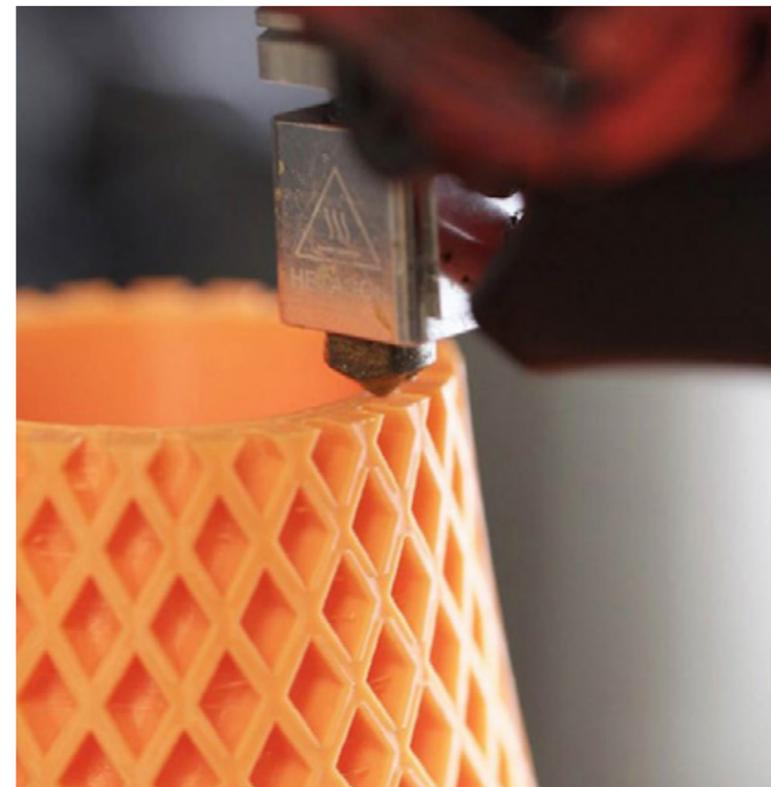


**Figure 3.2.2** FDM print in progress (left) and sectional diagram of printing mechanism (right).

in this research operate at the scale of 500 to 10,000 microns. This research views the 'oversized' print clay layers as an opportunity to break from ideals of efficiency inherited from other technologies and materials. By utilizing material deformation, ceramic 3D printing can disassociate the print layer with the universal manufacturing language of 3D printing and form design languages unique to the material behaviour of clay.

## 3.3 TRANSLATING DIGITAL TO PHYSICAL

In a typical 3D printing workflow, digital geometries are converted to tool paths using software that contours geometry based on inputs of materiality and function. This software is commonly referred to as a slicer. As the market for consumer-grade 3D printers continues to grow, many slicers are prioritizing universal application and user-friendly interfacing. Popular slicers used in the consumer market, such as Cura, provide a foundational platform, allowing custom print settings for different printers and materials to be imported. 3D printer manufacturers, such as Potterbot, will provide calibrated print settings for their printers that can be easily imported into a slicer. Optimization principles of minimizing print time and maximizing material usage are the underlying standards on which many slicers operate. These optimization principles are helpful when paired with the ever-increasing print resolution of resins and plastics. However, they do not address unpredictable and emergent properties that are inherent to clay deformation. As Dimitris Gourdoukis states,

the adoption of standardized protocols "serves the designer to the extent that it helps her or him to realize a preconceived architectural idea."[9]

The first phase of this research was conducted using the slicer Simplify 3D. After three months of experimentation, it was concluded that Simplify 3D could not fully support the study of material deformation. The tool paths of subsequent research phases are produced in grasshopper and exported directly to the printers. Two state-of-the-art publications were pivotal in supporting the development of visual scripting tool paths from the ground up. The first text, *Advanced 3D Printing With Grasshopper: Clay and FDM* by Diego Garcia Cuevas and Gianluca Pugliese, outlines a framework for experimentation with G-code generation.[10] The second text, *Algorithms-Aided Design* by Arturo Tedeschi, provided more advanced techniques for generating parametric tool paths.[11]

Parameters such as extrusion rate, print speed, and z-axis variability are defined globally in Simplify 3D. Defining these parameters as constants lead to prints that better reflect their digital counterparts while minimizing unpredictable material behaviour. Most slicers come with features to combat deformation, such as rastered infill patterns and overhang support systems. Using slicers to experiment with controlled deformation adds an unnecessary degree of abstraction to the workflow. Digital geometry must be modelled in a way that anticipates print parameters. Parametric tool path generation allows the user to individually isolate and manipulate

---

9.   Gourdoukis, "Digital Craftsmanship," 52.

10.   García Cuevas and Pugliese, *Advanced 3D Printing*.

11.   Tedeschi, *AAD Algorithms-Aided Design*.
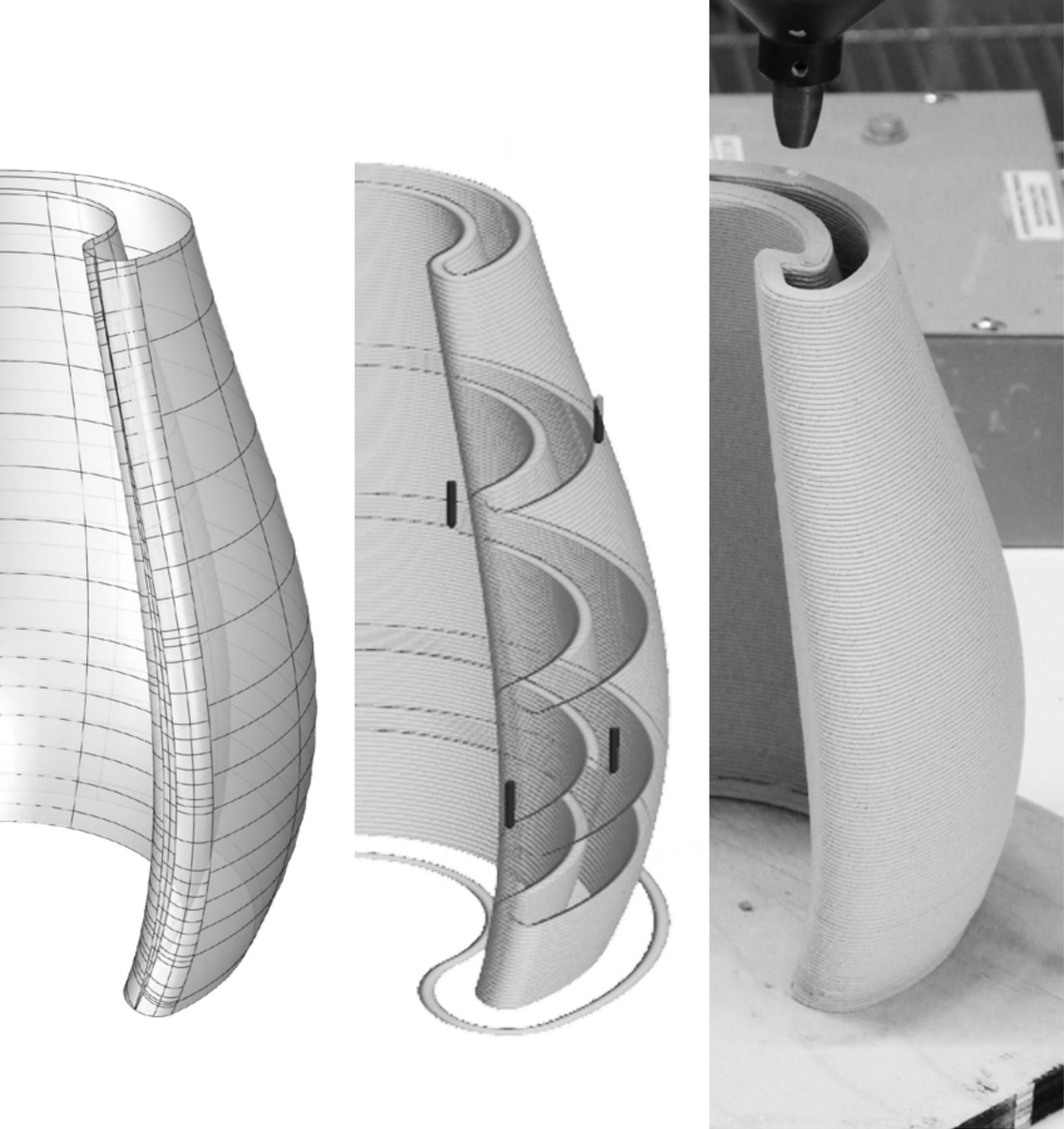
**Figure 3.3.1** Workflow from digital geometry (left), to tool path generated by slicer software (middle), to physical print (right).
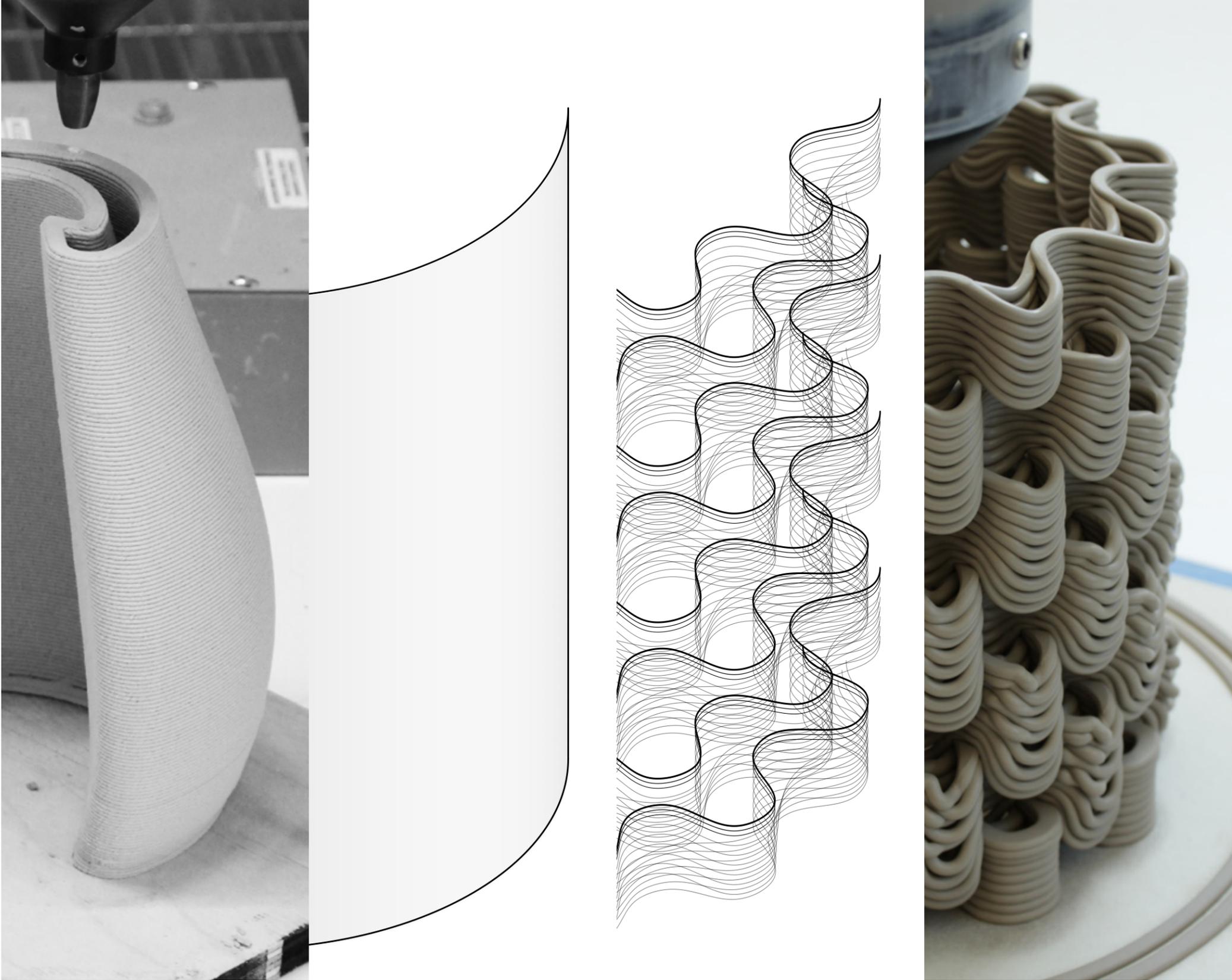
**Figure 3.3.2** Workflow from digital geometry (left), to abstracted tool path generated in grasshopper (middle), to physical print (right).

every aspect that forms a tool path. Custom G-code generation provides access to many printer functions relating to clay deformation that most slicers are not equipped with. The functions listed below represent the most significant contributors to slicer incompatibility within this body of research:

1. **Non-planar printing–** Clays' ability to deform during wet-processing allows small changes in layer height to compound over a print, resulting in structurally stable z-axis variability.
2. **Extrusion variability–** Can be altered to embed patterns in the thickness of a print wall. This thesis utilizes fluctuations in extrusion rate to facilitate variable light transmission through non-porous porcelain shades. Current slicers lock extrusion as a constant, prioritizing stability and uniformity over materially responsive functions.
3. **Intersecting geometries–** Slicers typically require a closed geometry with no intersecting faces to generate a tool path. As clay is wet-processed, overlapping walls can help prevent collapse and form multi-layered formal expressions.
4. **Seam generation–** The ability to deconstruct the tool path and reconstruct the seam is critical to producing clean prints in clay.



**Figure 3.3.3** Material studies that all stem from 100mm x 100mm x 200mm base geometry.

**Figure 3.3.4** Examples of non-planar printing (left) and extrusion variability (right).

**Figure 3.3.5** Examples of geometry intersection (left) and seam generation (right).

## 3.4 CLASSIFYING THE PRINT LAYER

The the plasticity of clay, when harnessed by LDM, represents a new world of formal languages. The striations left by the extruder are inherent to all ceramic artifacts manufactured with this technology. The print layer or tool mark of a digitally fabricated ceramic artifact can operate on a wide range of scales. How the manufacturer addresses the tool mark of the printing process directly affects the topology of the 3D printed clay vessel. Through this lens of examination, three categories of expression start to emerge from the broader field of LDM with clay: tool path as a byproduct of form definition, tool path as an expression of ornament, and tool path as a function of performance. These categories employ a variety of digital tools and exist on a spectrum with substantial room for overlap.

### Tool Path as a Byproduct of Form

The first category represents tool paths that are contours of their digital counterparts, prioritizing form over ornament. These prints typically utilize low step heights that maximize lamination from layer to layer and reduce deformation. Ornament often destabilizes the print, leading to a negotiation between the form's complexity and the ornament's complexity. Contouring can facilitate more complex asymmetrical forms as it represents the least abstracted translation of the digital geometry to the physical print. The more linear translation of digital input to physical output allows this category of expression to utilize a wide range of slicers.
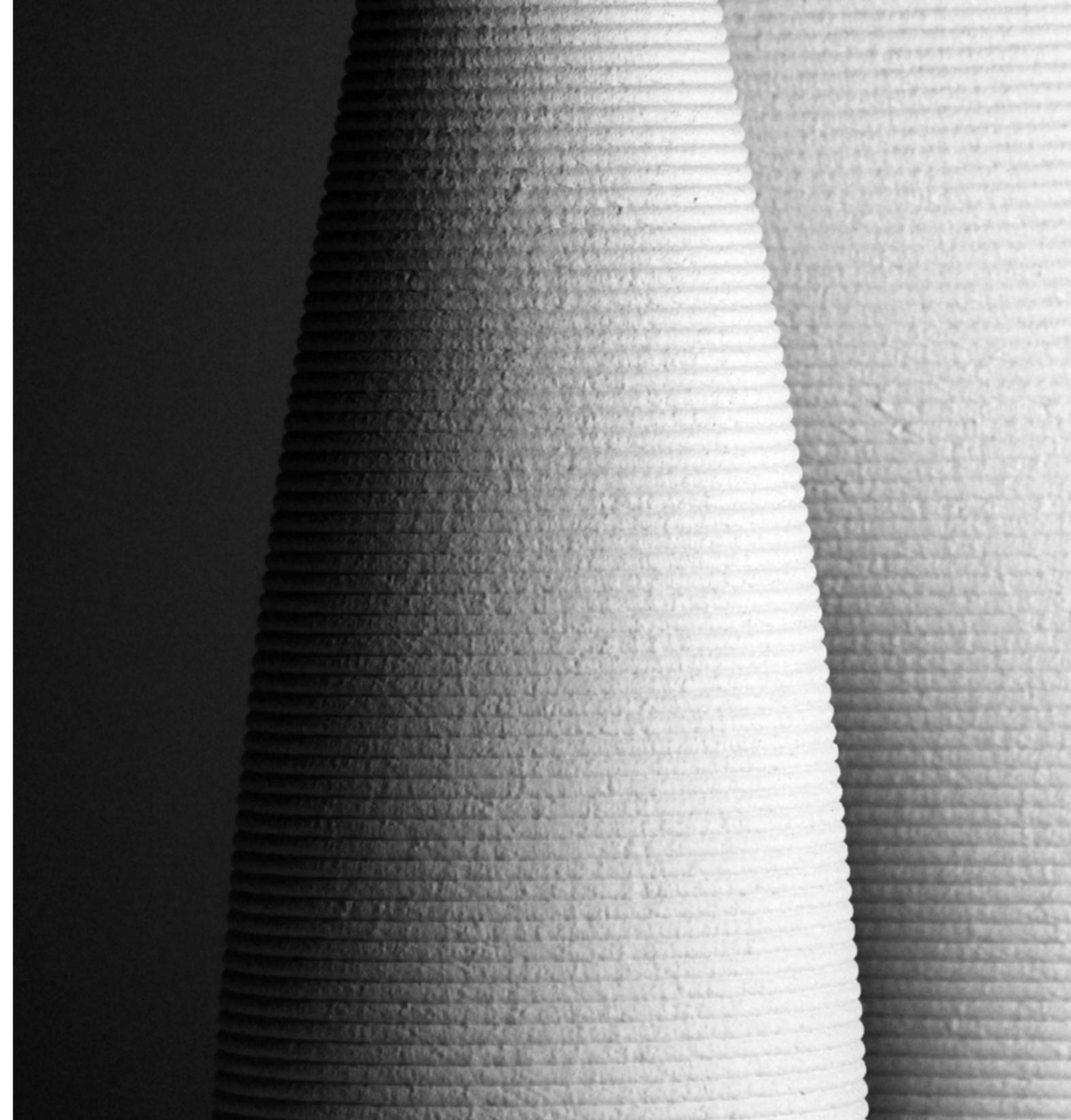


**Figure 3.4.1** Early material studies utilized light washes across non-porous surfaces.

At one end of the spectrum, post-processing physical interventions can completely erase the print layer. Printing to the minimum step height tolerances and either rubbing out the print layers manually or applying an opaque glaze will fill the print layers' ridges, creating a monolithic finish. Jonathan Keep is a ceramic artist who has produced many bodies of works that utilize these manufacturing methodologies. One of his most recent works, 'Icebergs,' is a series of porcelain prints generated using 'noise' inputs. The random inputs in form generation create geometries that mimic the erosion of icebergs.[12] In this series of explorations, the print layer serves the complexity of the overall form by being constant and minimal. A white glaze is then applied to further accentuate the form and reduce print layer visibility.

Oliver Van Herpt is a ceramic artist that utilizes analog methods to generate ornament. Many of his prints are simple tubular forms comprising soft facets or undulations. These works do not express material deformation through digital manipulation of the print layer. Instead, they rely on pre and post-processing physical interventions to embed ornament. His project 'Colourful White' generates ornament by layering pigment into the clay body. The result is a "motion blur effect that made them look as if they were moving even though they were sitting still."[13] The print layer facilitates the blurring effect as pigments are dispersed coiled up the porcelain tube.



Figure 3.4.2 Early material studies utilized light washes across non-porous surfaces.

---

12.    Keep, "Iceberg Series."

13.    van Herpt, "Colorful White."

**Figure 3.4.3** Iceberg Field by Johnathan Keep.



**Figure 3.4.4** Iceberg interior detailing by Jonathan Keep.



**Figure 3.4.5** Colorful White by Olivier van Herpt.



**Figure 3.4.6** Colorful White print in progress.

## Tool Path as an Expression of Ornament

Category two harnesses deformation of the print layer to express ornament. Digital and physical interventions can temporarily displace the print bead from the form to create patterns on a print's surface. The plasticity of clay allows the print layer to be pulled away from the primary structure to hang freely, forming a 'loop.' In this category, the design language of 'looping,' 'weaving,' and 'braiding' becomes present despite clay extrusion being more akin to non-woven textiles. Visual parallels can be drawn between the movement of the clay extrusion and traditional woven structures such as wicker baskets. Ornament expressed through print layer manipulation can be perceived as separate geometry attached or embedded into a form that provides structural support.

In this category slicers and custom tool path generation can be used with significant impact. However, some forms of tool path generation are better suited to generate certain forms of ornament. Patterns spanning multiple layers, such as diamond facet meshes that translate to braided patterns when printed (see Figure 3.4.7), are easier to create by using a slicer's geometric processing logic. A few emerging products cater to designers who want to explore material deformation in clay without learning to generate custom tool paths with coding and visual scripting languages. Potterware by Emerging objects is slicer software geared towards creating surface patterns with clay 3D printers. The program allows for basic looping and weaving patterns to be generated over imported forms. While lacking many



**Figure 3.4.7** Preliminary material behaviour study, exploring 'braided' patterns generated from non-porous tessellations.

niche functions that clay printing can accommodate, this software allows for an easy and intuitive point of entry for users exploring material deformation in 3D printed ceramic artifacts.

'Bad Ombres' by Emerging Objects is an excellent example of a project that bridges categories one and two. This project is printed with two different clay bodies to form a vertical colour gradient, embedding ornament into the form. Loops on these vessels do not directly contribute to structural stability. Instead, they add decorative elements that protrude from the base vessel. As stated by Emerging Objects, these loops "celebrate the object and the individual extrusion of clay by liberating particular extrusions from the vessel, suggesting the material is defying gravity with petal-like extrusions of multiple clay bodies."[14]

'SEKI' by Erin Hunt (in collaboration with Kelly Devitt-Steenhagen, and Ingrid Lilligren) is a project that captures the diversity of ornament that can be achieved through material deformation. 'SEKI' is a catalogue of eight unique vases that utilize ornament using looping, braiding, spiralling and weaving patterns. The vases are then finished using glazes formulated to enhance the qualities of the patterns across the vase through layering and pooling effects. Throughout these pieces, the form of the non-porous vase is maintained while the middle third of the vase is abstracted by patterns that utilize clay's unique deformation properties.[15]



**Figure 3.4.8** Potterware interface and resulting print.
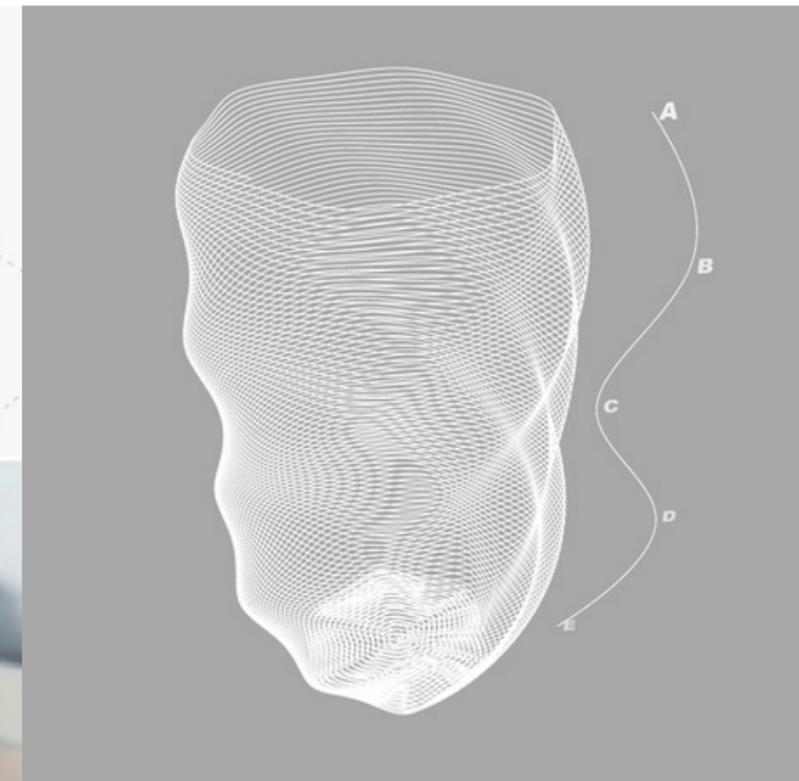
**Figure 3.4.9** Potterware interface.

14. Rael et al., "Bad Ombres V.2."

15. Linsey Hunt, "Seki."

**Figure 3.4.10** Bad Ombres V2 by Emerging Objects.



**Figure 3.4.11** SEKI by Erin Hunt.

## Tool Mark as a Function of Performance

Category three utilizes the tool path to create ornament as well as harness material performance. In category two, ornament and form can be distinguished separately within a print. In this category, ornament, form, and structure are perceived holistically. Form and ornament take on structural and performative characteristics. Material deformation is no longer utilized for purely ornamental purposes. Category three takes shape in porous print structures, non-planar printing, or other methods that obscure the continuity of print layers through high degrees of deformation. This high degree of material deformation means that the translation from digital to physical becomes further abstracted. Custom tool path generation is of great benefit here. Most slicers do not support surface porosity, layer-by-layer control, non-planar printing, and other critical functions to harness material performance. Custom G-code generation and material computation require in-depth research on material behaviour. As a result, this category is less established than the previous two. Performative deformation differs from many conventions of additive manufacturing, making it extremely difficult to achieve similar effects with any other material or technology. In this space of ornament as form and material deformation as methodology, the limitations of this unique technology can be pushed.

'Clay Non-Wovens' by David Rosenwasser, Sonya Mantell, and Jenny Sabin is a project that blurs the decorative and performative qualities of the tool path. 'Clay Non-Wovens' is a series of light



**Figure 3.4.12** Full scale prototypes utilizing porous tool paths generated in grasshopper.

screens produced by layering print coils across a horizontal surface. This project posits that "the traditional clay coil is to be reconsidered as a structural fibre rather than a tool for solid construction."[16] 'Clay Non-Wovens' seeks to celebrate the fabrication process rather than erase it.

'InFormed Ceramics: Multi-axis Clay 3D Printing on Freeform Molds' challenges current manufacturing methodologies for architectural ceramic systems by leveraging the same robotic arm for different production phases.[17] Each of the nineteen panels of the project is first conceived of as a foam formwork to facilitate non-planar printing of clay using a multi-axis clay extruder. Three different end-effectors are utilized on the same arm to support complex clay forms: a hotwire cutter shapes the formwork, a spindle refines the formwork into continuous curves, and lastly, a multi-axis extruder prints custom tool paths.

'Spatial Print Trajectory: controlling Material Behavior with Print Speed, Feed Rate, and Complex Print Path' posits that current digital fabrication techniques for extruding successive planar layers "uses an excess of material and is a time-consuming process that does not take advantage of the viscous properties of clay."[18] This project explores voxel structures created by 'return-loops' formed by a tool path of anchors and dragging coils.


**Figure 3.4.13** Non-woven clay prints in progress.
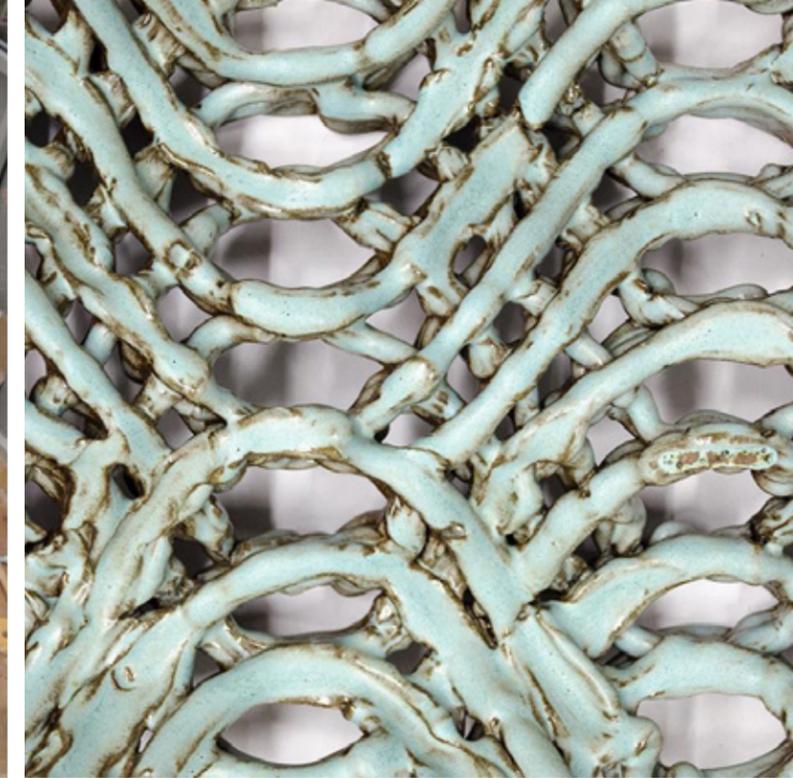

**Figure 3.4.14** Non-woven clay panel glazed.
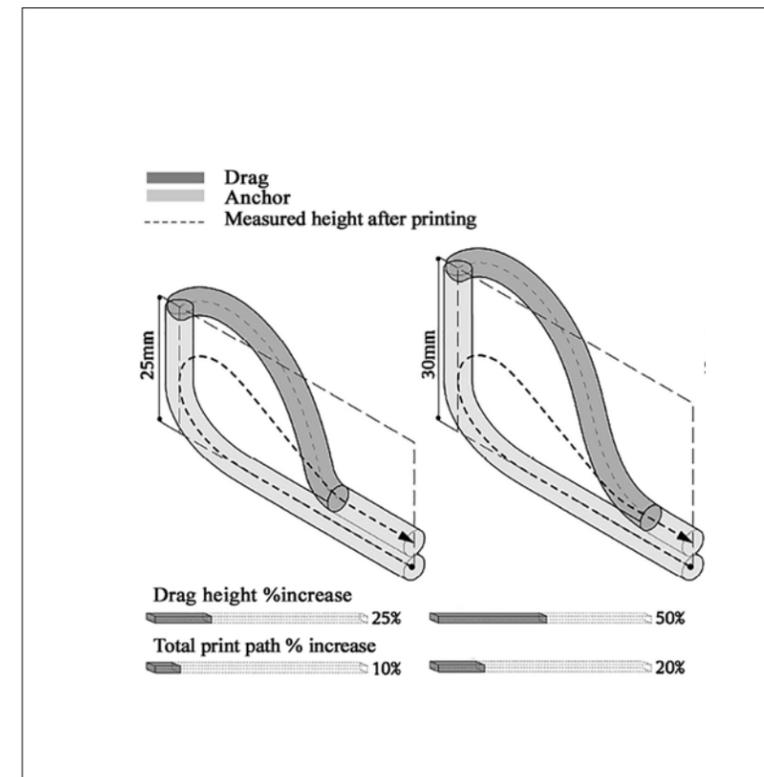

**Figure 3.4.15** Diagram of anchor generation.
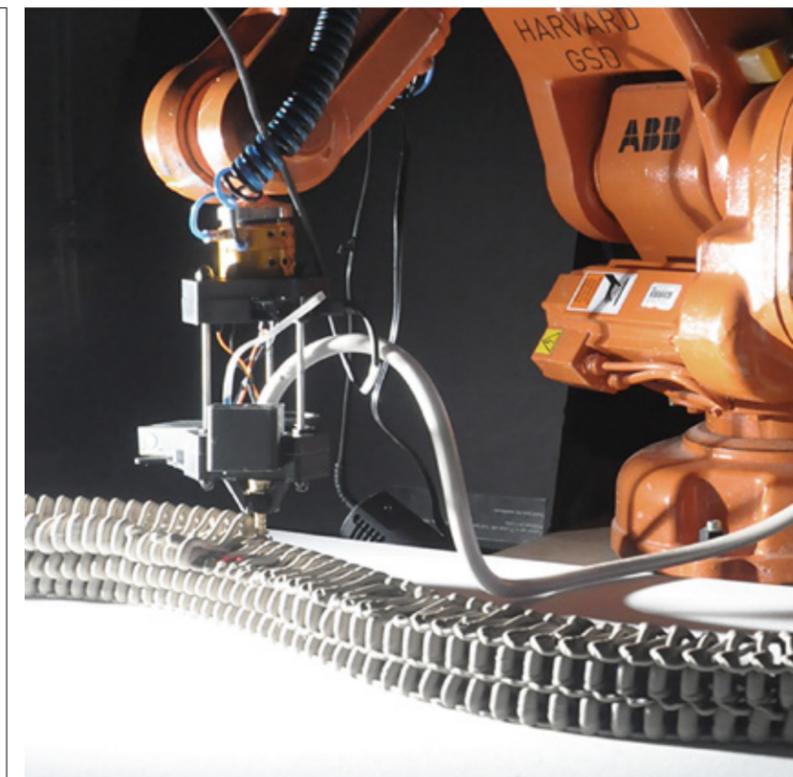

**Figure 3.4.16** Double curved surface print in progress.

---

16.  Rosenwasser et al., "Clay Non-Wovens," 502.

17.  Ko et al., "InFormed Ceramics," 302.

18.  AlOthman et al., "Spatial Print Trajectory," 169.
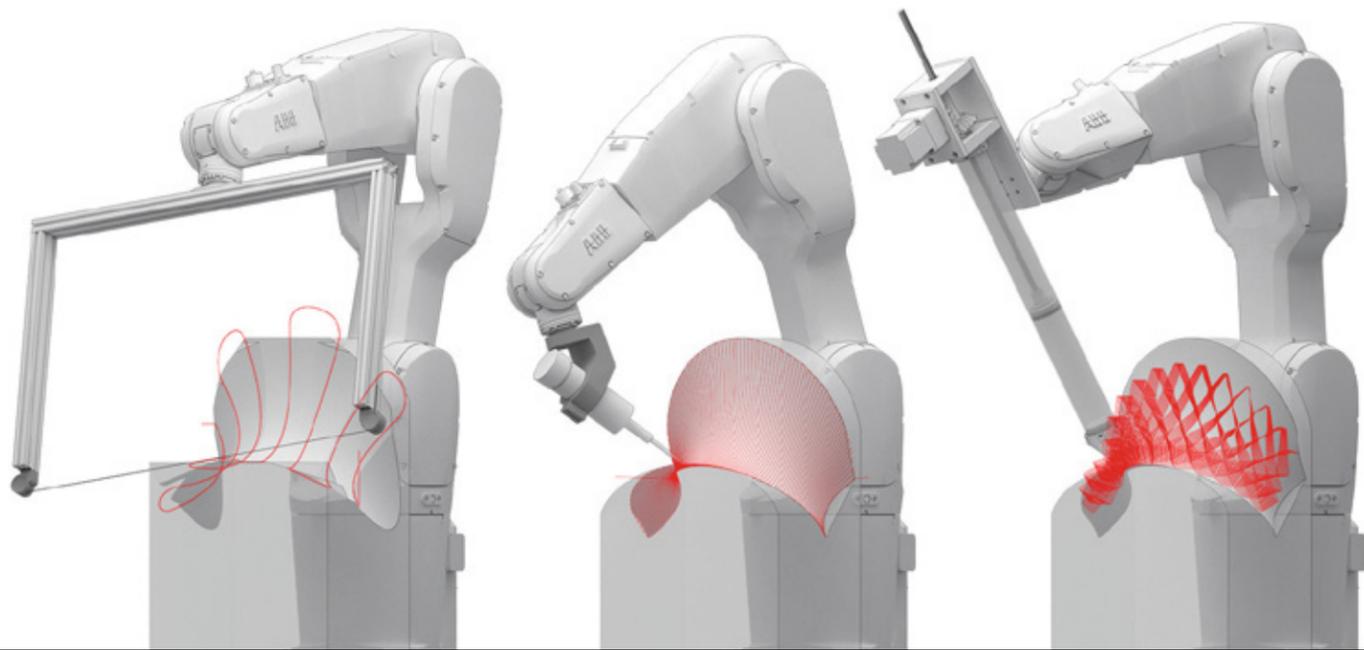
**Figure 3.4.17** Diagram of spindle and clay extrusion strategies on same surface.



**Figure 3.4.18** Onsite installation of final panels.

# PART 4

## METHODOLOGY

## 4.1 OVERVIEW

The research methodology consists of two phases of computational development. Each phase utilizes one of two digital workflows: 'Mesh to Slicer' and 'Grasshopper to G-Code.'

Material explorations in the first phase utilize the print coil ornamentally. This phase helped identify relationships between digital parameters and material behaviour for crafting texture and sculptural relief across ceramic surfaces. The second phase of computational development looked to harness material behaviour by designing tool paths that utilize the print coil performatively. This phase comprises the development of four light screen typologies. Two parameters are essential to understanding the computational methods:

1. **Number of layers in a print pattern**– Consecutive print layers are grouped and vertically tessellated across a print to create light apertures. The number of layers used to generate a pattern determine aperture size (Figure 4.1.1).

2. **Wave divisions**– Refer to the horizontal pattern occurring across a print layer. Within the digital workflow, print layers are conceived of as contours that subdivide a digital surface into horizontal lines. These horizontal lines represent the tool path. Contours are then subdivided into a series of points. Points are displaced to create tool path variability. This displacement results in the transformation of the tool path into a series of wave-like curves (Figure 4.1.2).

'S' Tool Path Section     'M' Tool Path Section     'L' Tool Path Section     'XL' Tool Path Section
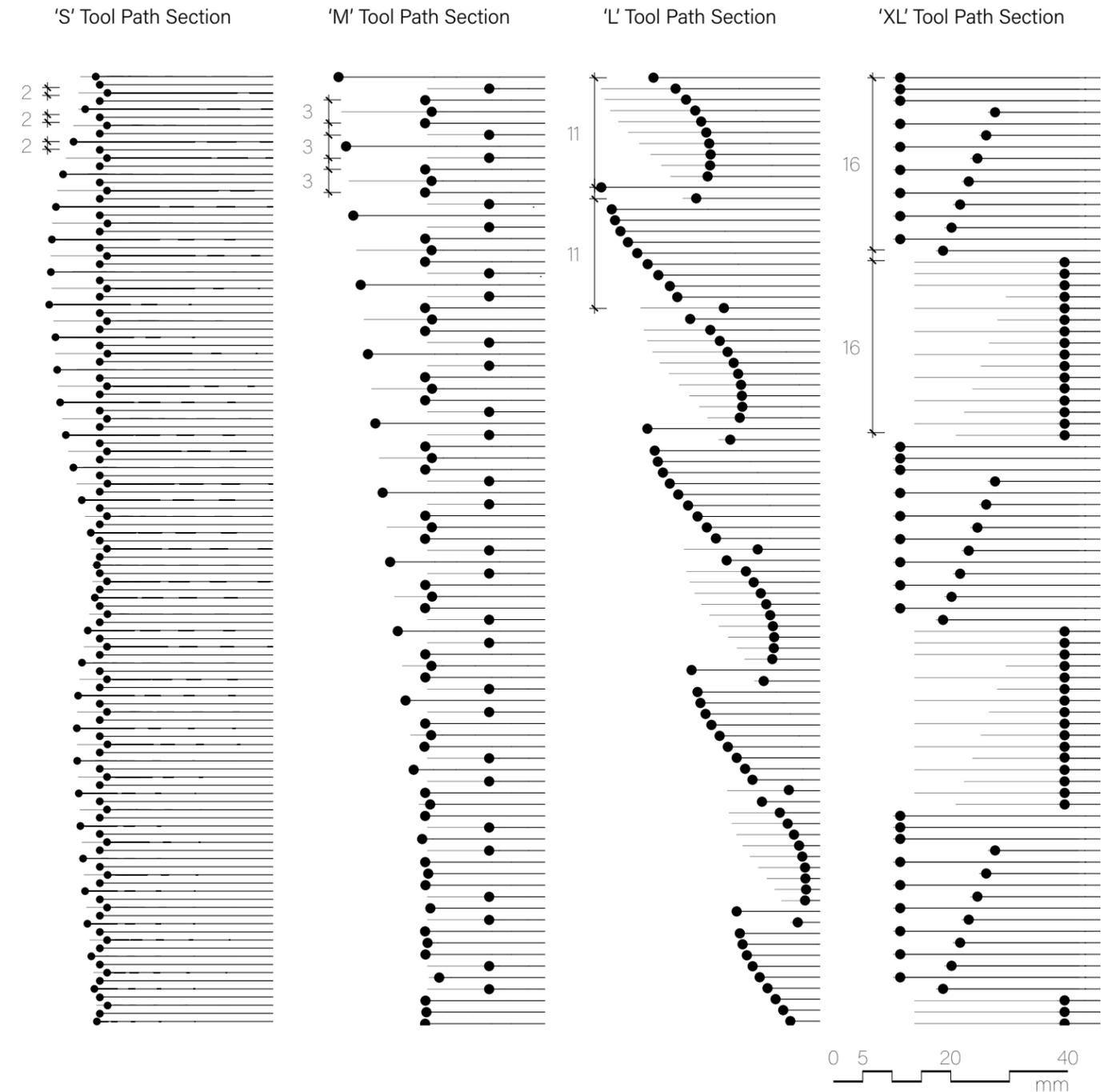


**Figure 4.1.1** Comparison of number of layers in each print pattern.

The four light screen typologies in the second phase of computational development are categorized by the number of layers required to create apertures. Although the formal expressions, illumination, plastic deformation and structural stability differ substantially between light screen typologies, the number of layers in a print pattern remains a universally significant parameter in dictating form. The 'Small' (S) typology consists of non-porous geometries that rely on the translucency of porcelain to diffuse light. The 'Medium' (M), 'Large' (L), and 'Extra-Large' (XL) typologies rely on the plasticity of stoneware to create openwork structures that scatter light across distinct sectional conditions.

The final prototypes within each light screen typology capitalize on both clay's working properties and ceramic performance characteristics. Graded light scattering effects across these pieces are a product of strategic shifts in the design of the tool path to produce distinct sectional conditions. In the porcelain prototypes, brightness increases when sectional depth is minimized. In stoneware prototypes, brightness increases the further layers are pulled apart in the X-Y axis. However, increased porosity and thin wall sections promote instability. Since none of the prototypes in this research utilize formwork to provide structural support during wet-processing, tool paths must be carefully considered to prevent structural failure. The final prototypes attempt to push the structural and formal limitations of the material, maximize the manufacturing capabilities of the machines utilized, and harness the relationship between light and ceramic surfaces.



*0-1*

*0-0-1-1*

*0-1-2-3-4-3-2-1-0*
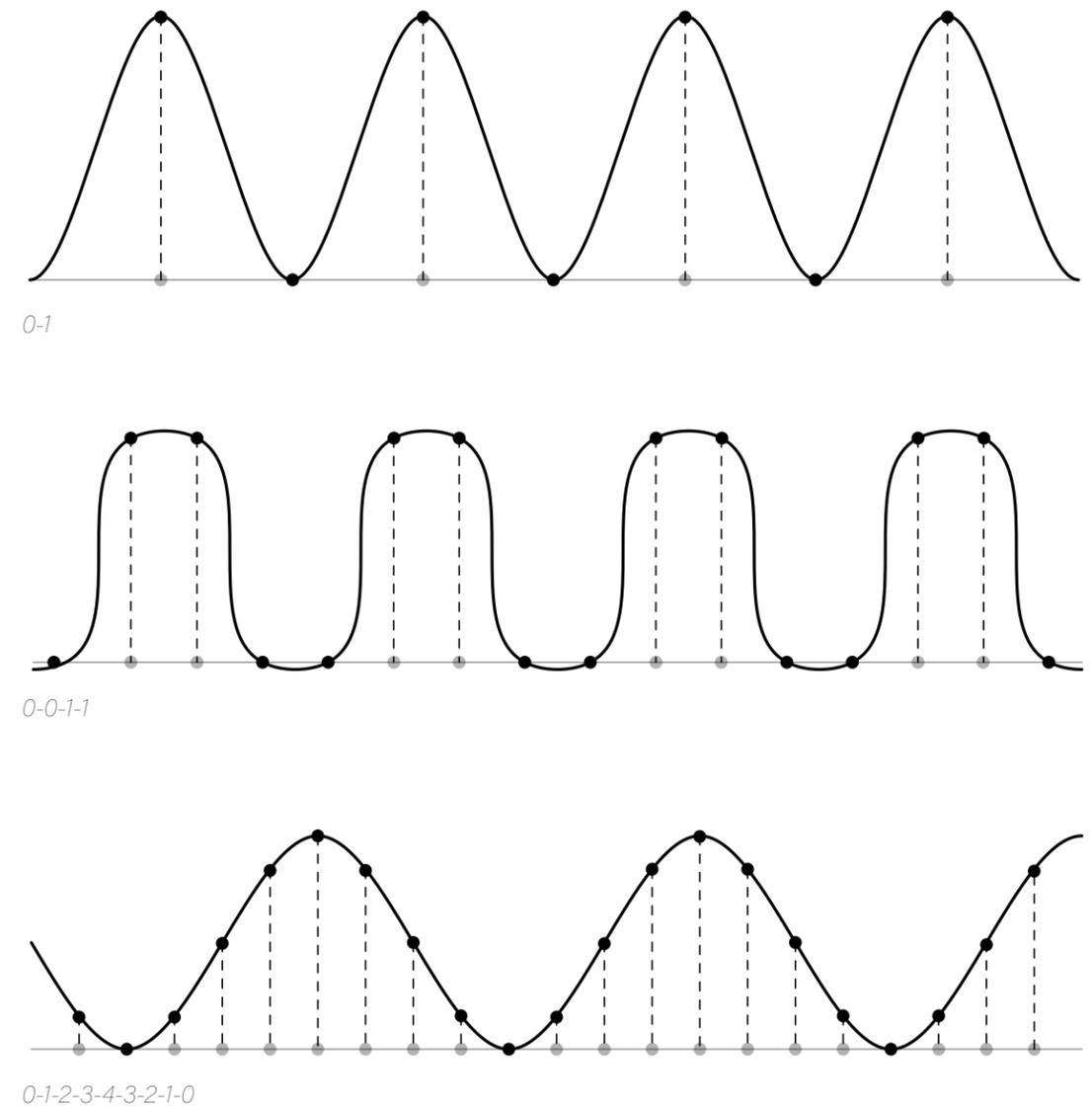
**Figure 4.1.2** Waves in a print layer constructed from displaced base points.

# 'S' TYPOLOGY



# 'M' TYPOLOGY



# 'L' TYPOLOGY
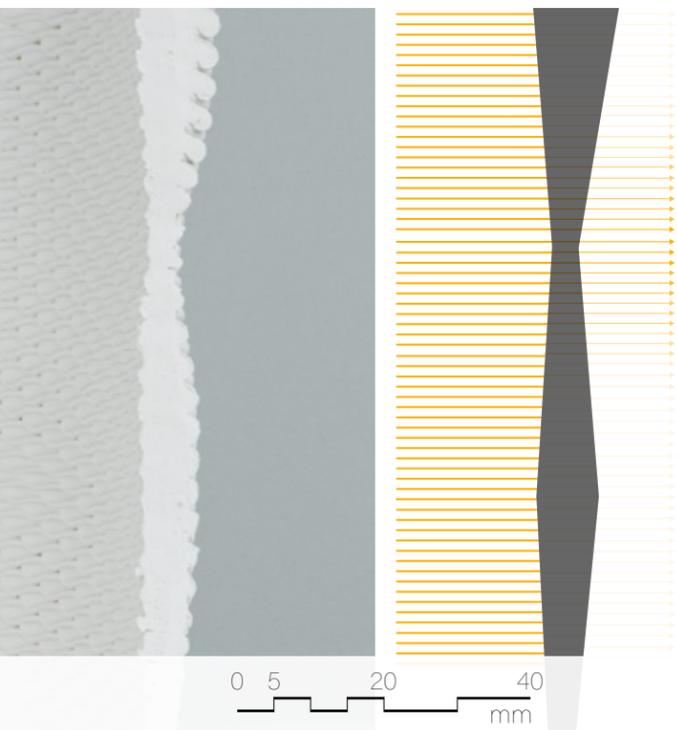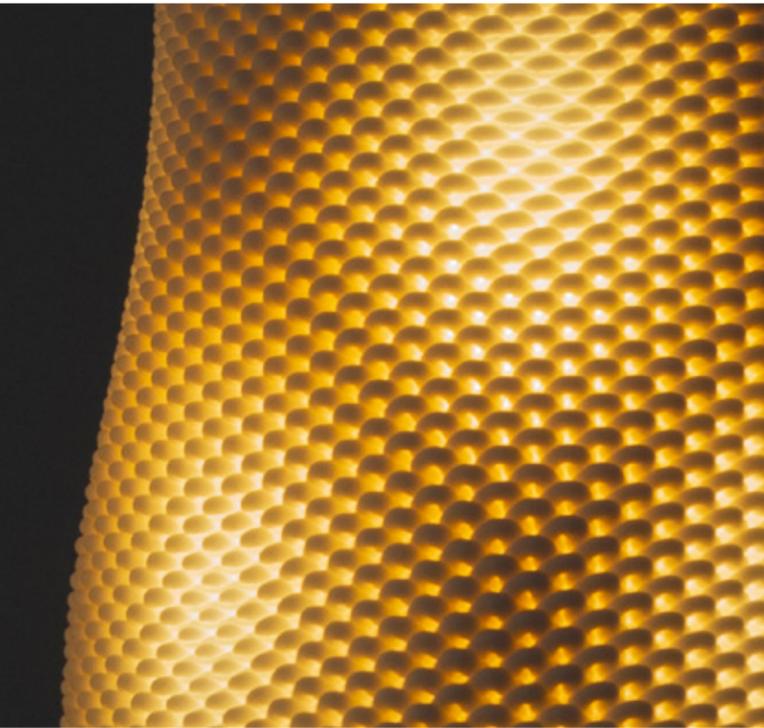


# 'XL' TYPOLOGY



**Clay Body:** Polar Ice, cone 6 porcelain.
**Lighting Effect:** Extrusion variation in the printing process regulates diffuse light transmission through the fired ceramic body to generate light scattering effects.
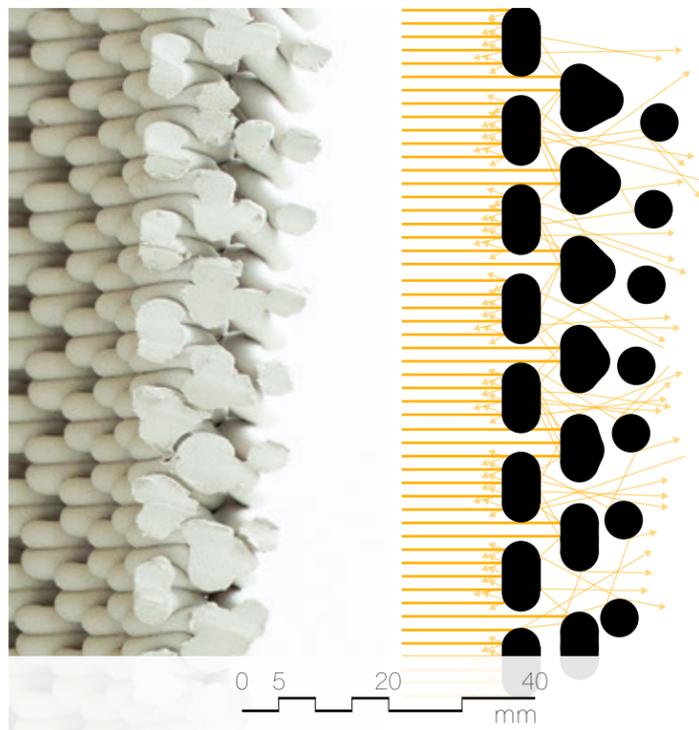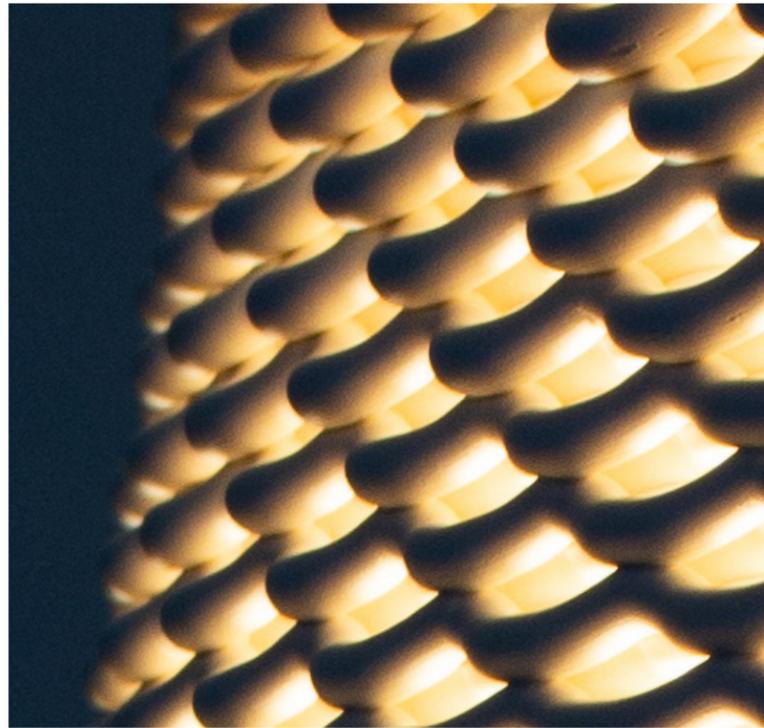
**Clay Body:** PSH 516, cone 6 stoneware.
**Lighting Effect:** Single print layers are staggered to create a multi-layered screen that scatters and diffuses light.
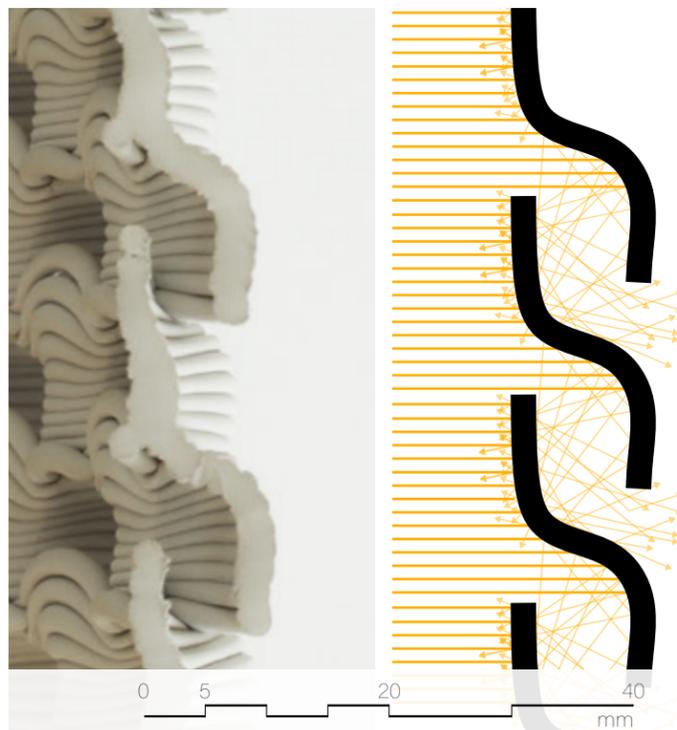
**Clay Body:** PSH 516, cone 6 stoneware.
**Lighting Effect:** Controlled deformation is utilized to create scoops that direct light downward, shielding the viewer from glare.
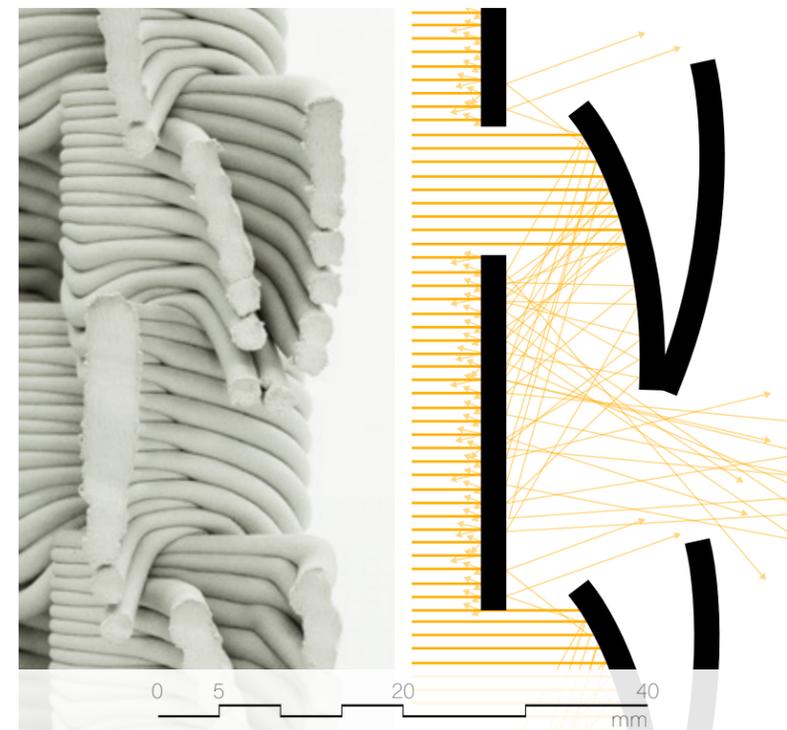
**Clay Body:** PSH 516, cone 6 stoneware.
**Lighting Effect:** Controlled deformation and extrusion variation are utilized to create light shelves that scatter incident light to prevent glare.

## Digital to Physical Workflows

**Mesh to Slicer**– This workflow consists of 3D modeled meshes generated in Rhinoceros 6, and translated into G-Code via slicer software, Simplify 3D. The first series of prints utilized this workflow primarily due to ease of use: no coding knowledge is required to produce 3D prints this way. However, this workflow limits the ability to easily manipulate geometric expressions at the scale of a single print coil. Figure 4.1.4 illustrates the limitations on print parameters set by the slicer software: speed and extrusion rate must remain fixed.

**Grasshopper to G-code**– This workflow consists of generating a continuous curve in Grasshopper that represents a potential tool path. The curve control points are manipulated to create patterns using a variety of techniques such as image mapping and attractor points. Once the tool path is set, a secondary script translates the curve into a series of coordinate points. Those coordinates are packaged with an extrusion rate and print speed in a text document to create a G-code file for the printer. All experiments in Phase 2 of computational development are a product of parametric G-Code generation in Grasshopper. A G-Code file is divided into lines of commands. Within this body of research, a typical line of commands consists of 3 values:

**G1**– This denotes a linear movement, typically followed by Cartesian coordinates. Curvilinear tool paths are created using minute linear movements. Therefore, the proximity of coordinates between two
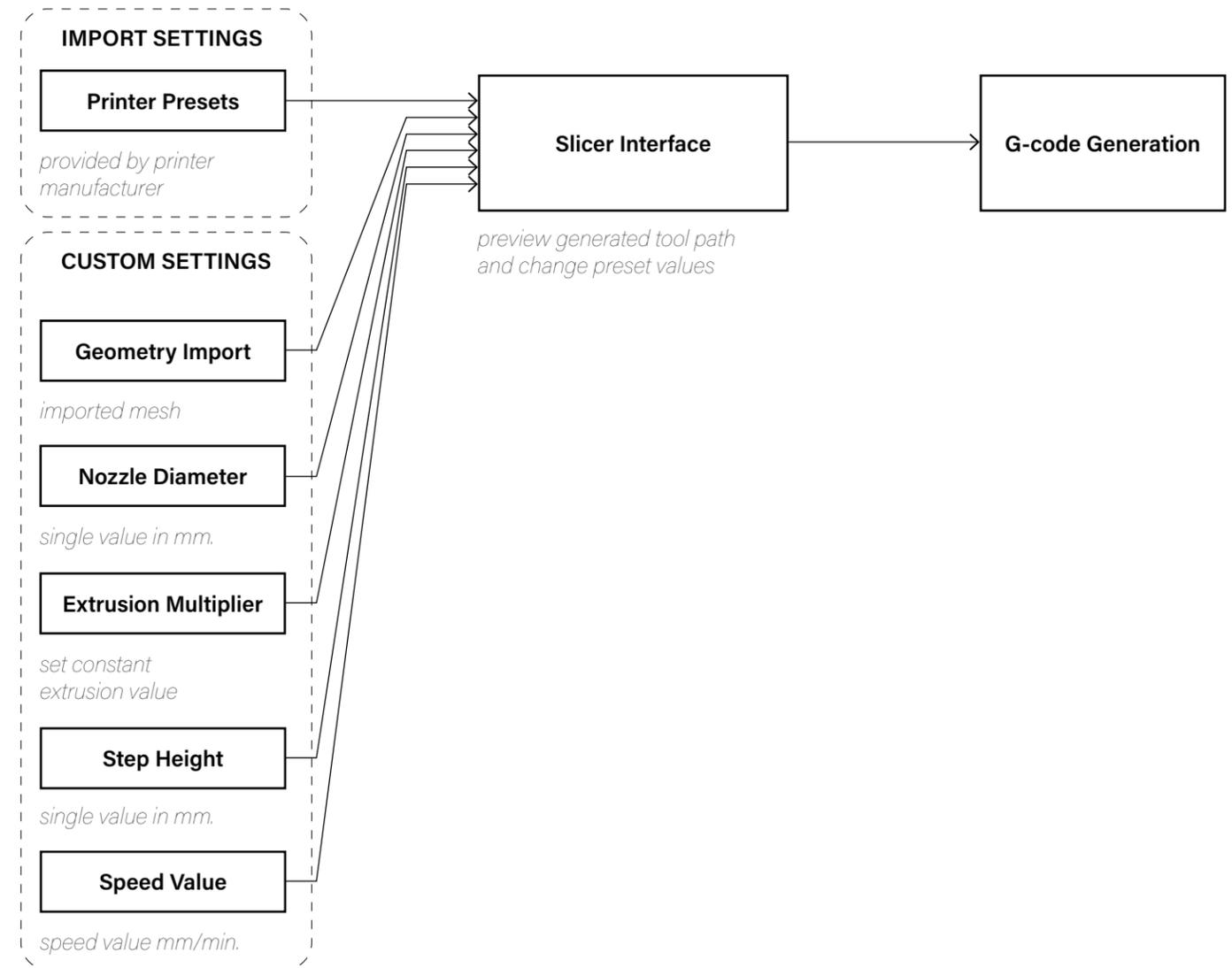


**Figure 4.1.4** Principle inputs of mesh-to-slicer workflow.

command lines determines how 'smooth' curves will print- otherwise known as 'print resolution.'

**F**– The speed at which the printer executes movement. This value is measured in mm/minute.

**E**– A compounding value that dictates how much material is extruded during a single movement. Print speed, layer height, and tool path geometry can all impact E value. E value has a significant impact on plastic deformation during wet processing. The equation to derive this value requires a filament radius. Since clay remains malleable throughout the printing process, there is no optimal equation for this value.



**PRINCIPLE INPUTS**

Geometry Generation
*surface/brep*

Step Height
*single value in mm.*

Vertically Tesselated Print Pattern Number
*number of layers that create the repeating sequence*

Wave Division
*single value*

Vector Generation
*image map/control pts.*

Print Resolution
*single value in mm.*

Extrusion Domain
*min.-max. extrusion values*

E. Value Generation
*image map/control pts.*

Speed Value
*speed value mm/min.*

Print Layer Generation
*surface contoured to create list of curves*

Pattern Dispatch
*print layers organized to receive alternating patterns*

Base Points
*print layer curves divided into number of points*

Wave Generation
*vectors applied to base points to create waves and reconstructed into a continuous tool path*

G-code coordinates
*the tool path curve is divided by print resolution*

Extrusion Variation
*g-code coordinates used to map new extrusion values*

G
E
F

G-code Generation

**Figure 4.1.5** Principle inputs of grasshopper to G-code workflow.

## 4.2 PRELIMINARY STUDIES

The first series of tests are predominantly concerned with harnessing clay's working properties rather than its ceramic performance characteristics. All experiments covered in this section were generated using a 'mesh to slicer' digital workflow. These deformation studies were a means to decode the physical and digital parameters required to achieve specific formal expressions utilizing the Potterbot XLS-1. The works in the chapter are divided into three categories that mark the chronological progression of the digital workflow: from standardized fabrication protocols defined in Simplify 3D to custom tool path generation in Grasshopper. The three categories are: unitary geometries, non-porous spliced geometries and porous spliced geometries.

### Unitary Geometries

The studies in the category were the first series of prints produced for this thesis. As stated previously, these studies did not address material behaviour concerning light. Harnessing the working properties of clay, such as controlled deformation and viscoelasticity, was the primary focus. These studies are categorized as unitary geometries because they were all modeled and sliced from a single, continuous digital geometry. Modeling 3D prints as continuous closed meshes is the fastest and most reliable way to ensure a slicer can process an imported geometry with minimal material deformation.

## UNITARY GEOMETRIES
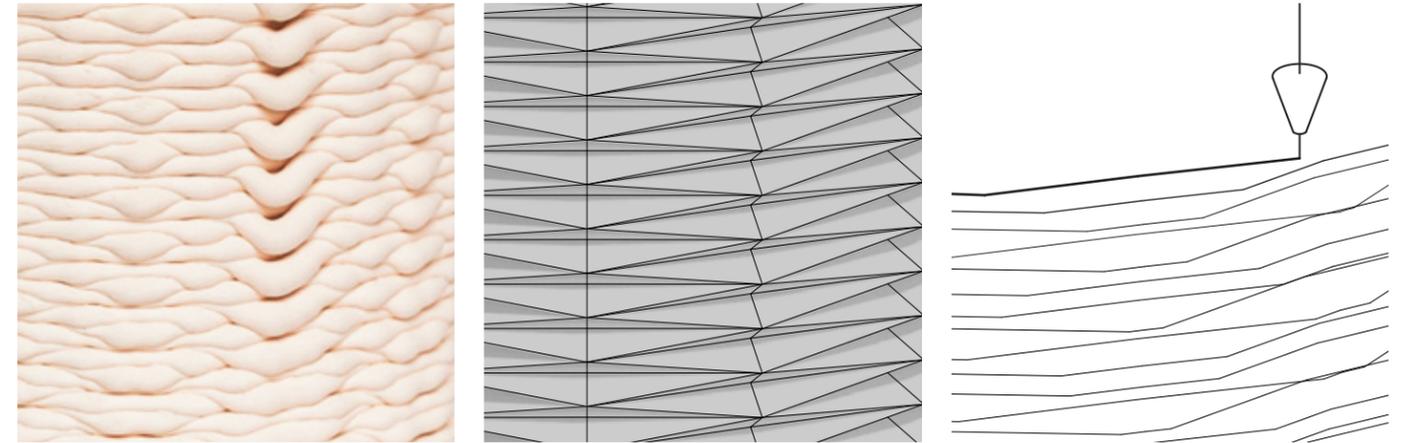


**Figure 4.2.1** Non-porous facet pattern, unglazed PSH-516.
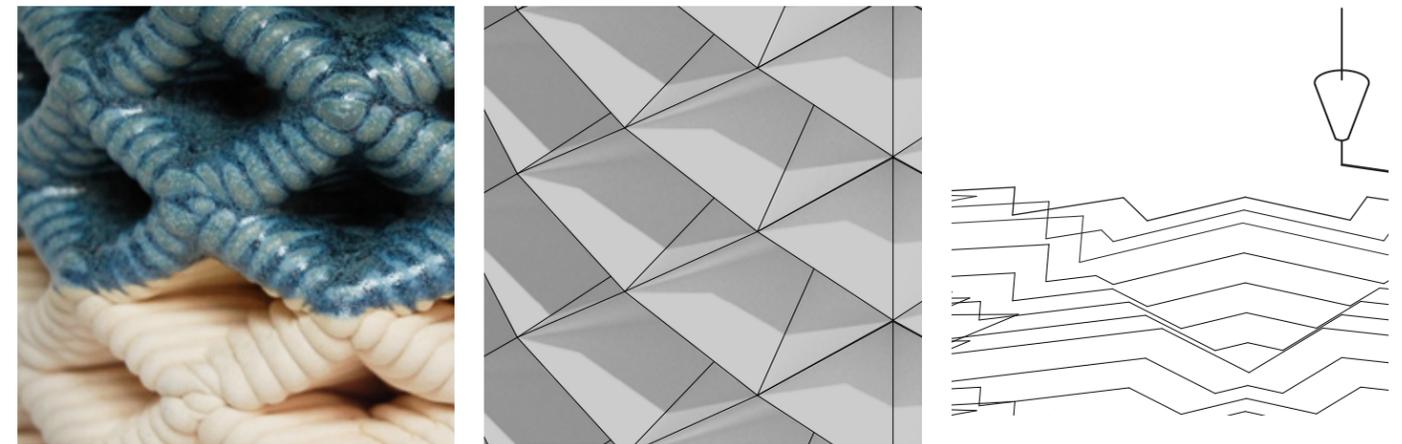


**Figure 4.2.2** Non-porous exterior braided pattern, Variegated Slate Blue glaze on PSH-516.
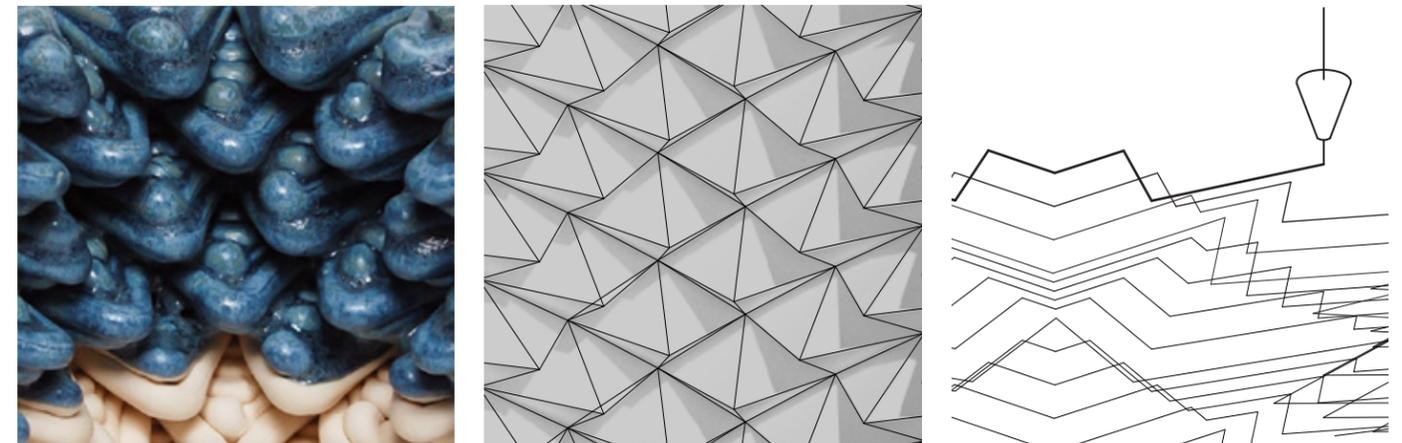


**Figure 4.2.3** Non-porous interior braided pattern, Variegated Slate Blue glaze on PSH-516.

Patterns with a large number of layers can achieve multi-directional effects. The pattern in Figure 4.2.2 repeats after ten layers. The weaving effect is also mirrored vertically and horizontally. The resulting physical outputs vary drastically between the interior and exterior of the geometries. While the print coils on the interior take on a 'woven' or 'braid'-like effect, the exterior yields a matrix of bulbous forms. Modeling continuous forms allows for a broad expression of deformation across multiple layers but has limitations when expressing deformation on the scale of a single print layer. These forms are also designed to be non-porous, limiting their possible interactions with light.

UNITARY GEOMETRIES CONT.
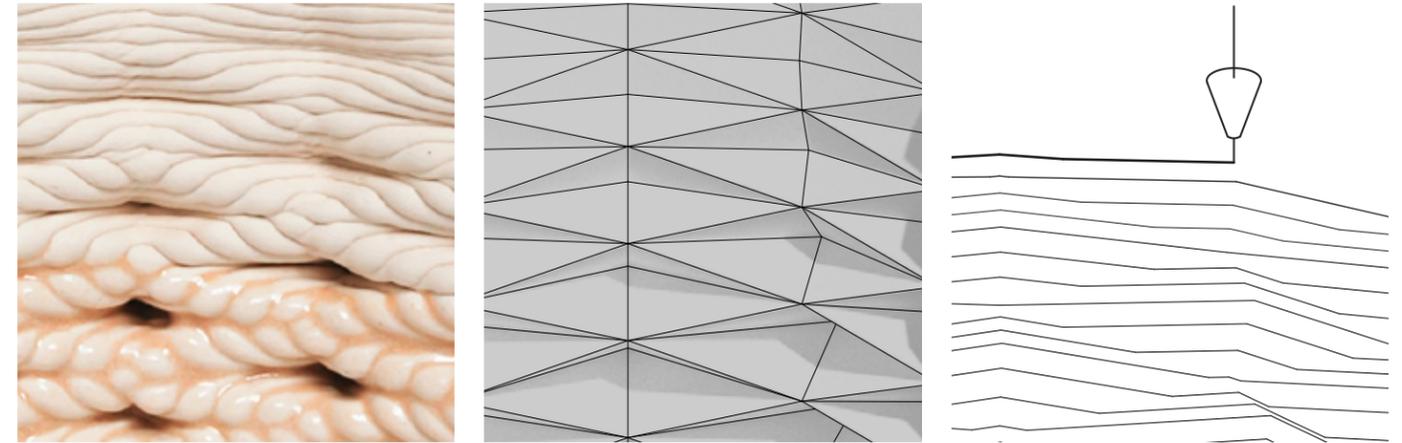


**Figure 4.2.4** Non-porous braid facet gradient pattern, Bone glaze on PSH-516.
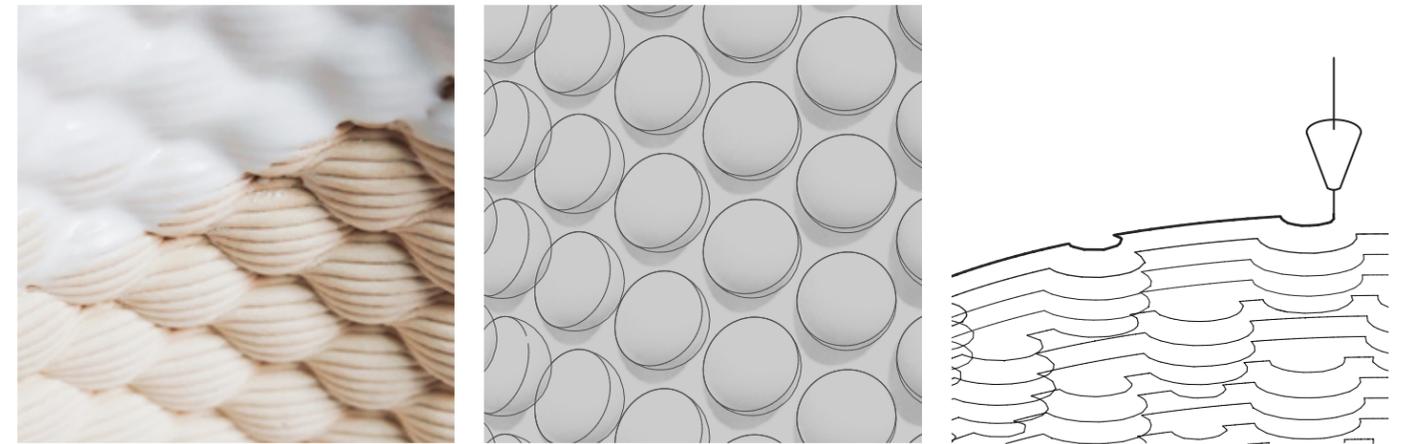


**Figure 4.2.5** Non-porous interior dome weave pattern, Maiolica glaze on PSH-516.

## Non-Porous Spliced Geometries

The geometries in this category remain non-porous but begin to manipulate form at the smallest possible resolution; that of a single print layer. Each print layer was modeled as a continuous mesh and then stacked to form the entire geometry. This workflow also began to address ideas of internalizing controlled deformation patterns into a digital model to bypass efficiency protocols of Simplify 3D.

Figure 4.2.6 is an example of a porous digital mesh that has a non-porous physical counterpart. The geometry was subdivided into 2.5mm surface extrusions to achieve a weaving effect. These extrusions each represent a single print layer. Print layers are then subdivided into wave divisions that are scaled proportionately to the nozzle diameter. Every alternating print layer was then rotated about the center of the entire geometry by the width of a single wave. The alternating layer structure creates the perceived effect of 'weaving.' In this print, the rotation of alternating layers results in vertical striping.

Figure 4.2.7 was created using a similar digital model as Figure 4.2.6 but yielded very different results. Although both prints used the same 2.5mm step height and 5.5mm nozzle diameter, figure 4.2.7 has precisely double the wave divisions and an asymmetrical wave profile. While the exterior surface reads as a matrix of points, the interior surface preserves some of the linear quality of the print coils and layer structure. Although the physical prints in this category remain non-porous, the digital models are highly porous.

## NON-POROUS SPLICED GEOMETRIES
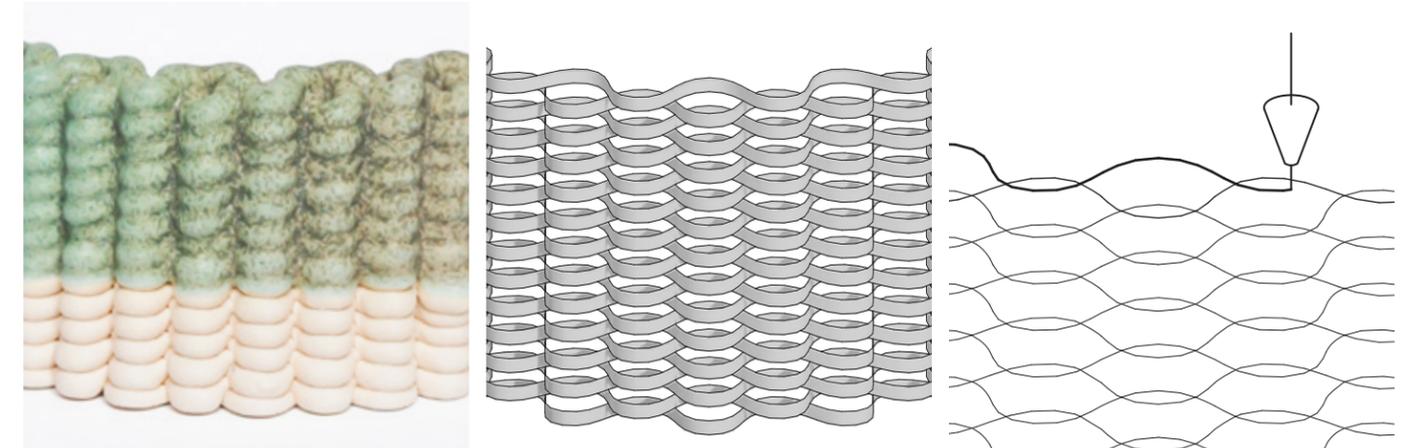


**Figure 4.2.6** Non-porous weave pattern, ASM1 glaze on PSH-516.
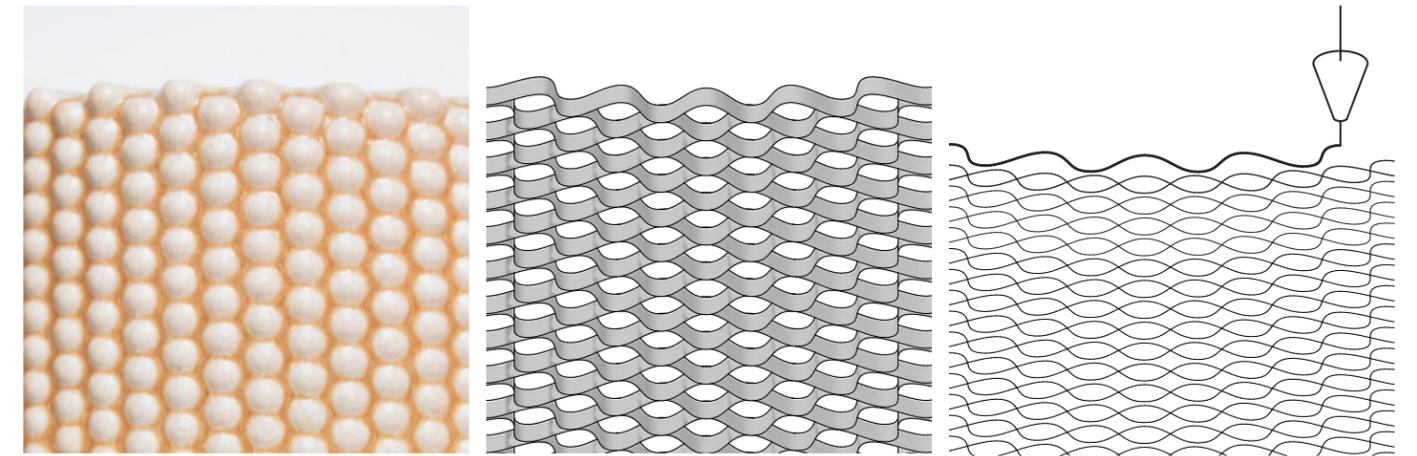


**Figure 4.2.7** Non-porous exterior weave texture, Bone glaze on PSH-516.
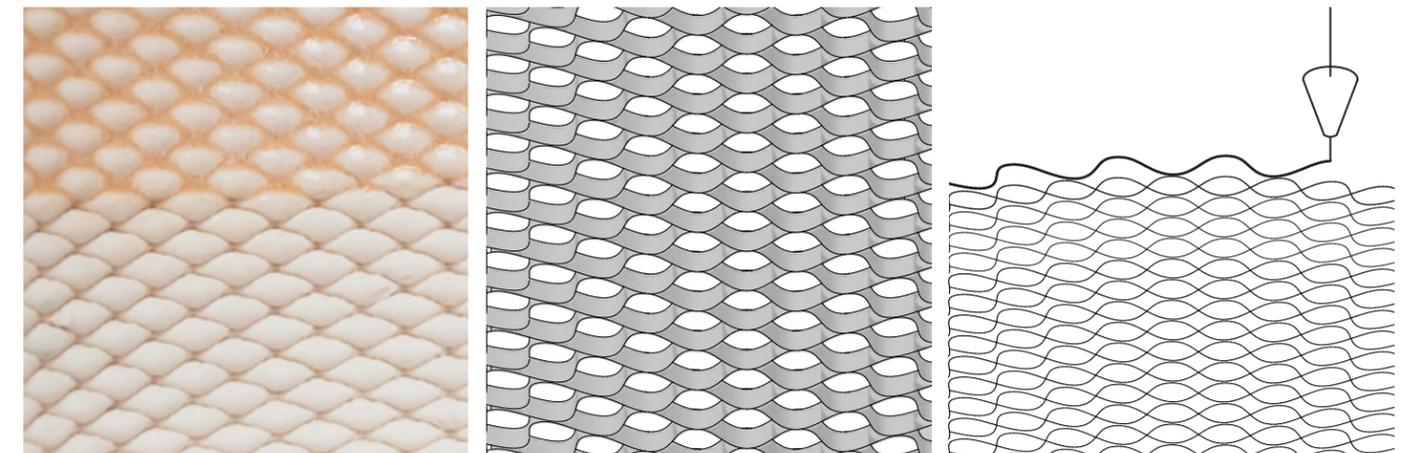


**Figure 4.2.8** Non-porous interior weave texture, Bone glaze on PSH-516.

Using the same wave geometry at the level of the single print coil can have different effects based on how sequential print layers are rotated. Figure 4.2.9 uses the same principle of creating wave divisions as Figures 4.2.6 and 4.2.7. It also uses the same print parameters. However, print layers in Figure 4.2.9 are rotated by one-third of the width of a single wave, resulting in a three-layer tessellation across the entire geometry. The change in angle of rotation also alters the directional quality of the pattern, creating a spiral. A similar directional effect occurs in Figure 4.2.10. Waves are not evenly distributed across the entire print layer as in prior experiments- they only occur once per layer. A 1mm step height makes the structure impermeable despite print coils undergoing a high degree of deformation as they pull away from the supporting structure.

## NON-POROUS SPLICED GEOMETRIES CONT.
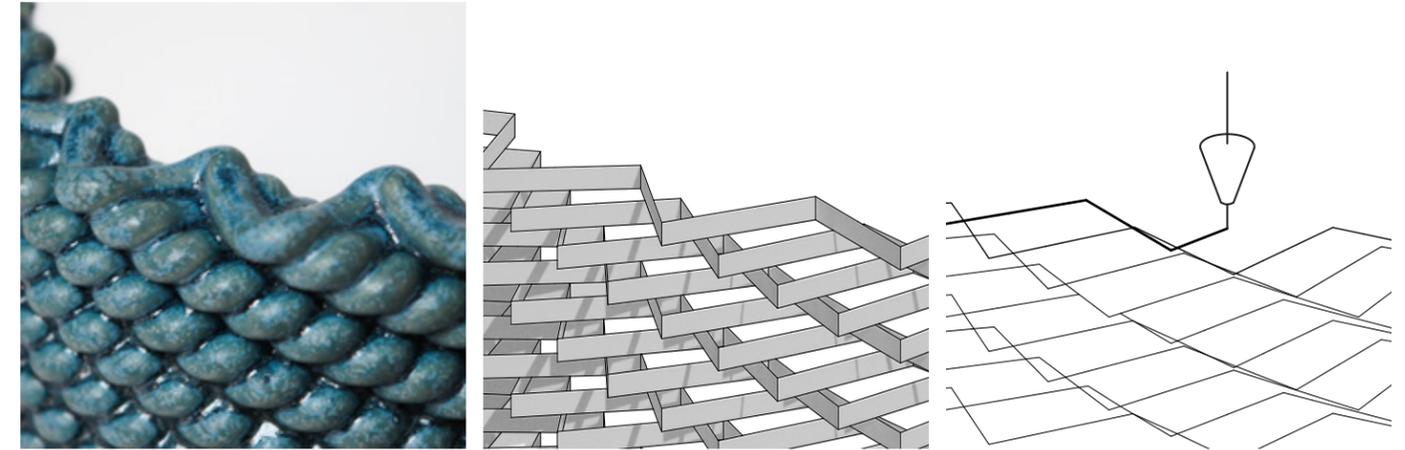


**Figure 4.2.9** Non-porous spiral pattern, Variegated Slate Blue glaze on PSH-516.
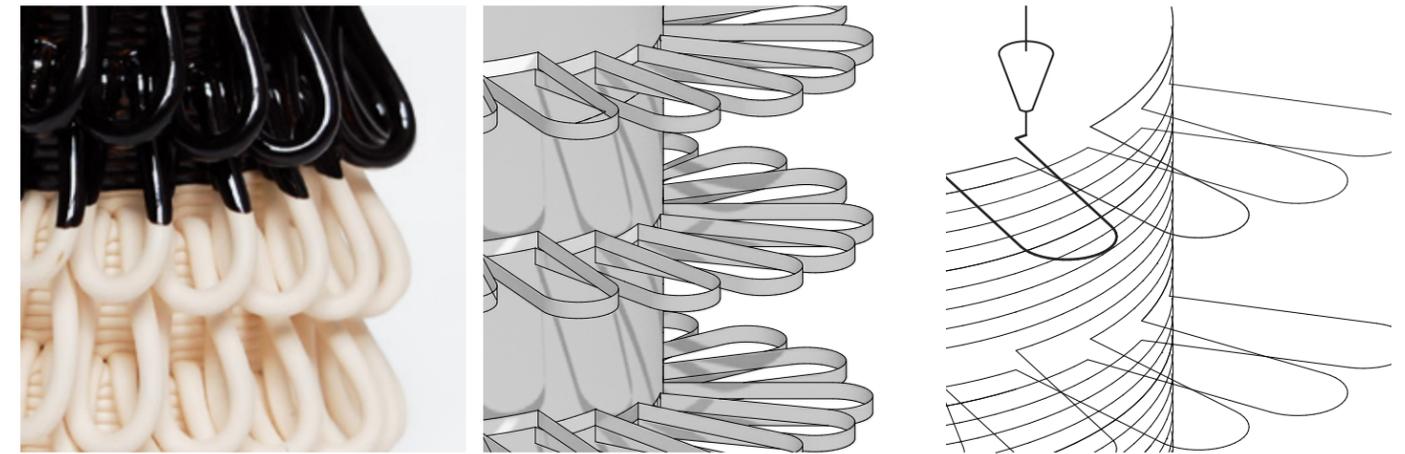


**Figure 4.2.10** Non-porous spiral looping pattern, Licorice glaze on PSH-516.

## Porous Spliced Geometries

The following porous geometries examine how print coils can be used to diffuse and scatter light. At this point, the focus of the research methodology shifted from print coil expression as a function of ornament to print coil deformation to yield specific material performance characteristics. These geometries represent preliminary attempts at 3D printed openwork light screens.

Figure 4.2.11 was intended to determine the minimum required offset between print layers to leave visible gaps in the geometry. These voids were intended to produce a graded light effect-diffusing increasing amounts of light as gaps between layers widen. Figure 4.2.11 was modeled as a series of extrusions, each representing a 1mm step height. The porous area of the print consists of alternating print layers being pulled back several centimeters into the interior of the geometry. Gradation in the size of the apertures is created by increasing the number of layers pulled back. Nozzle diameter, speed, and extrusion rate are critical in determining aperture size because they impact how much material is deposited at a given location across the print.

In Figure 4.2.11, there is a direct relationship between the location of the light source and the viewer, creating an opportunity for glare to occur. Figure 4.2.12 uses the same method of pulling back layers to produce a series of light apertures. However, Figure 4.2.12 takes advantage of material deformation to create sectional overlaps



**Figure 4.2.11** Porous hung coil pattern, ASM1 glaze on PSH-516.

in the geometry. Print layers are staggered along the X-Y axis to create shelf-like structures instead of pulling back material to the same location. Print coils are illuminated based on their proximity to the light source, creating graded illumination as light washes across the surface of the stoneware. Although the shelves do not overlap in the digital model, print coils sag over 10mm across the entire width of the apertures. This allows for an indirect relationship between the light source and the viewer's line of sight. The light shelves in Figure 4.2.12 also direct light downwards, casting light and shadow on the surface below.

Although utilizing a mesh to slicer workflow is a viable means of developing 3D printed ceramics, any minute changes using this methodology entail complete remodeling. Modeling can be done using a parametric workflow. However, the print parameters remain external and need to be re-assessed within the slicer. Layer height, number of wave divisions, wave geometries and shifts between layers or waves in the X-Y axis cannot be altered independently of one another. As an iterative design process, this workflow presents some critical limitations. Since digital geometries differ substantially from their physical counterparts, mesh to slicer workflows do not allow for rapid responses to emergent material behaviour. Parametrizing and isolating these variables allows for more efficient rapid prototyping. It also permits users to establish relationships between digital geometries and G-Code variables not otherwise accessible through slicer software. In order to bypass these limitations, the following four light screen typologies were generated using a mesh to slicer workflow.



**Figure 4.2.12** Porous light shelves, Unglazed PSH-516.

## 4.3 'S' TYPOLOGY

Brightness and light scattering in the Small ('S') typology are primarily regulated by porcelain thickness. Material thickness at a given location determines the amount of light transmission across the clay body. Graded light transmission is achieved using two digital tooling operations:

1. **Extrusion Variability–** Unique to the 'S' and 'XL' typologies.
2. **Waves–** Contours that expand and contract in amplitude to change the sectional distribution of material.

The final 'S' prototypes illustrate the relationship between these two sets of parameters. Both sets of parameters are attached to a set of variable domains that control material deposition and wave amplitude relative to the exact locations on the prototypes:

1. **Variable Extrusion Domain–** 0.2 to 0.6 *consistent throughout series.
2. **Variable Wave Amplitude Domain–** 2.5mm to 8mm *range is within these values but changes across each prototype.

While the variable extrusion domain does not change across the series, wave amplitude is vertically graded. When waves expand, additional material is deposited along the X-Y axis resulting in diminished brightness. This produces greater contrast between areas of variable light transmission. The apertures in the final 'S' prototype



**Figure 4.3.1** Final 'S' prototype series.
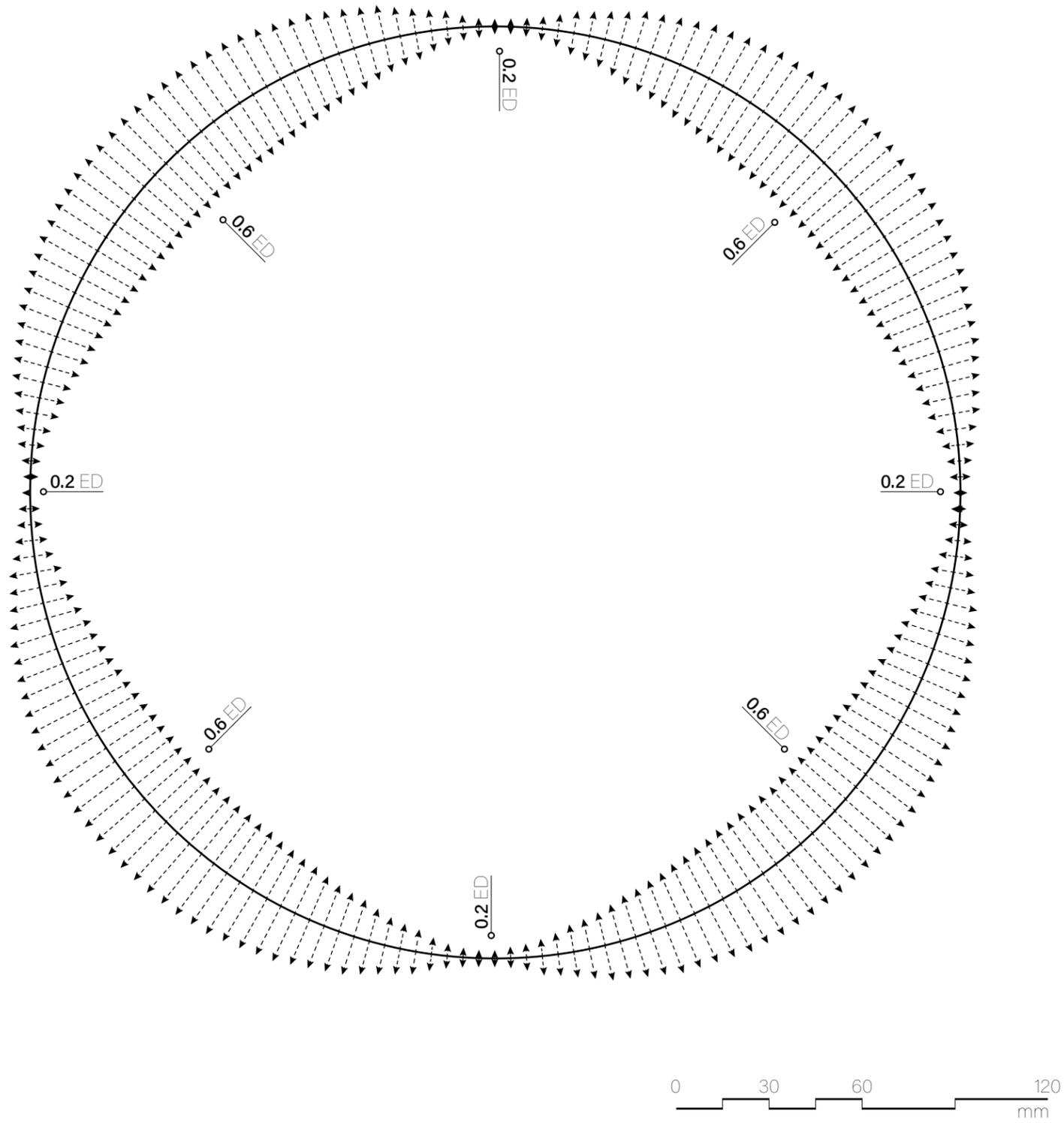
**Figure 4.3.2** 'S' typology extrusion domain (ED) plan.

0   30   60   120
mm
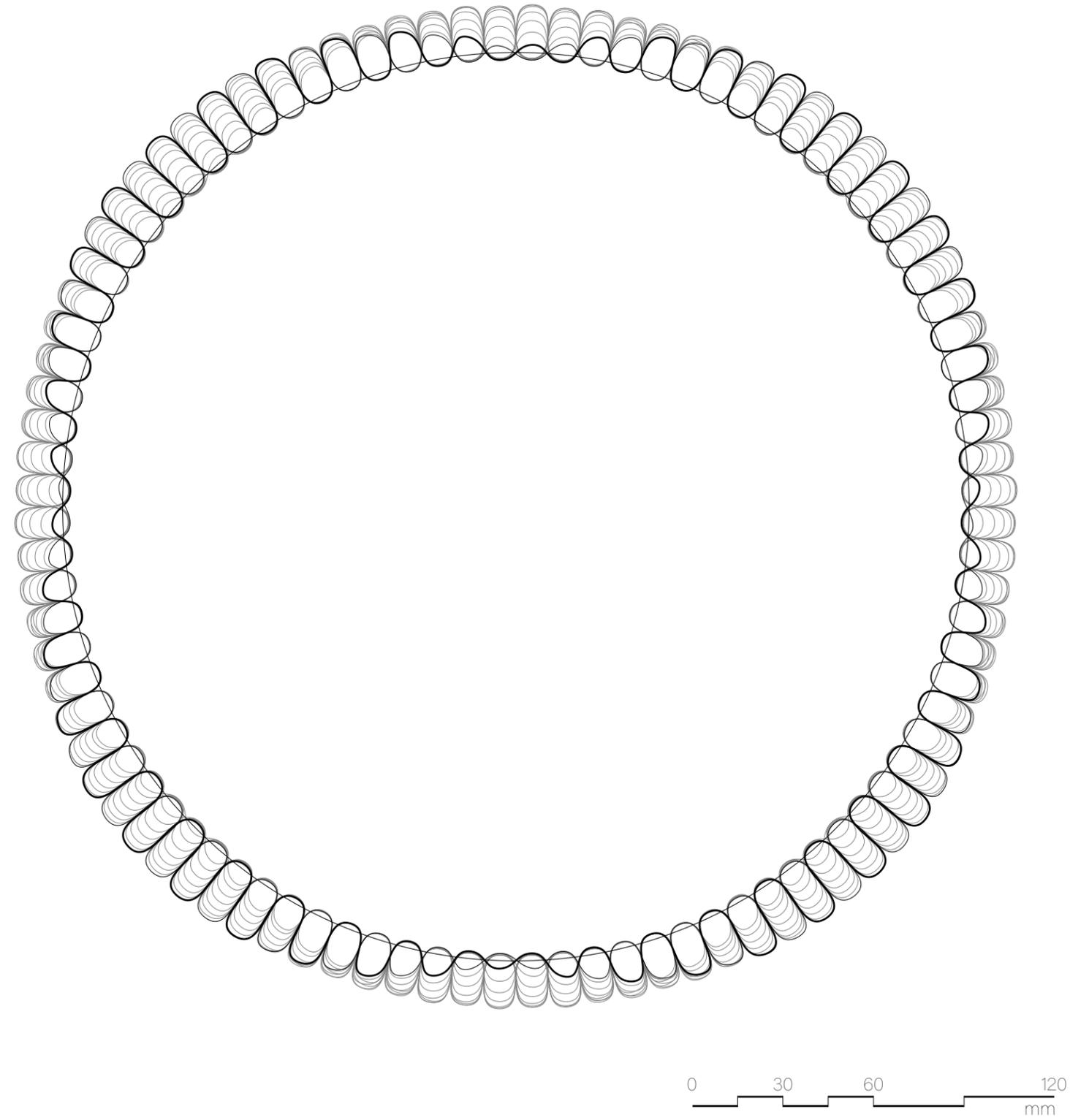


**Figure 4.3.3** 'S' typology tool path plan.

0   30   60   120
mm
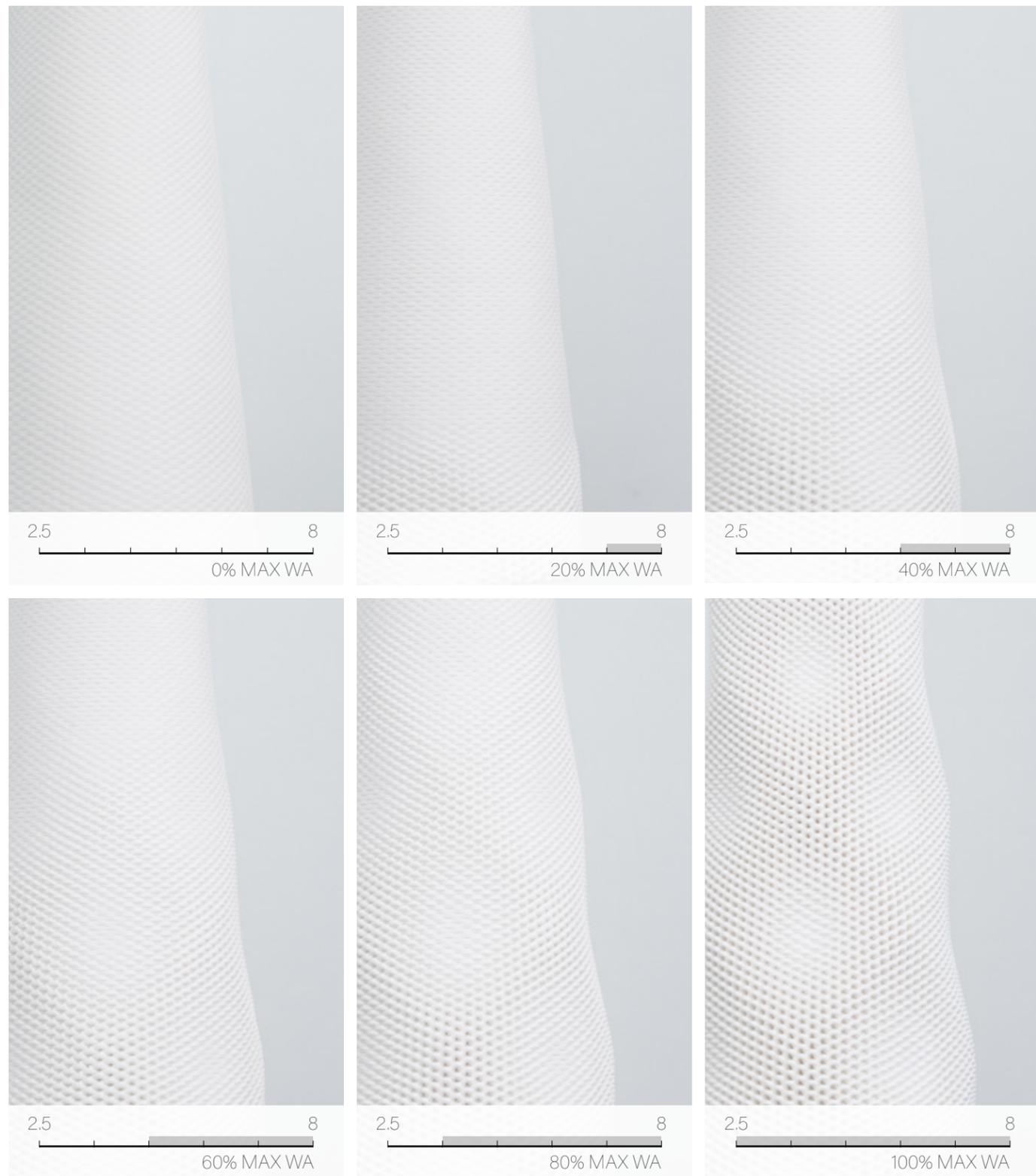
**Figure 4.3.4** Wave amplitude (WA) variation diagram.
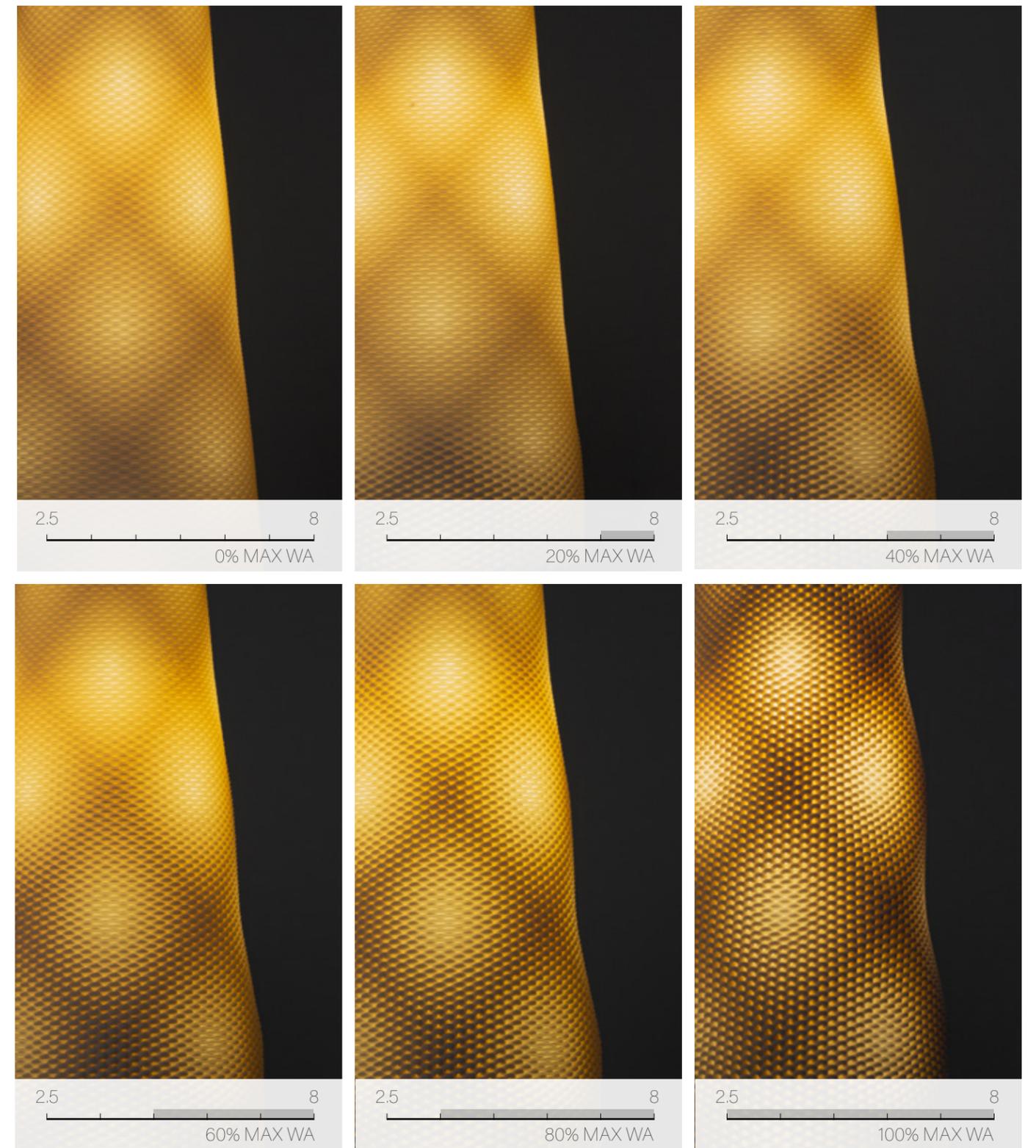


**Figure 4.3.5** Illuminated wave amplitude (WA) variation diagram.

consist of four vertically tessellated layers. The first and third layers remain the same throughout the print. Wave amplitude across these layers operates using a fixed domain. The material is evenly deposited, and light transmission remains constant. The second and fourth layers have identical geometries, staggered to facilitate displacement in the Z-axis. These layers have variable domains that control their wave amplitudes and alter brightness and light scattering depending on their length. When wave amplitudes are set to a fixed value (Figure 4.3.4), extrusion variability is very difficult to perceive when the light fixture is off.

The final 'S' prototypes function as a series of pendants. The pendants are printed upside-down to accommodate a base plate that fixes the hardware to the rest of the shade. Each pendant is designed to utilize a full 1400cc cartridge of clay on the Lutum 4.

## Plastic Deformation and Structural Collapse

Extrusion variability is the most significant contributor to plastic deformation and structural failure in the 'S' typology. Uneven distribution of material results in severe warping during wet-processing, drying and firing. Variable section thicknesses must be evenly distributed about all axis to prevent warping and collapse. Thin segments in wall sections result in buckling. Figures 4.3.25-4.3.30 in the 'S' index illustrate the relationship between buckling and material distribution: the more a pattern repeats across all axes,
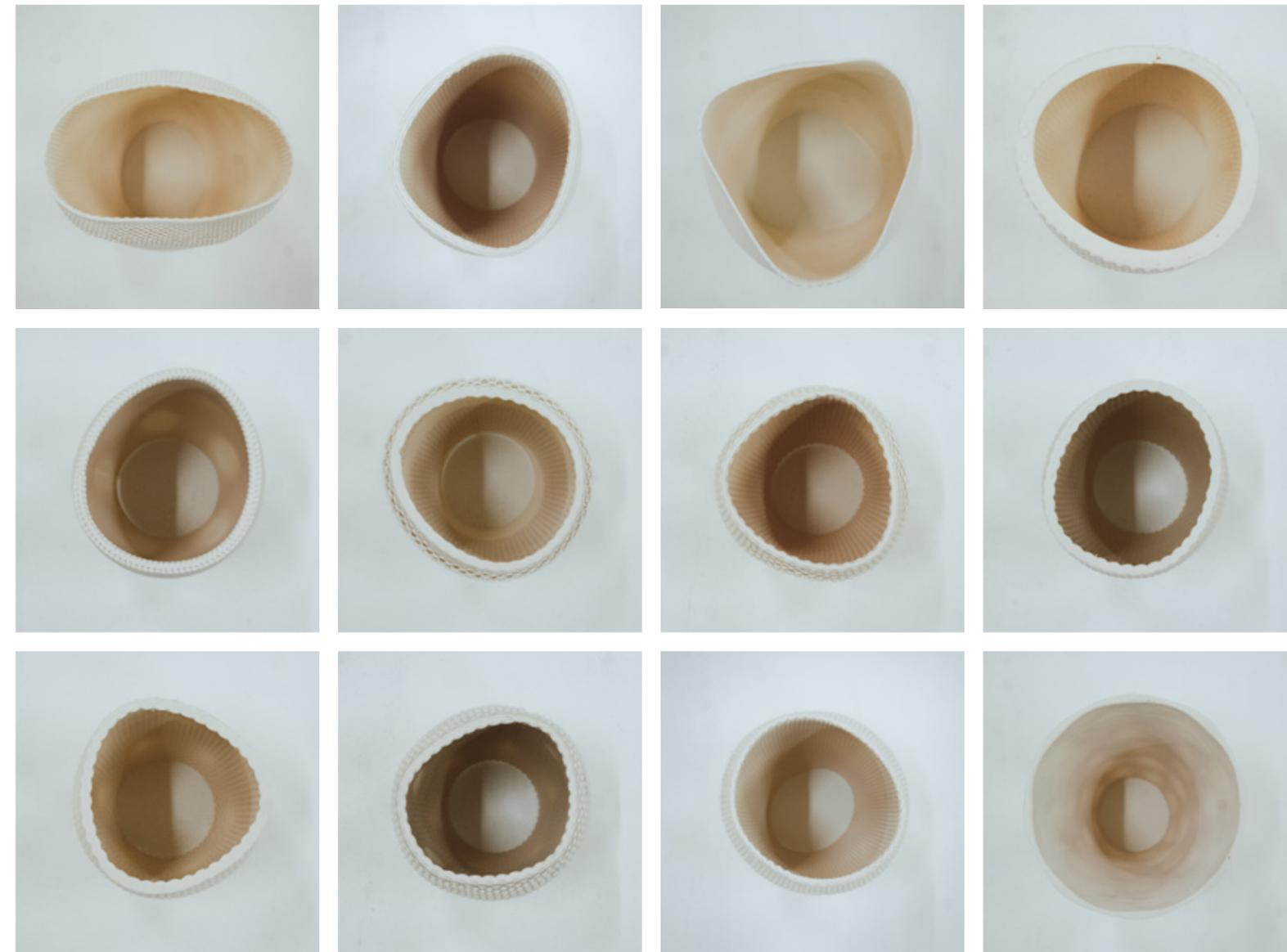


**Figure 4.3.6** Documented buckling during the firing process.

the less the porcelain warps. The final prototypes in the 'S' typology consist of a series of rhombi that transmit increasing gradients of light at their center. Four rhombi are tessellated along the diameter of each pendant and vertically distributed across the entire porcelain surface. The repetitive distribution of the pattern serves to minimize deformation.

Due to the thinness of the print coils required to transmit light, the 'S' typology cannot support dramatic overhangs or highly contoured surfaces. Staggering layers of material causes prints to collapse since there is limited surface area for layers to adhere to one another.

## Extrusion Domains

While iterations of 'M,' 'L,' and 'XL' focused on digitally crafting and maximizing aperture size, 'S' development was primarily driven by the attunement of porcelain's working properties. Due to high failure rates, over fifty percent of the research was spent on achieving the precise consistency required to print LF and PI. Without a pug mill to mechanically de-air and smooth the clay, this manual process is highly labour and time-intensive.

The 'S' typology had to mitigate the shadow, glare and interreflection created when sectionally layering a material with diffuse light transmission (see Part 2.6: Fired Ceramic Traits). Rather than increasing brightness as per the stoneware screens in the 'M,' 'L' and 'XL' stoneware typologies, staggering and overlapping material in the porcelain 'S' typology often has the effect of diminishing brightness. As a result, subtle tool path tessellations were determined to be the most suitable patterns to work in conjunction with extrusion variability. Print coils in the 'S' typology are formally expressed as 'loops' (see Part 4.4: 'M' Typology – Tool Path Variations).

Therefore, digital design development focused on establishing a set of variable domains related to extrusion and wave amplitude that minimize structural failure and printer failure.
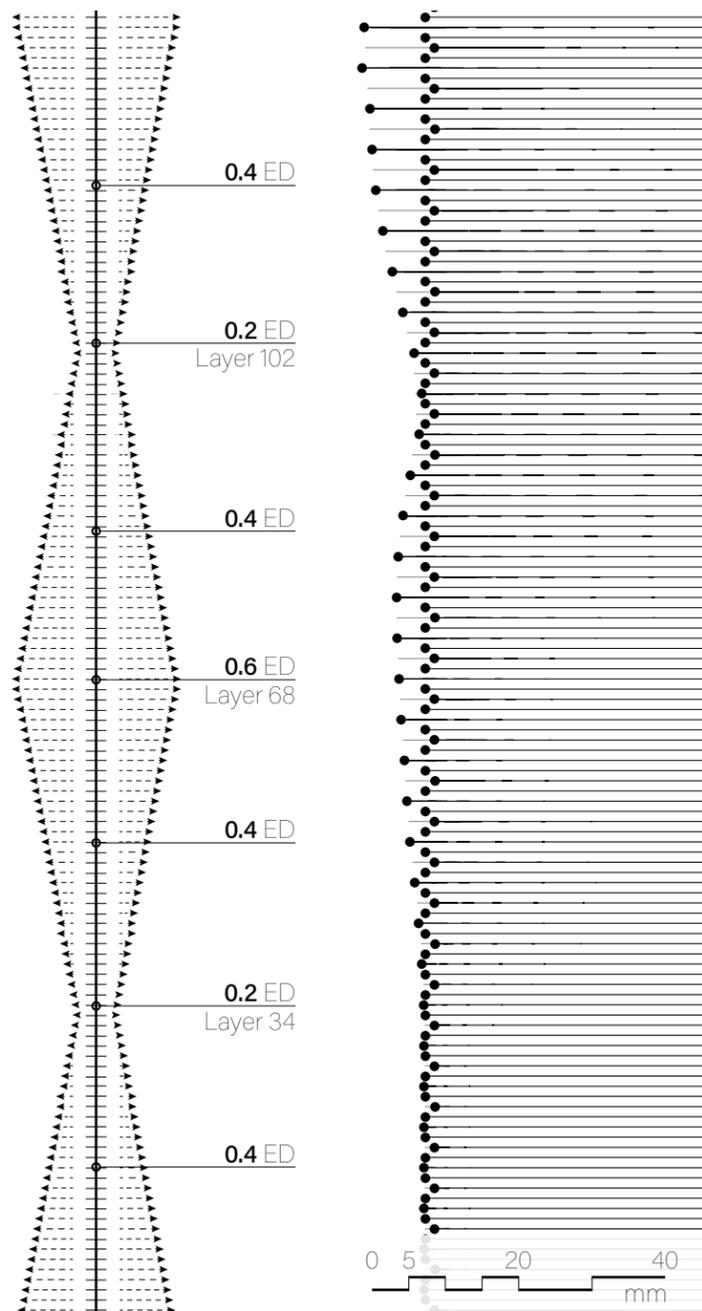
**Figure 4.3.7** Tool path section and extrusion domain (ED) map.

0.4 ED

0.2 ED
Layer 102

0.4 ED

0.6 ED
Layer 68

0.4 ED

0.2 ED
Layer 34

0.4 ED

0    5        20              40
                              mm
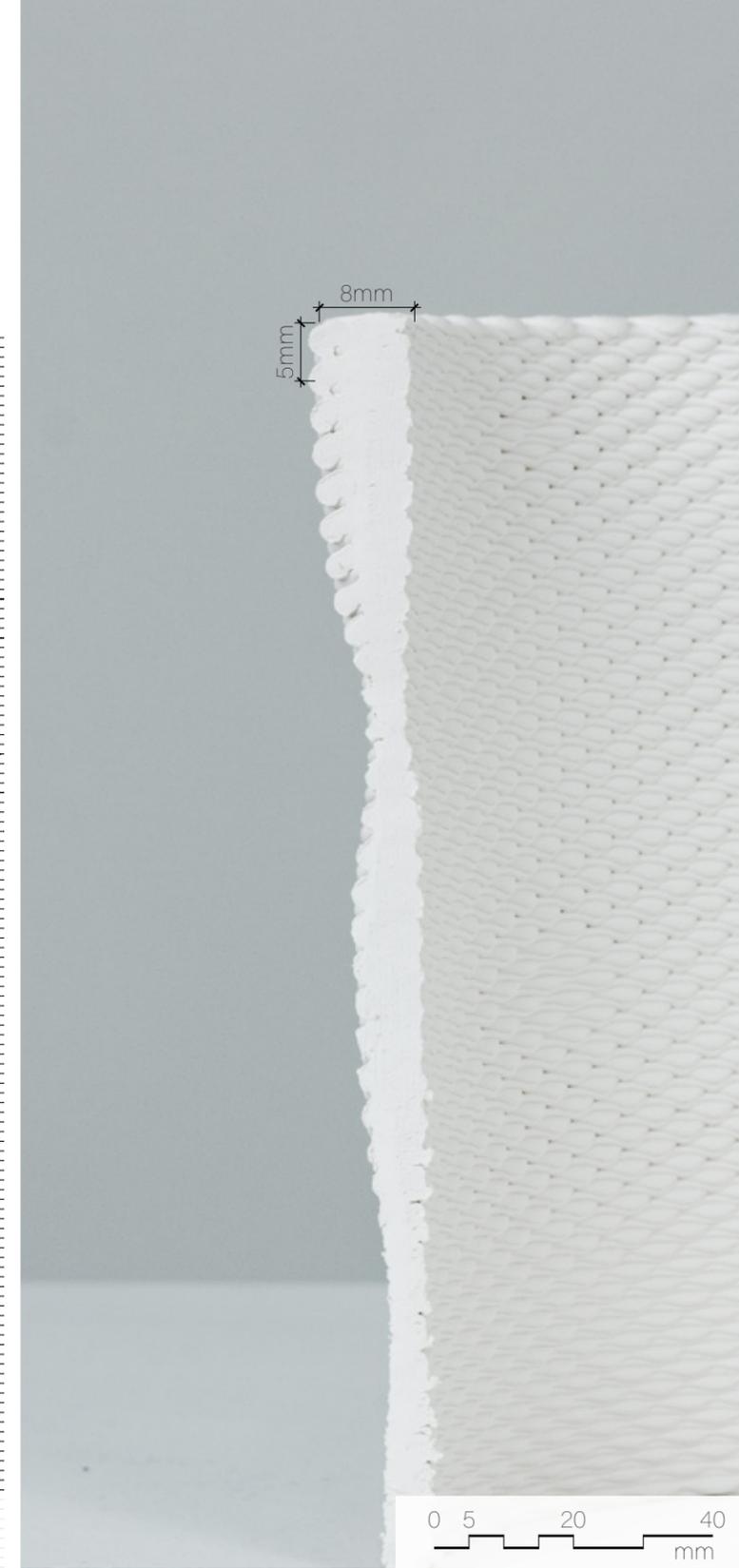
**Figure 4.3.8** Physical print section.

8mm

5mm

0    5        20              40
                              mm
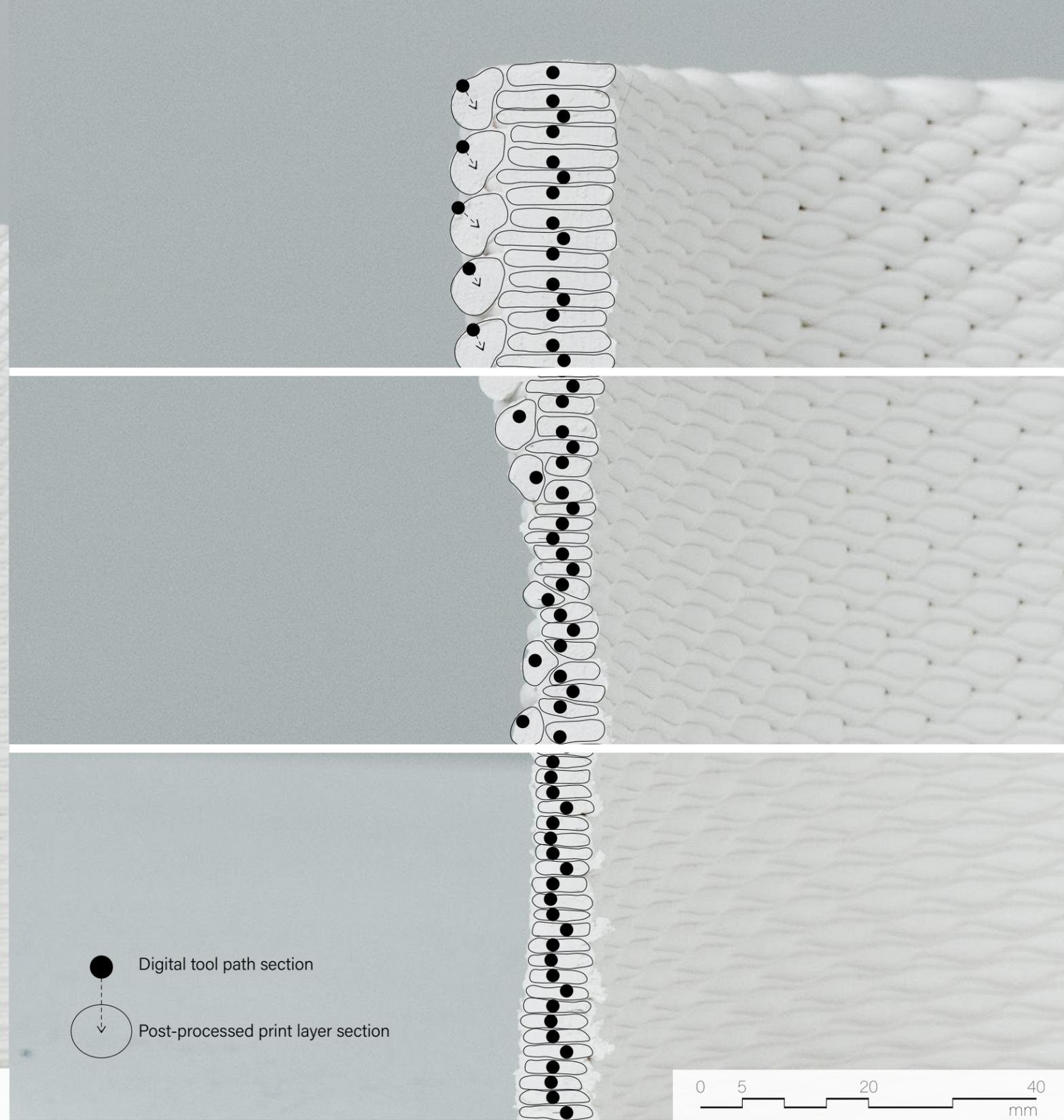
**Figure 4.3.9** Deformation of tool path mapped onto physical print.

● Digital tool path section

○ Post-processed print layer section

0    5        20              40
                              mm

01

0 5    20     40
mm



02

0 5    20     40
mm



03

0 5    20     40
mm
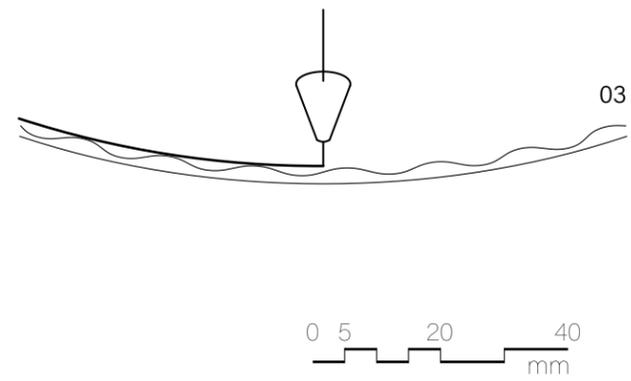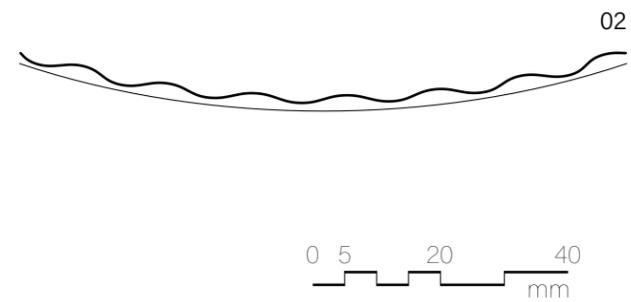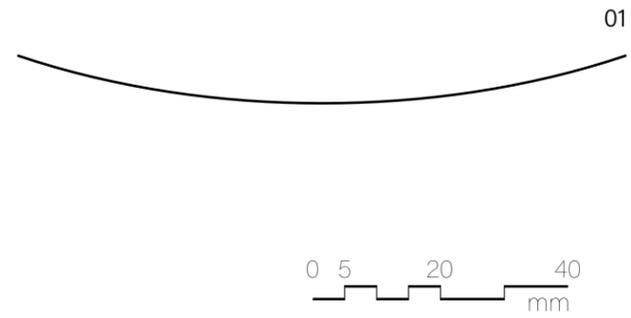
**Figure 4.3.10** Variable extrusion print layers 01, 02, 03.



04

0 5    20     40
mm



05

0 5    20     40
mm



06

0 5    20     40
mm
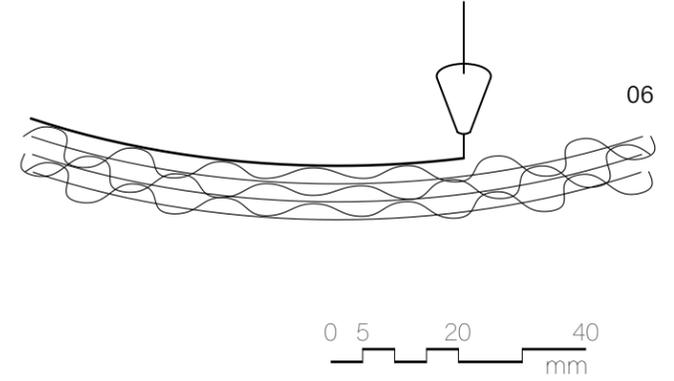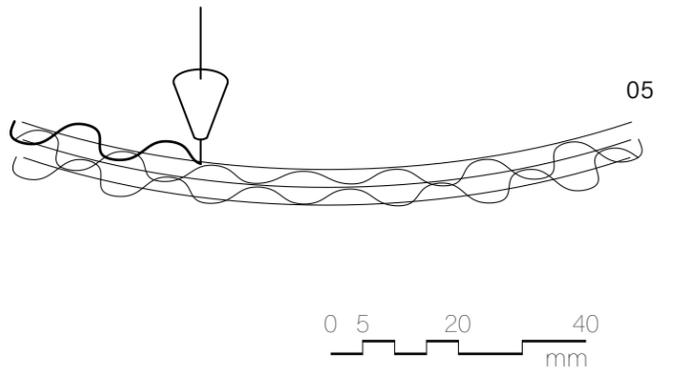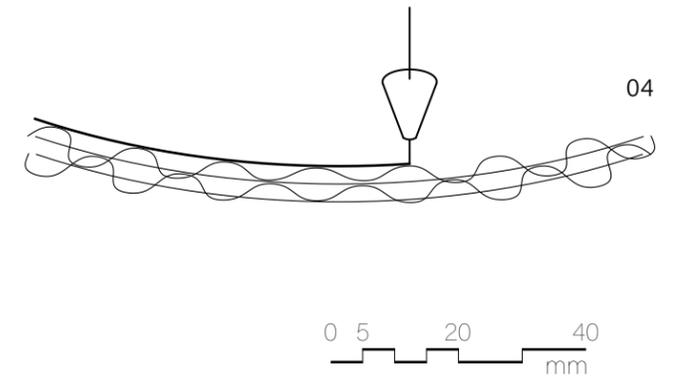
**Figure 4.3.11** Variable extrusion print layers 04, 05, 06.

07

0  5      20        40
mm

08

0  5      20        40
mm

09

0  5      20        40
mm
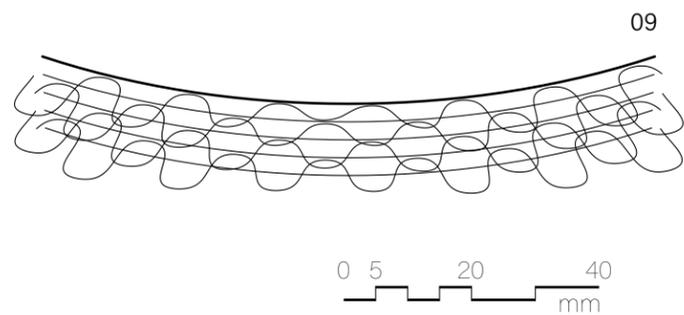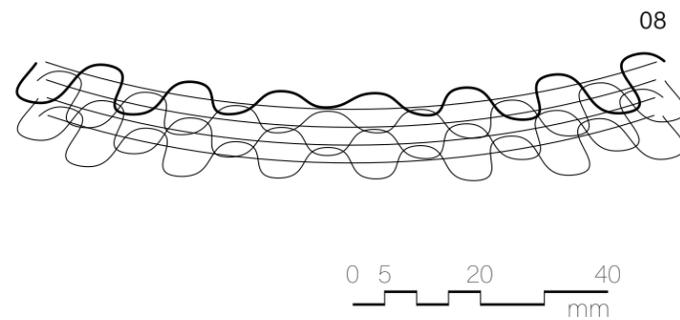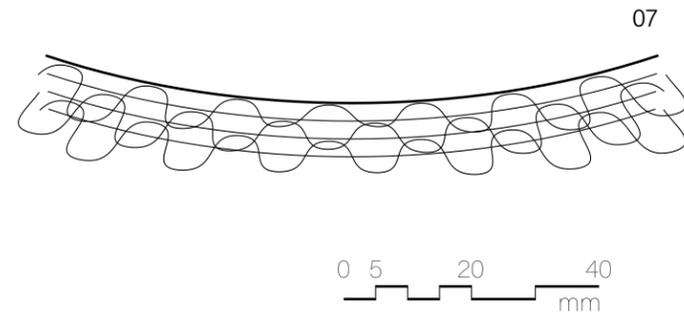
**Figure 4.3.12** Variable extrusion print layers 07, 08, 09.
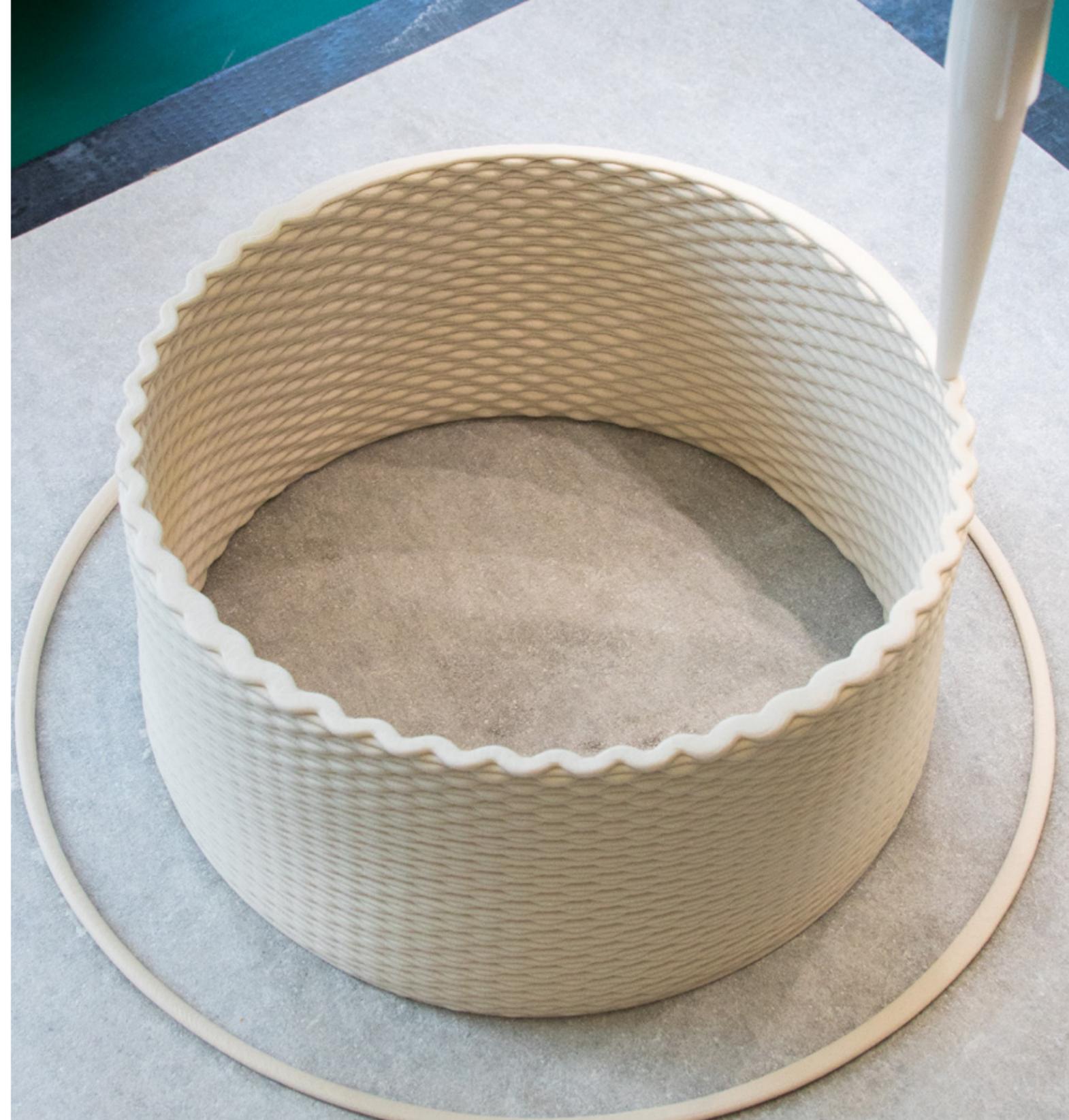


**Figure 4.3.13** 'S' prototype print in progress.

**Figure 4.3.14** 'S' prototype series, front view.

**Figure 4.3.15** Illuminated 'S' prototype series, front view.

Figure 4.3.16 Illuminated 'S' prototype series.

## 'S' Index

This index consists of 2 sets of prototypes ordered chronologically. The first set consist of extrusion variability experiments applied to 100mm x 100mm x 200mm tubes. The second set focuses on extrusion and wave distribution in relationship to warping during the firing process.



**Figure 4.3.17** Clear liner glaze on Laguna Frost, fired to cone 6, 90mm x 90mm x 180mm, extrusion variability.



**Figure 4.3.18** Clear liner glaze on Laguna Frost, fired to cone 6, 90mm x 90mm x 180mm, extrusion variability.

**Figure 4.3.19** Clear liner glaze on Laguna Frost, fired to cone 6, 90mm x 90mm x 180mm, 2 layer sequence (x2), extrusion variability.



**Figure 4.3.21** Clear liner glaze on Laguna Frost, fired to cone 6, 90mm x 90mm x 180mm, extrusion variability.



**Figure 4.3.20** Clear liner glaze on Polar Ice, fired to cone 6, 90mm x 90mm x 80mm, 2 layer sequence (x2), extrusion variability.



**Figure 4.3.22** Clear liner glaze on Laguna Frost, fired to cone 6, 90mm x 90mm x 180mm, extrusion variability.

**Figure 4.3.23** Unglazed Laguna Frost, fired to cone 6, 90mm x 90mm x 180mm, 2 layer sequence (x2), extrusion variability.



**Figure 4.3.25** Unglazed Laguna Frost, fired to cone 6, 90mm x 90mm x 90mm, 2 layer sequence (x2), extrusion variability.



**Figure 4.3.24** Clear liner glaze on Polar Ice, fired to cone 6, 90mm x 90mm x 80mm, extrusion variability.
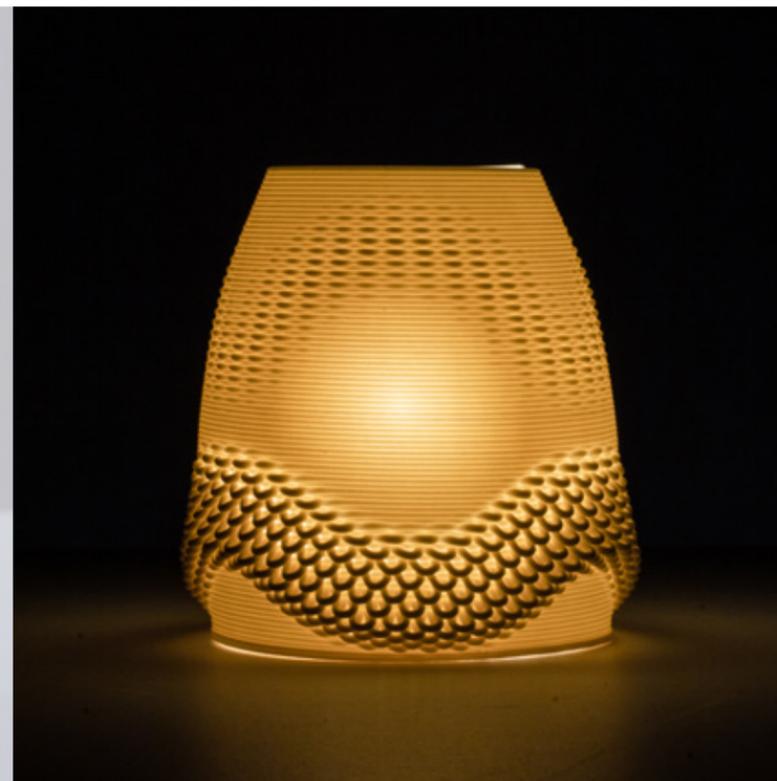


**Figure 4.3.26** Unglazed Laguna Frost, fired to cone 6, 90mm x 90mm x 90mm, 2 layer sequence (x2), extrusion variability.

**Figure 4.3.27** Unglazed Laguna Frost, fired to cone 6, 90mm x 90mm x 90mm, 2 layer sequence (x2), extrusion variability.



**Figure 4.3.29** Unglazed Laguna Frost, fired to cone 6, 90mm x 90mm x 90mm, 2 layer sequence (x2), extrusion variability.



**Figure 4.3.28** Unglazed Laguna Frost, fired to cone 6, 90mm x 90mm x 90mm, 2 layer sequence (x2), extrusion variability.



**Figure 4.3.30** Unglazed Laguna Frost, fired to cone 6, 90mm x 90mm x 90mm, 2 layer sequence (x2), extrusion variability.

**Figure 4.3.31** Clear liner glaze on Polar Ice, fired to cone 6, 160mm x 160mm x 300mm, 2 layer sequence (x2), extrusion variability.



**Figure 4.3.33** Unglazed Laguna Frost, fired to cone 6, 160mm x 160mm x 300mm, 2 layer sequence (x2), extrusion variability.



**Figure 4.3.32** Unglazed Laguna Frost, fired to cone 6, 160mm x 160mm x 300mm, 2 layer sequence (x2), extrusion variability.

## 4.4 'M' TYPOLOGY

Brightness and light scattering in the Medium ('M') typology are controlled by aperture size. The apertures in the final 'M' prototype are vertically graded. This vertical shift creates three distinct lighting conditions that form horizontal bands across the body of the screen. The apertures in the final 'M' prototype consist of three vertically tessellated layers. Each layer is composed of a series of waves. Waves expand and contract in amplitude to change the sectional distribution of material across the three horizontal bands. In the first and third layers of the pattern, waves remain consistent. These waves are symmetrically distributed about the interior and exterior of the print. The second layer controls porosity: waves expand and contract in amplitude using a set of variable amplitude domains. These domains change the geometry of the print coil and regulate light levels.

The final 'M' prototype functions as a table lamp. The center of the shade houses the light source, similar to the chimney of an oil lamp. The top of the form tapers to obscure the light source. This decrease in the diameter of the screen condenses the print coils, causing them to deform at the top of the geometry. A steel support structure, modelled after butane stoves, elevates the shade 150mm from the table's surface below to increase illumination. The final 'M' prototype is designed to utilize a full 3600cc cartridge of clay on the Potterbot XLS-1.



**Figure 4.4.1** Final 'M' prototype with steel hardware.

## Plastic Deformation and Structural Collapse

Maximizing aperture size is the most significant contributor to plastic deformation and structural collapse in the 'M' typology. As porosity increases, so does deformation and risk of collapse. The surfaces to which patterns are digitally mapped form a structural datum line within each piece. Brightness increases when waves expand and pull away from this structural datum line, creating openings in the wall section. Instability is most aggravated when the clay is asymmetrically distributed about the structural datum.

In the final 'M' prototype, this sectional shift occurs along the most highly contoured area of the shade. As a result, this area of the piece requires physical intervention to prevent collapse during printing. A heat gun is used to reduce moisture and stiffen the clay during the process. Without this treatment, the piece consistently buckles. Similar sectional conditions were tested on tubular forms requiring no intervention. A decrease in step height or a reduction in wave amplitude may be utilized to mitigate these issues at the expense of diminishing brightness. With these considerations in mind, applying heat was the most appropriate solution to preventing structural collapse.



**Figure 4.4.2** Structural collapse of 'M' prototype during print.

**Figure 4.4.3** 'M' typology tool path plan.

0    30    60    120
mm
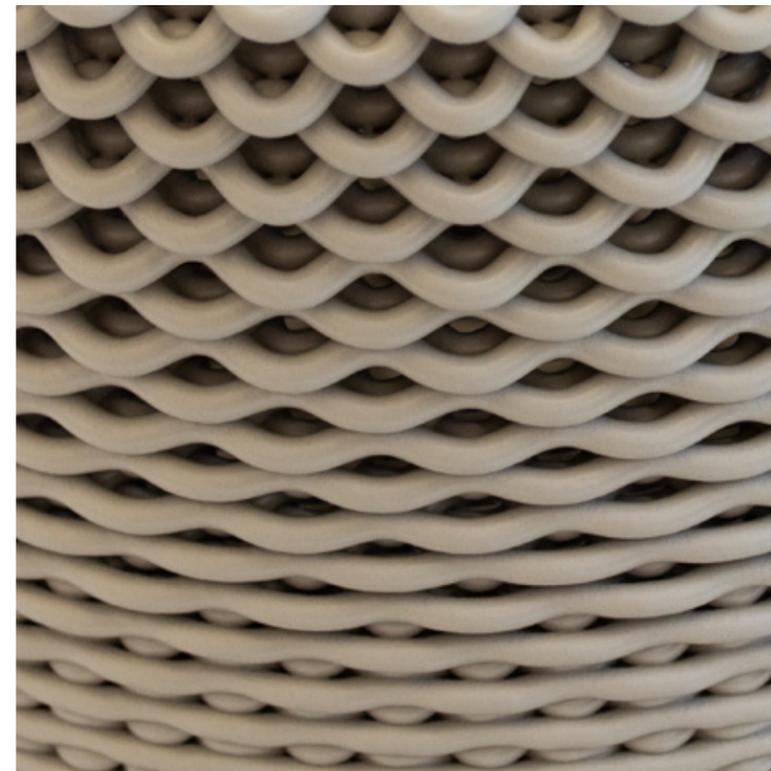


**Figure 4.4.4** Exterior loop profile.
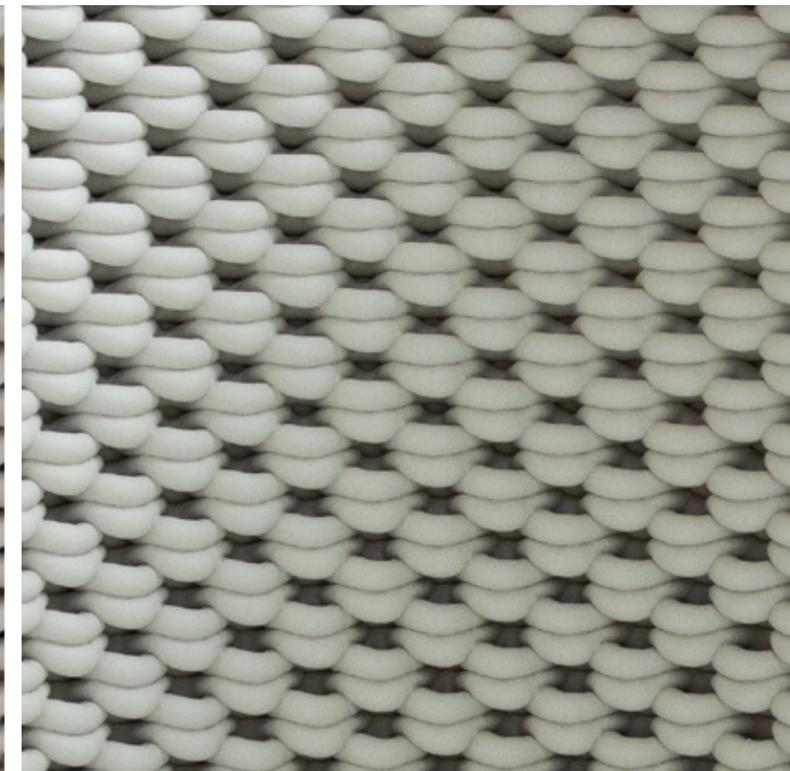


**Figure 4.4.5** Interior loop profile.
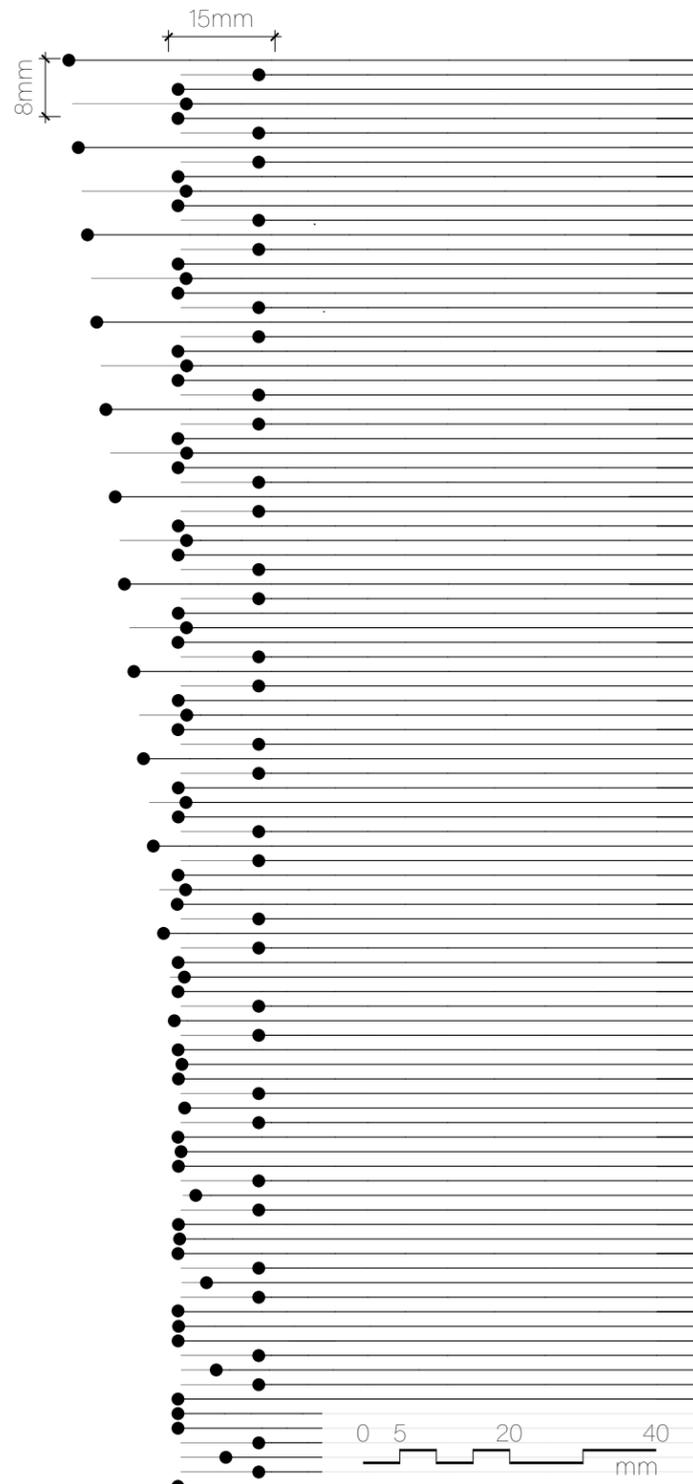
**Figure 4.4.6** Tool path section.



**Figure 4.4.7** Physical print section.
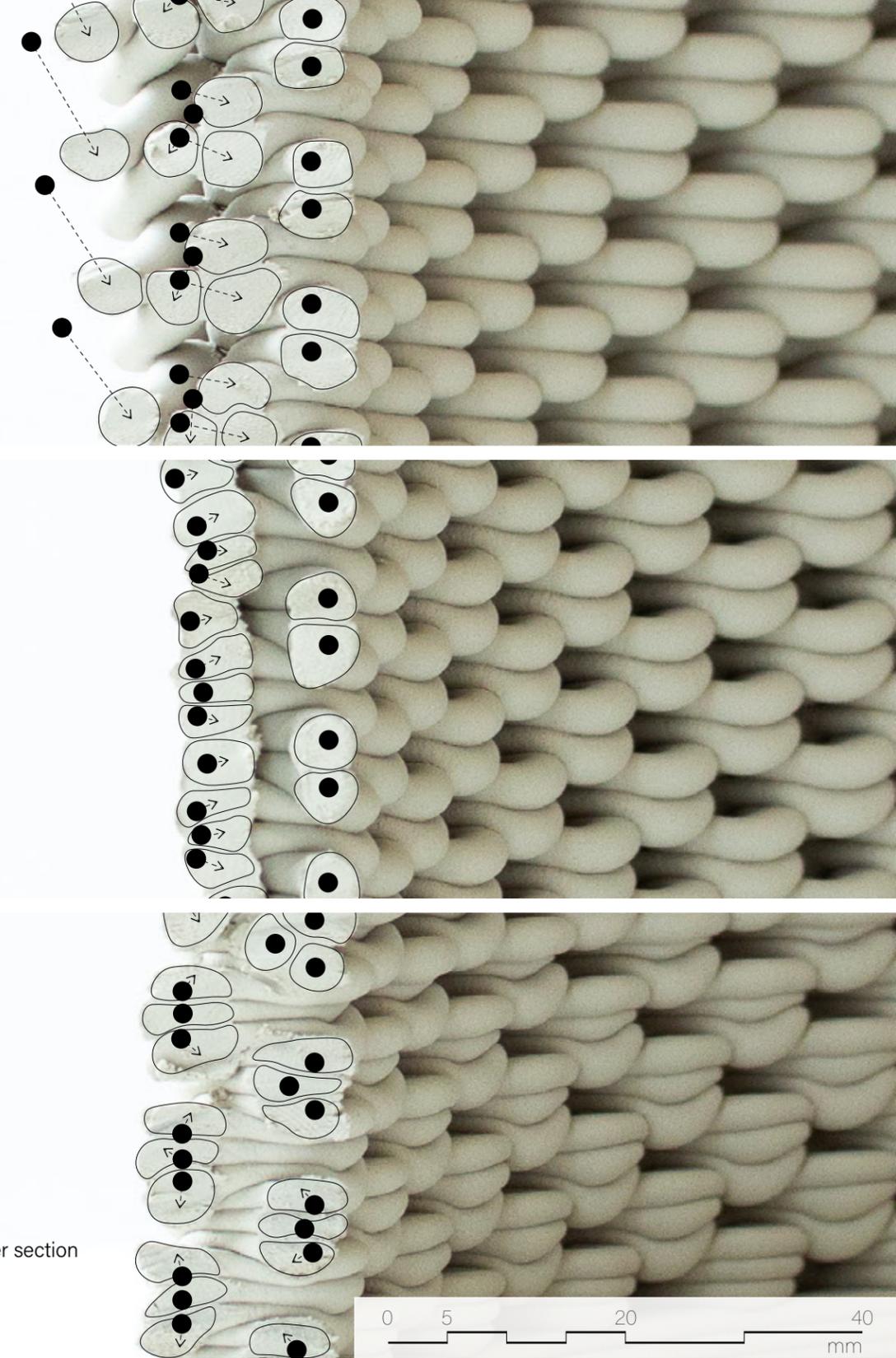


● Digital tool path section

Post-processed print layer section

**Figure 4.4.8** Deformation of tool path mapped onto physical print.

01

0 5 20 40
mm

02

0 5 20 40
mm

03

0 5 20 40
mm
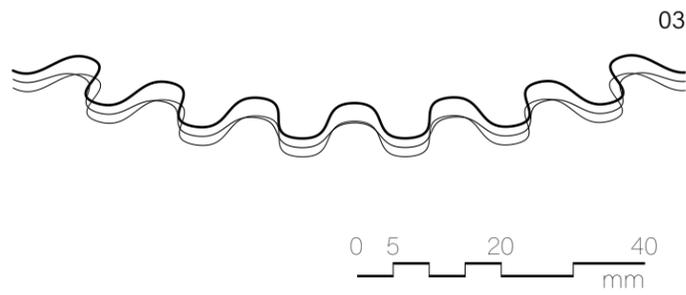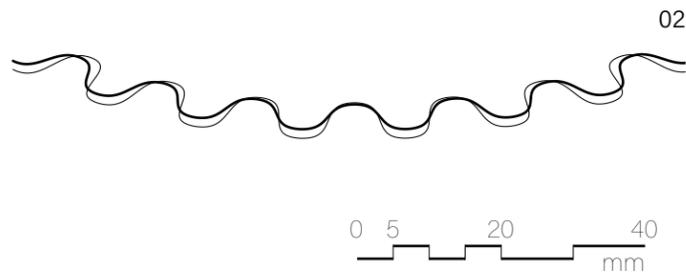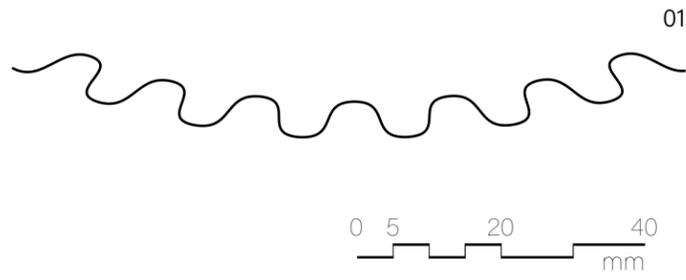
**Figure 4.4.9** Loop print layers 01, 02, 03.

04

0 5 20 40
mm

05

0 5 20 40
mm

06

0 5 20 40
mm
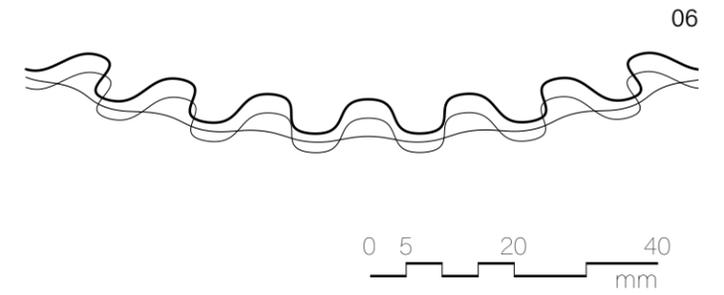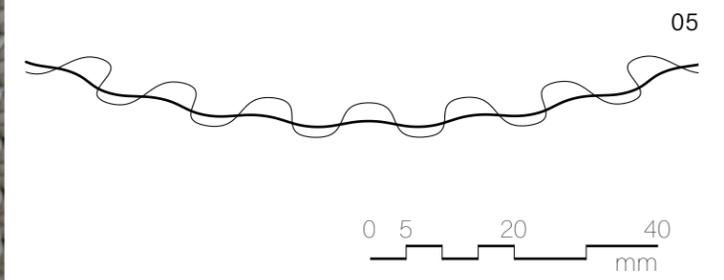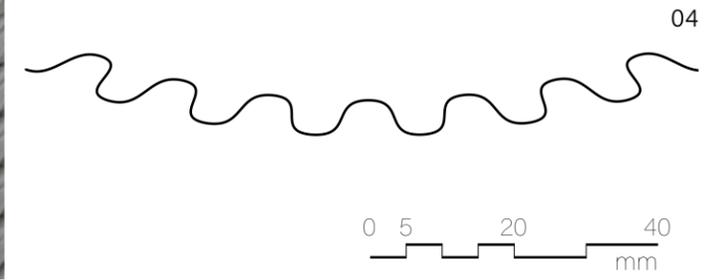
**Figure 4.4.10** Loop print layers 04, 05, 06.

07

0  5      20        40
mm

08

0  5      20        40
mm

09

0  5      20        40
mm
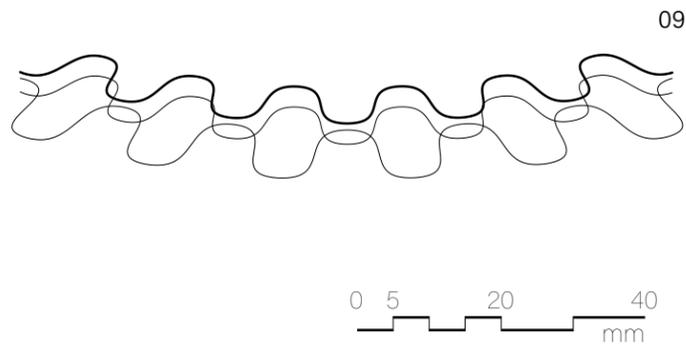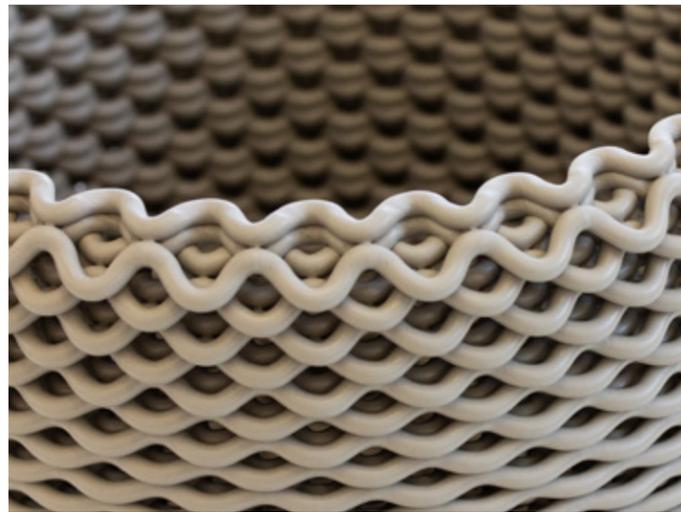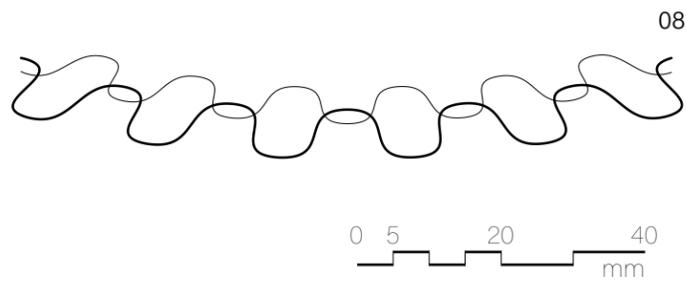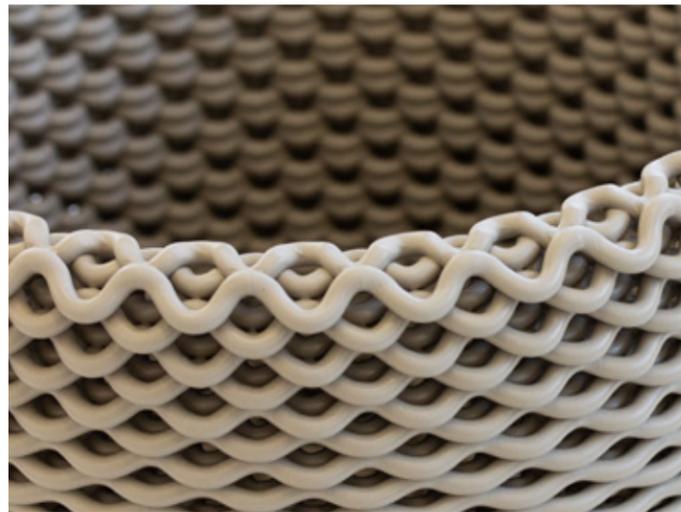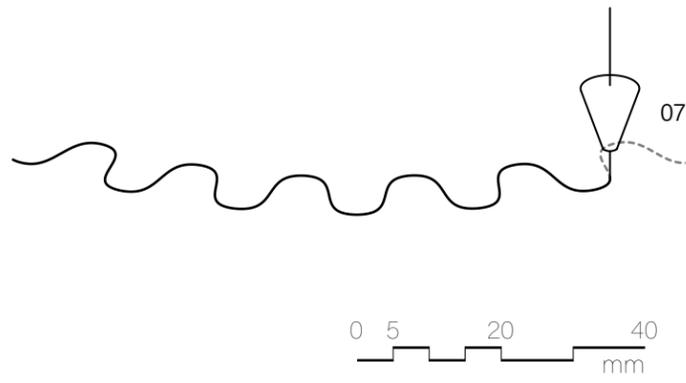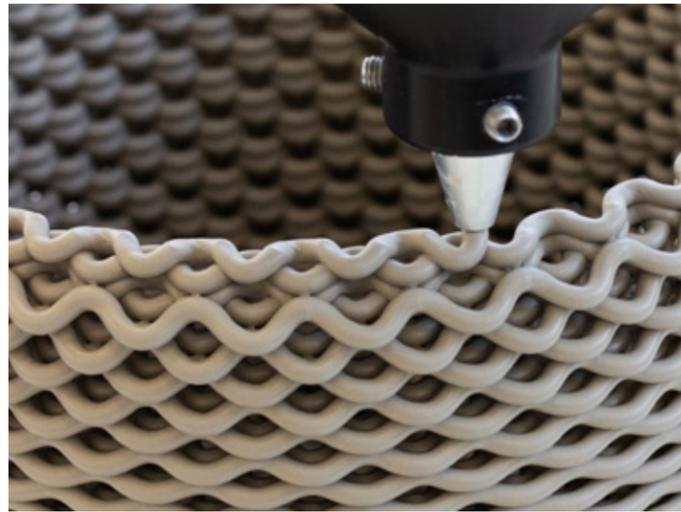
**Figure 4.4.11** Loop print layers 07, 08, 09.

**Figure 4.4.12** 'M' prototype print in progress.

**Figure 4.4.13** 'M' prototype, front view.

**Figure 4.4.14** Illuminated 'M' prototype, front view.

**Figure 4.4.15** Illuminated 'M' prototype.
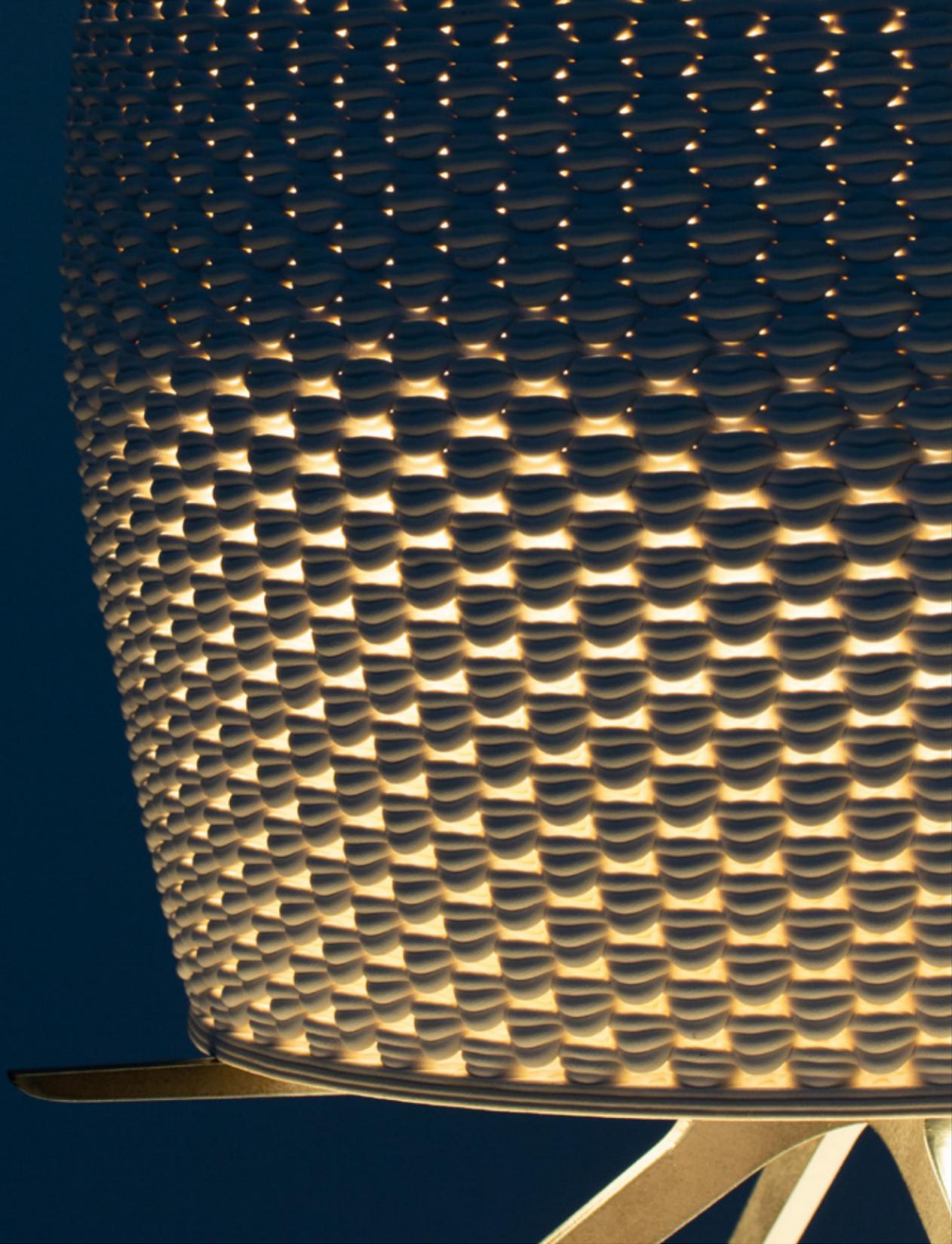
**Figure 4.4.16** Illuminated 'M' prototype, base detail.
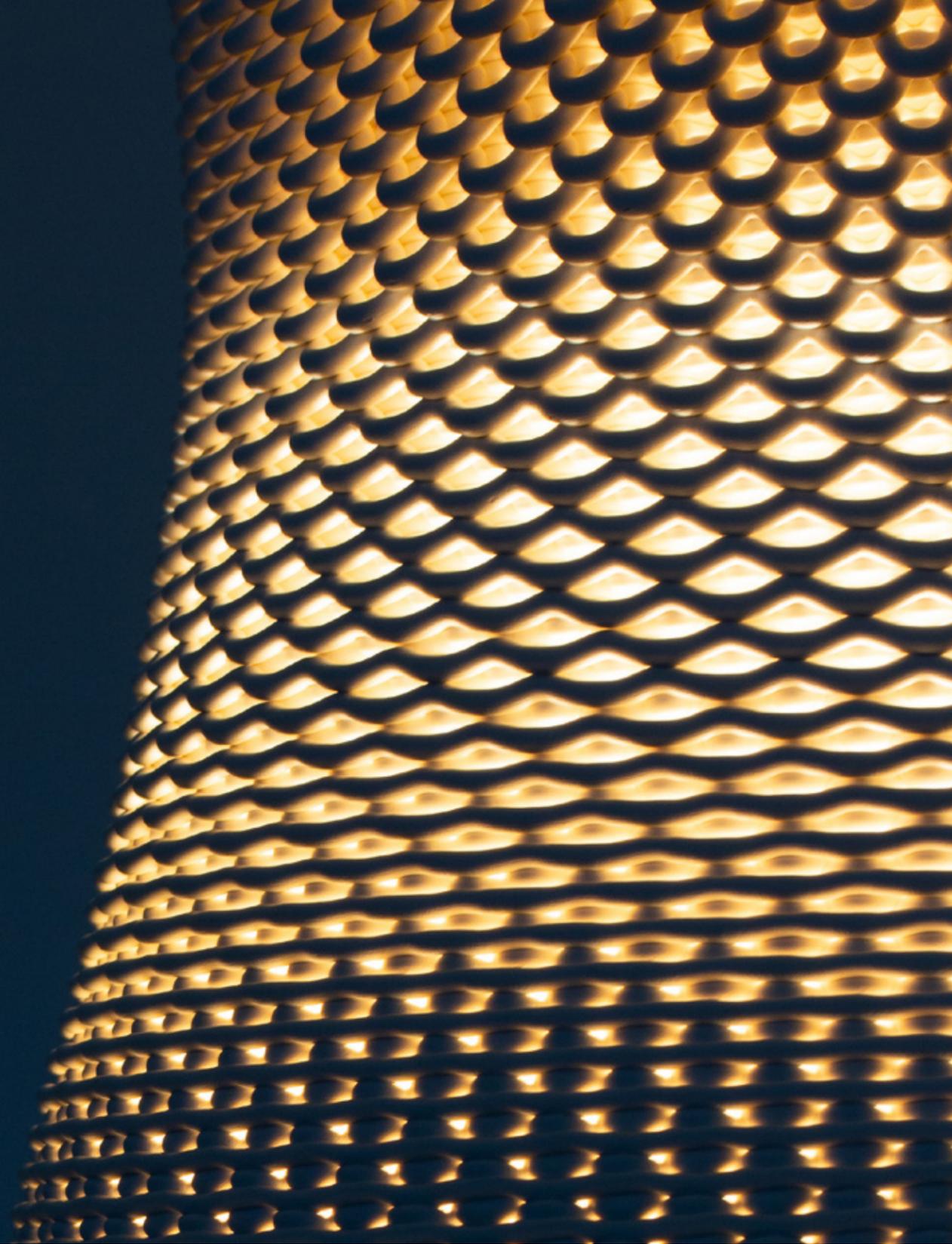


**Figure 4.4.17** Illuminated 'M' prototype, chimney detail.

Tool Path Variations

Four distinct formal languages emerged in relation to the way that print coils are expressed in the 'M' typology: loops, inverted loops, oversized/overhanging loops and spirals.

1.  **Loops–** are expressed as individual print coils, whereas spirals are perceived as groupings of print layers. The print coils in the final 'M' prototype are expressed as loops. These types of loops are grouped into sequences of three layers. The first and third layers provide structural support, while the second layer changes to vary light conditions across the piece.
2.  **Inverted loops–** are also grouped into sequences of three layers (Figure 4.4.23). The first and third layers change to grade light conditions across the piece, while the second layer provides structural support.
3.  **Oversized or overhanging loops–** operate using the same layer structure (Figure 4.4.21). However, these loops are elongated to hang past the bottom of prints to form light screens that take on floral qualities. These experiments were printed on platforms to raise them above the print bed. Due to their thinness, overhanging loops are very fragile before and after firing.
4.  **Spirals–** are grouped into sequences of two layers, horizontally and vertically tessellated across pieces (Figure 4.4.20). Horizontally staggering layers creates 'spiraling' bands of linear light across the surface of the stoneware. The 'M' index illustrates the substantial overlap between these expressions of the print coil.
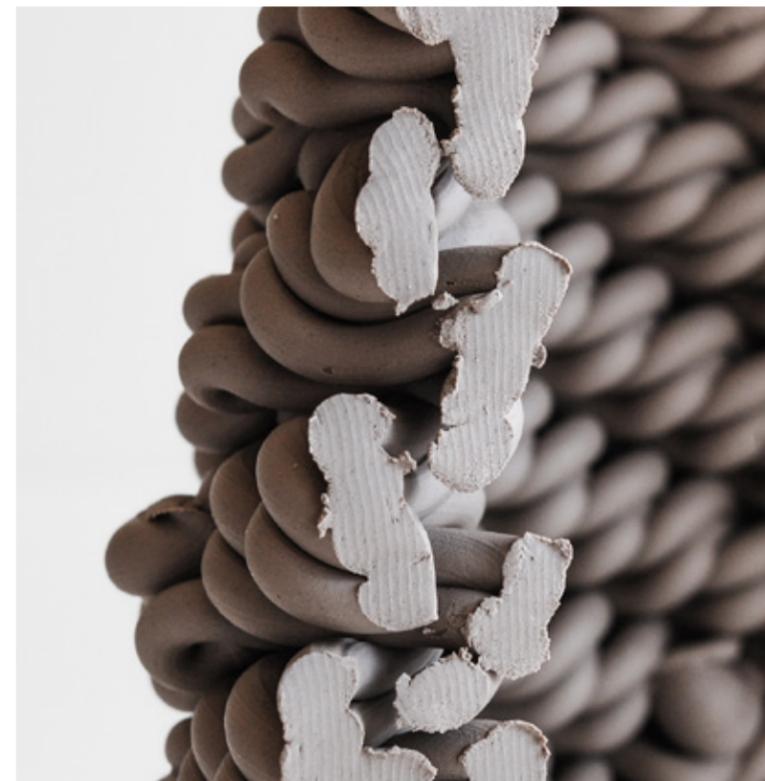


**Figure 4.4.18** Spiral pattern, section detail.
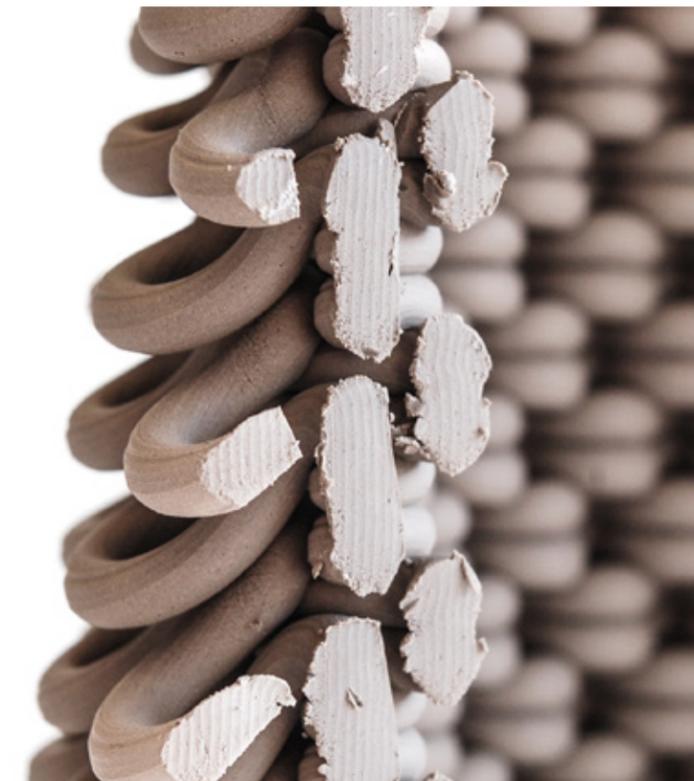


**Figure 4.4.19** Weave pattern, section detail.
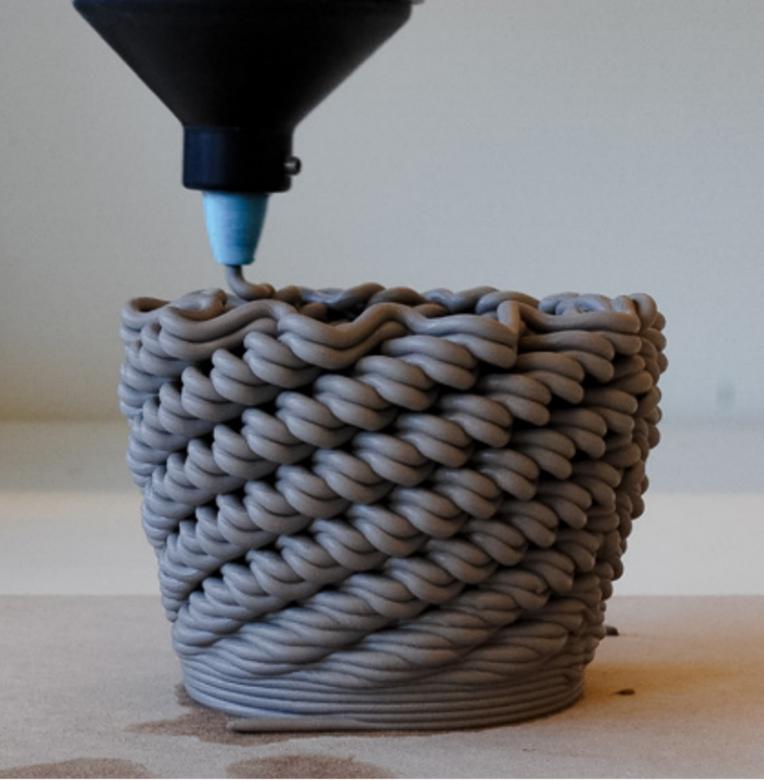
**Figure 4.4.20** Spiral pattern print in progress (left) and illuminated (right).
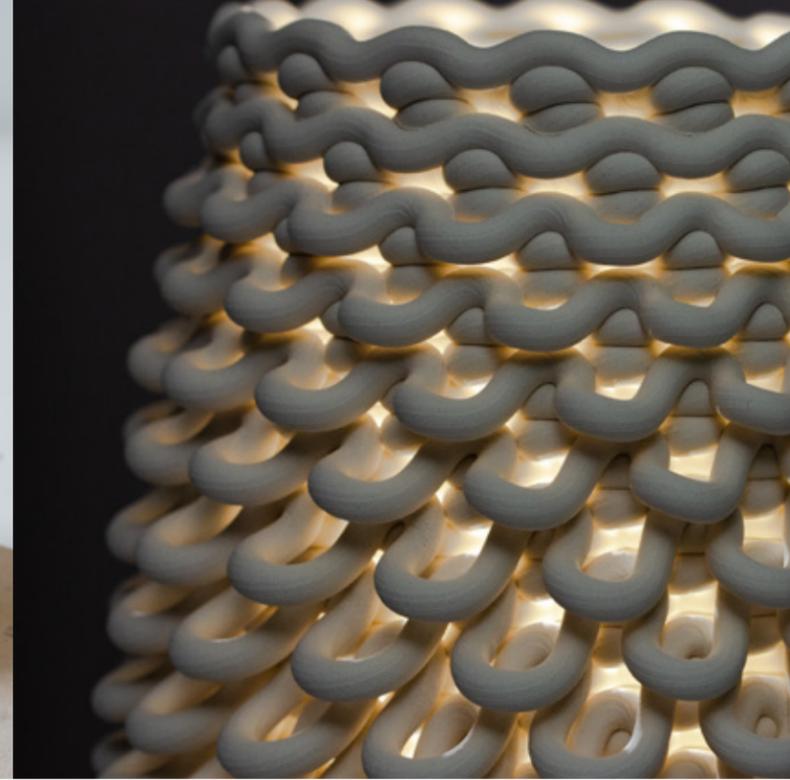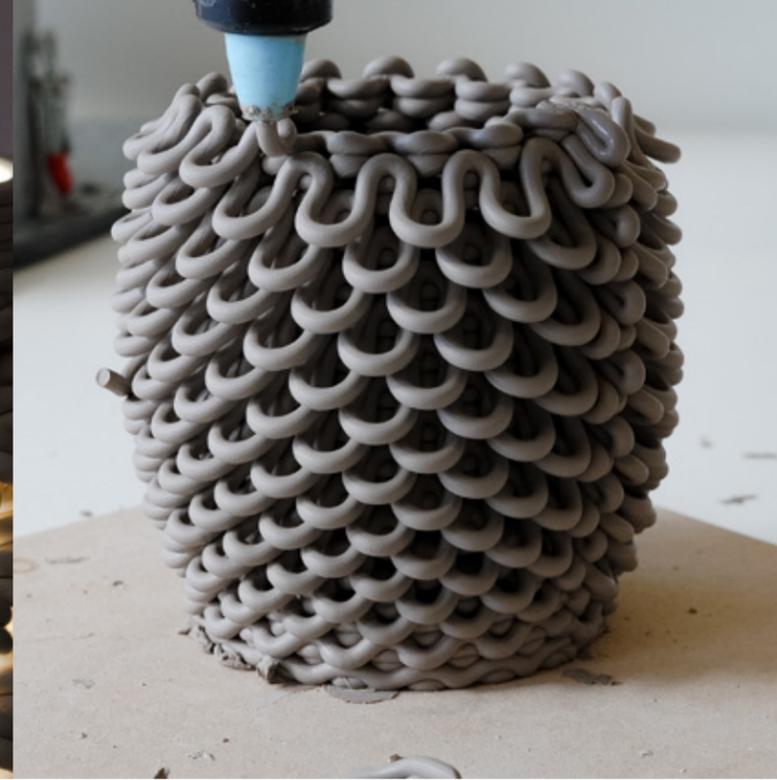
**Figure 4.4.22** Loop pattern print in progress (left) and illuminated (right).

**Figure 4.4.21** Oversized/Overhanging loop pattern print in progress (left) and illuminated (right).
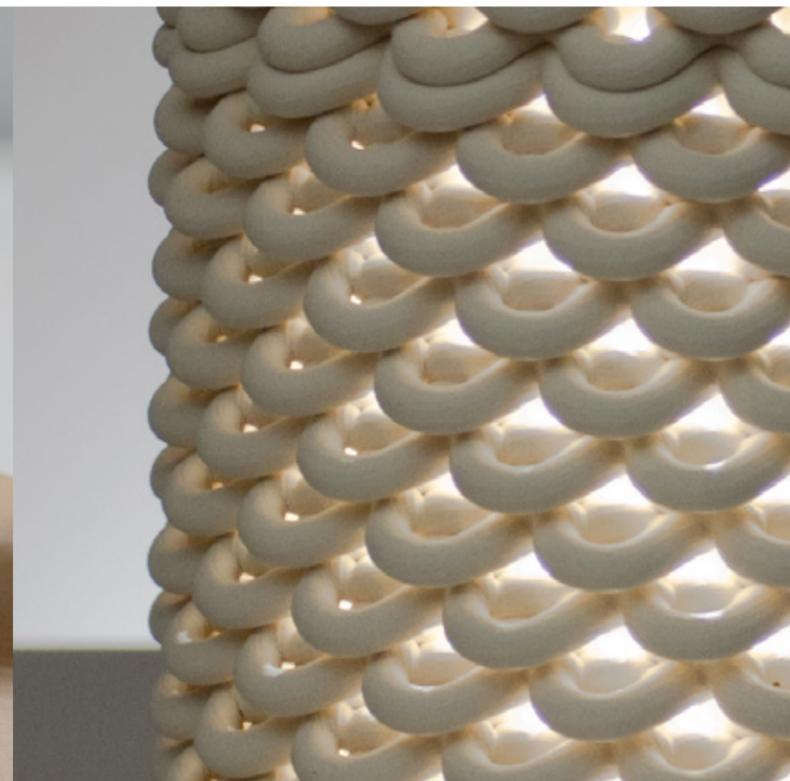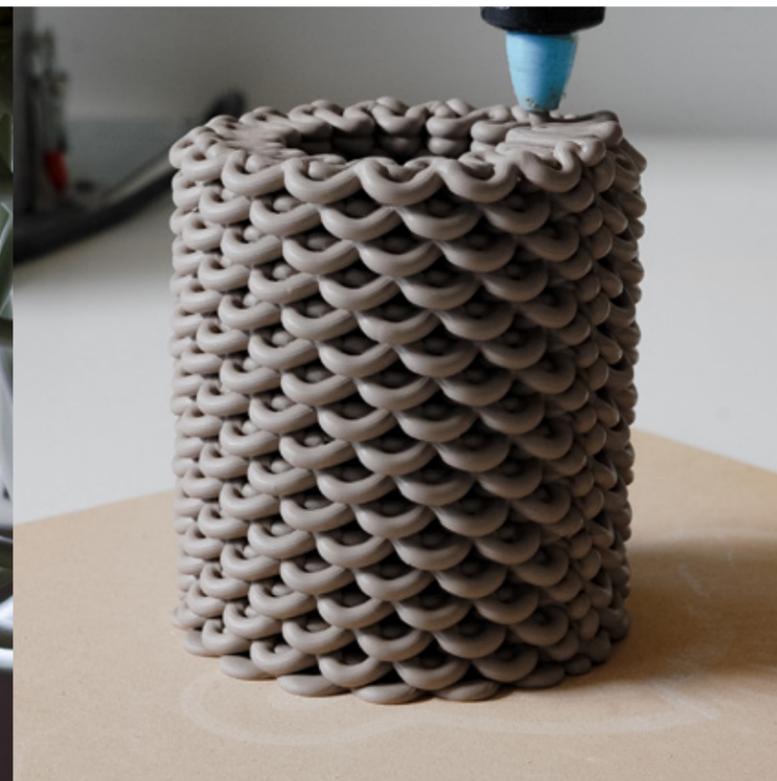
**Figure 4.4.23** Inverted loop pattern print in progress (left) and illuminated (right).

**Figure 4.4.24** Spiral pattern tool path plan (left) and physical print plan (right).



**Figure 4.4.25** Oversized/Overhanging loop pattern tool path plan (left) and physical print plan (right).

**Figure 4.4.26** Loop pattern tool path plan (left) and physical print plan (right).
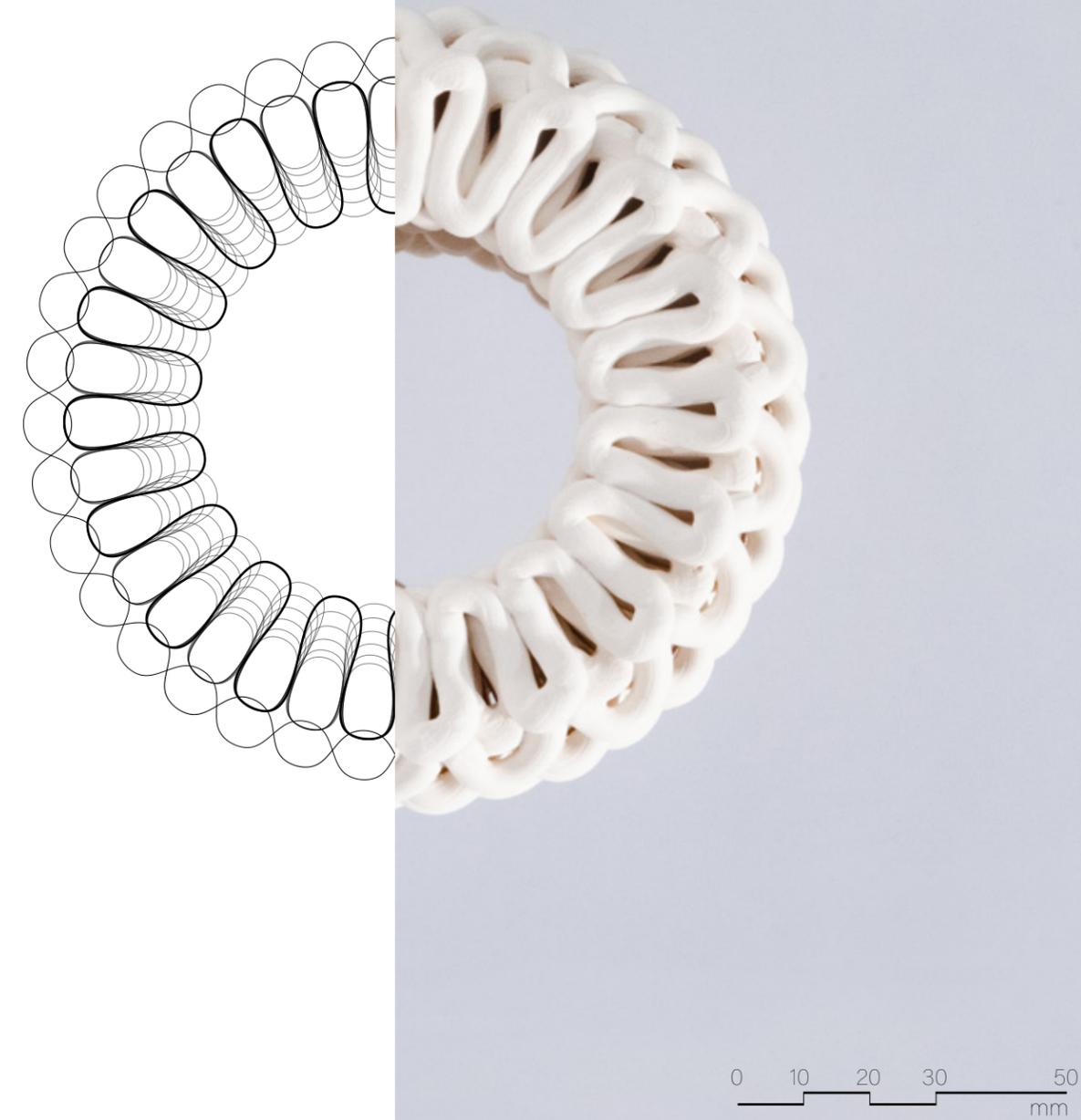


**Figure 4.4.27** Inverted loop pattern tool path plan (left) and physical print plan (right).

## Delamination

Extrusion rate and step height are critical parameters in preventing print delamination. For prints to maintain structural stability, deformation across layers must be mitigated before printing subsequent layers. This is referred to in this document as 'reformation' or 'stabilization.' The 'L' and 'XL' typologies use groups of six to twenty print layers, whereas the 'S' and 'M' typologies consist of two to three layers. The window for stabilization is much narrower in the 'S' and 'M' prototypes. Therefore, if the print section cannot be stabilized at a rate that corresponds to how quickly the material is being extruded and deformed, delamination occurs. This phenomenon is illustrated in several prints within the 'M' Index, including Figure 4.4.29. As formal inconsistencies compound, the print coil is eventually entirely displaced from the tool path. Non-planar printing can exacerbate this problem, as displayed in Figure 4.4.28. As a result, the final 'M' prototype has extrusion values and step heights specified to tenths of millimetres.



**Figure 4.4.28** Non-planar looping print studies displaying deformation and reformation.



**Figure 4.4.29** Examples of 'unwravelled' print studies.

## 'M' Index

This index consists of two sets of prototypes ordered chronologically. The first experiments are tool path/aperture studies applied to 100mm x 100mm x 200mm cylinders. These experiments display different print coil expressions and non-planar printing.

The second set consists of prototypes that maximize print cartridge capacity on the Potterbot XLS-1. These experiments focus on shaping the base surfaces to which tool paths are mapped and grading light effects across these surfaces.



**Figure 4.4.30** Unglazed PSH-515, fired to cone 04, 120mm x 120mm x 150mm, 2 layer sequence (x2).



**Figure 4.4.31** Unglazed PSH-515, fired to cone 04, 90mm x 90mm x 180mm, 2 layer sequence (x2).

**Figure 4.4.32** Unglazed PSH-515, fired to cone 04, 130mm x 130mm x 120mm, 2 layer sequence (x2).



**Figure 4.4.34** Unglazed PSH-515, fired to cone 04, 90mm x 90mm x 180mm, 3 layer sequence (x2).



**Figure 4.4.33** Unglazed PSH-515, fired to cone 04, 90mm x 90mm x 180mm, 3 layer sequence (x2).



**Figure 4.4.35** Unglazed PSH-515, fired to cone 04, 90mm x 90mm x 180mm, 3 layer sequence (x2), non-planar pattern.

**Figure 4.4.36** Unglazed PSH-515, fired to cone 04, 90mm x 90mm x 180mm, 3 layer sequence (x2), inverted loop pattern.



**Figure 4.4.38** Unglazed PSH-515, fired to cone 04, 90mm x 90mm x 160mm, 3 layer sequence (x3), spiral pattern.



**Figure 4.4.37** Unglazed PSH-515, fired to cone 04, 90mm x 90mm x 150mm, 3 layer sequence (x2), inverted loop pattern.



**Figure 4.4.39** Clear Linear glaze on Polar Ice, fired to cone 6, 90mm x 90mm x 180mm, 3 layer sequence (x2).

**Figure 4.4.40** Clear liner glaze on Polar Ice, fired to cone 6, 90mm x 90mm x 180mm, 2 layer sequence (x2), inverted loop pattern.



**Figure 4.4.42** Unglazed PSH-515, fired to cone 04, 90mm x 90mm x 180mm, 2 layer sequence (x4), spiral pattern.



**Figure 4.4.41** Clear Linear glaze on Polar Ice, fired to cone 6, 90mm x 90mm x 180mm, 2 layer sequence (x4), spiral pattern.



**Figure 4.4.43** Unglazed PSH-515, fired to cone 04, 90mm x 90mm x 180mm, 3 layer sequence (x4), spiral pattern.

**Figure 4.4.44** Unglazed PSH-515, fired to cone 04, 90mm x 90mm x 180mm, 2 layer sequence (x4), spiral patterning, non-planar pattern.



**Figure 4.4.46** Unglazed PSH-515, fired to cone 04, 90mm x 90mm x 150mm, 3 layer sequence (x3), hanging loops, spiral pattern.



**Figure 4.4.45** Unglazed PSH-515, fired to cone 04, 90mm x 90mm x 180mm, 3 layer sequence (x4), spiral pattern.
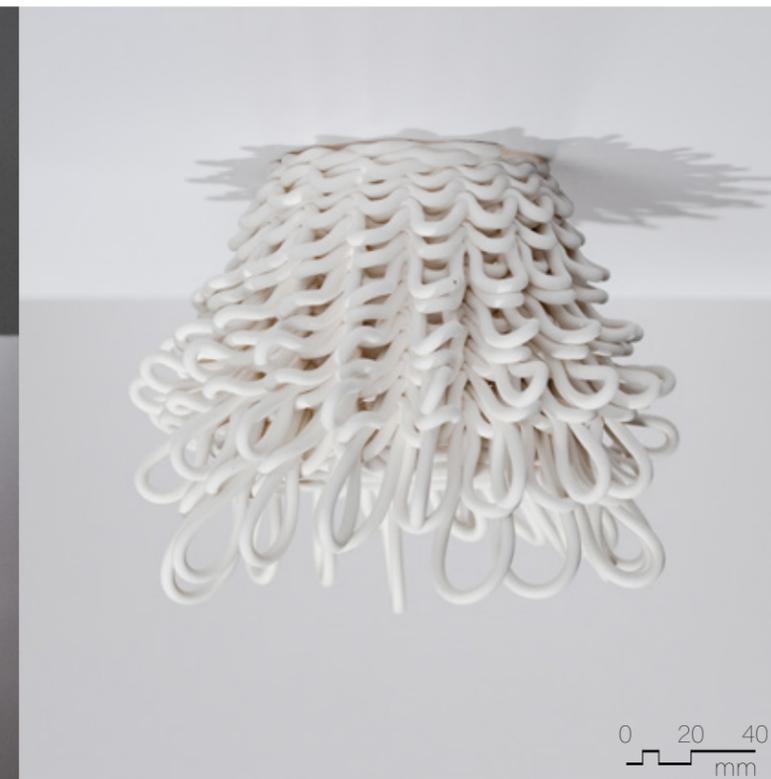


**Figure 4.4.47** Unglazed PSH-515, fired to cone 04, 90mm x 90mm x 150mm, 3 layer sequence (x2), hanging loops.

**Figure 4.4.48** Unglazed PSH-515, fired to cone 04, 90mm x 90mm x 150mm, 3 layer sequence (x3), hanging loops, spiral pattern.



**Figure 4.4.50** Unglazed PSH-515, fired to cone 04, 90mm x 90mm x 150mm, 3 layer sequence (x2), hanging loops.



**Figure 4.4.49** Unglazed PSH-515, fired to cone 04, 90mm x 90mm x 230mm, 3 layer sequence (x2), hanging loops.



**Figure 4.4.51** Unglazed PSH-515, fired to cone 04, 90mm x 90mm x 150mm, 3 layer sequence (x2), hanging loops.
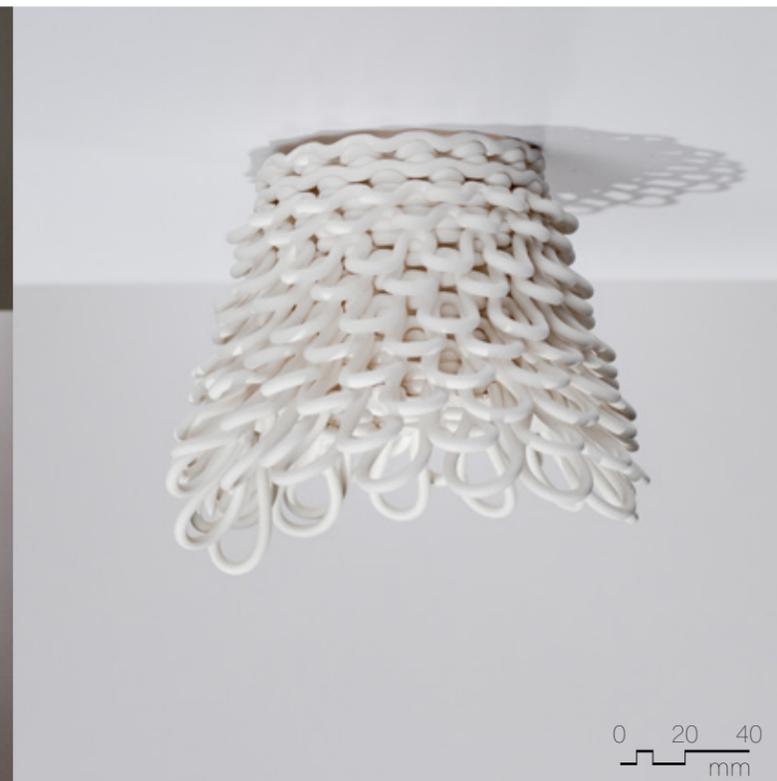
**Figure 4.4.52** Unglazed PSH-516, fired to cone 04, 230mm x 230mm x 340mm, 3 layer sequence (x2).
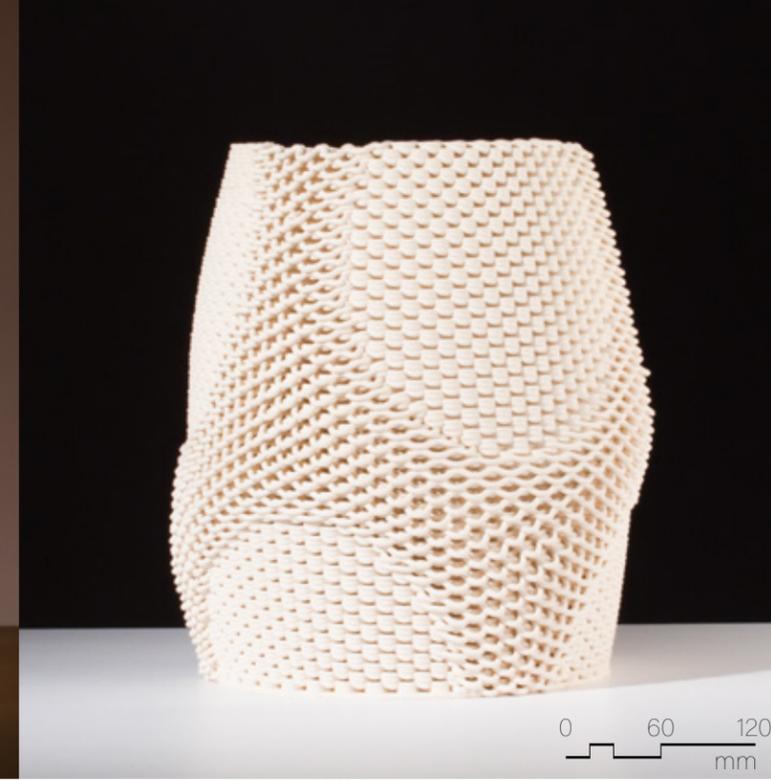
**Figure 4.4.54** Unglazed PSH-516, fired to cone 04, 230mm x 230mm x 340mm, 3 layer sequence (x2).

**Figure 4.4.53** Unglazed PSH-516, fired to cone 04, 230mm x 230mm x 340mm, 3 layer sequence (x2).
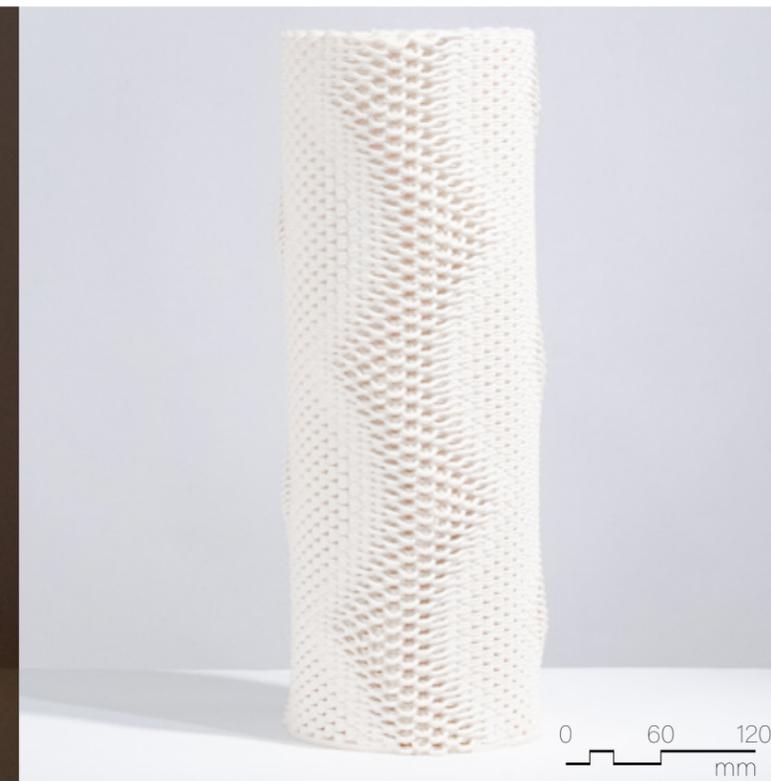
**Figure 4.4.55** Unglazed PSH-516, fired to cone 04, 220mm x 220mm x mm, 3 layer sequence (x2).

**Figure 4.4.56** Unglazed PSH-516, fired to cone 04, 260mm x 260mm x 400mm, 3 layer sequence (x2).

**Figure 4.4.58** Unglazed PSH-516, fired to cone 04, 260mm x 260mm x 400mm, 3 layer sequence (x2).

**Figure 4.4.57** Unglazed PSH-516, fired to cone 04, 260mm x 260mm x 400mm, 3 layer sequence (x2).

**Figure 4.4.59** Unglazed PSH-516, fired to cone 04, 260mm x 260mm x 400mm, 3 layer sequence (x2).

**Figure 4.4.60** Unglazed PSH-516, fired to cone 04, 280mm x 280mm x 350mm, 3 layer sequence (x2).

**Figure 4.4.62** Unglazed PSH Dark Granite, fired to cone 6, 280mm x 280mm x 350mm, 3 layer sequence (x2).

**Figure 4.4.61** Unglazed PSH-516, fired to cone 04, 280mm x 280mm x 350mm, 3 layer sequence (x2).

**Figure 4.4.63** Unglazed PSH-516, fired to cone 04, 280mm x 280mm x 350mm, 3 layer sequence (x2).

**Figure 4.4.64** Clear liner glaze on PSH-516, fired to cone 6, 280mm x 280mm x 350mm, 3 layer sequence (x2).



**Figure 4.4.65** Unglazed PSH-516, fired to cone 04, 300mm x 300mm x 350mm, 3 layer sequence (x2).

## 4.5 'L' TYPOLOGY

Brightness and light scattering in the Large ('L') typology are controlled by aperture size. The apertures in the final 'L' prototype are vertically graded. Brightness and light scattering gradually increase towards the bottom of the screen. The apertures in the final 'L' prototype consist of eleven vertically tessellated layers. Each layer is composed of a series of waves. Waves across these eleven layers gradually increase in amplitude, creating an opening at the top of each grouping of layers. Following the eleven-layer sequence, the vector domain that controls wave amplitude is reset to zero. Five print layers are required to restabilize material situated above voids in the geometry and allow layers to adhere to one another completely. Waves are horizontally staggered in the following eleven-layer sequence, creating rows of alternating light apertures. The formal language concerning how the print coils are expressed in the 'L' typology is referred to as 'scoops.'

The final 'L' prototype borrows formal elements from traditional ceramic table lamps. It has two components- housing and a shade. A steel frame hidden inside the housing supports the shade and light source. The shade is vertically flipped 180 degrees about its printed orientation to direct its apertures downwards. The pattern applied to the housing is ornamental- apertures are sealed to create a continuous surface. The housing and shade of the 'L' prototype are designed to utilize a full 3600cc cartridge of clay on the Potterbot XLS-1.



**Figure 4.5.1** Final 'L' prototype illuminated with steel hardware.

Plastic Deformation and Structural Collapse

Two strategies are implemented in the 'L' prototype to maximize aperture size and prevent structural failure:

1. **Interlocking scoops–** The second last layer of a scoop acts as the first layer of the next scoop (Figure 4.5.6). Interlocking scoops minimize the tendency for layers to splay outwards and cap the edge of each eleven layer grouping with a more robust print coil.

2. **Creating a geometry that mitigates the tendency of scoops to buckle–** The conical form of the shade exacerbates this tendency. A convex (outward-facing) scoop is placed between visible concave (inward-facing) scoops. Buckling is diverted to the convex scoops, deforming them into a series of flat planes (Figure 4.5.6).

The latter strategy in the tool path design also serves to direct incident light downwards and eliminate any direct glare caused by the light source. Apertures consisting of eleven layers were determined to optimize brightness and structural stability. The 'L' Index shows prior iterations of scoops that required higher volumes of clay to produce, diminishing brightness.



**Figure 4.5.2** Exterior scoop pattern.



**Figure 4.5.3** Interior scoop pattern.
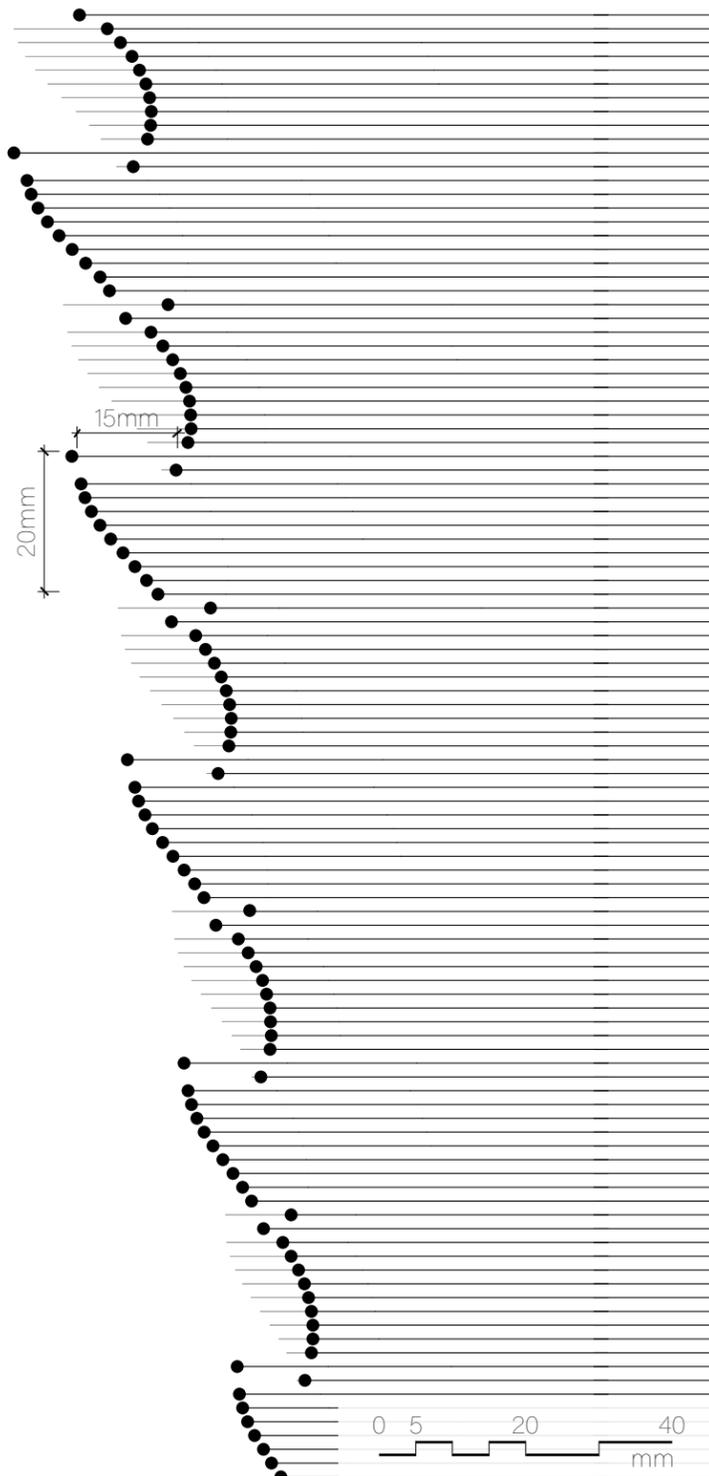
**Figure 4.5.4** Tool path section.

**Figure 4.5.5** Physical print section.

Digital tool path section

Post-processed print layer section
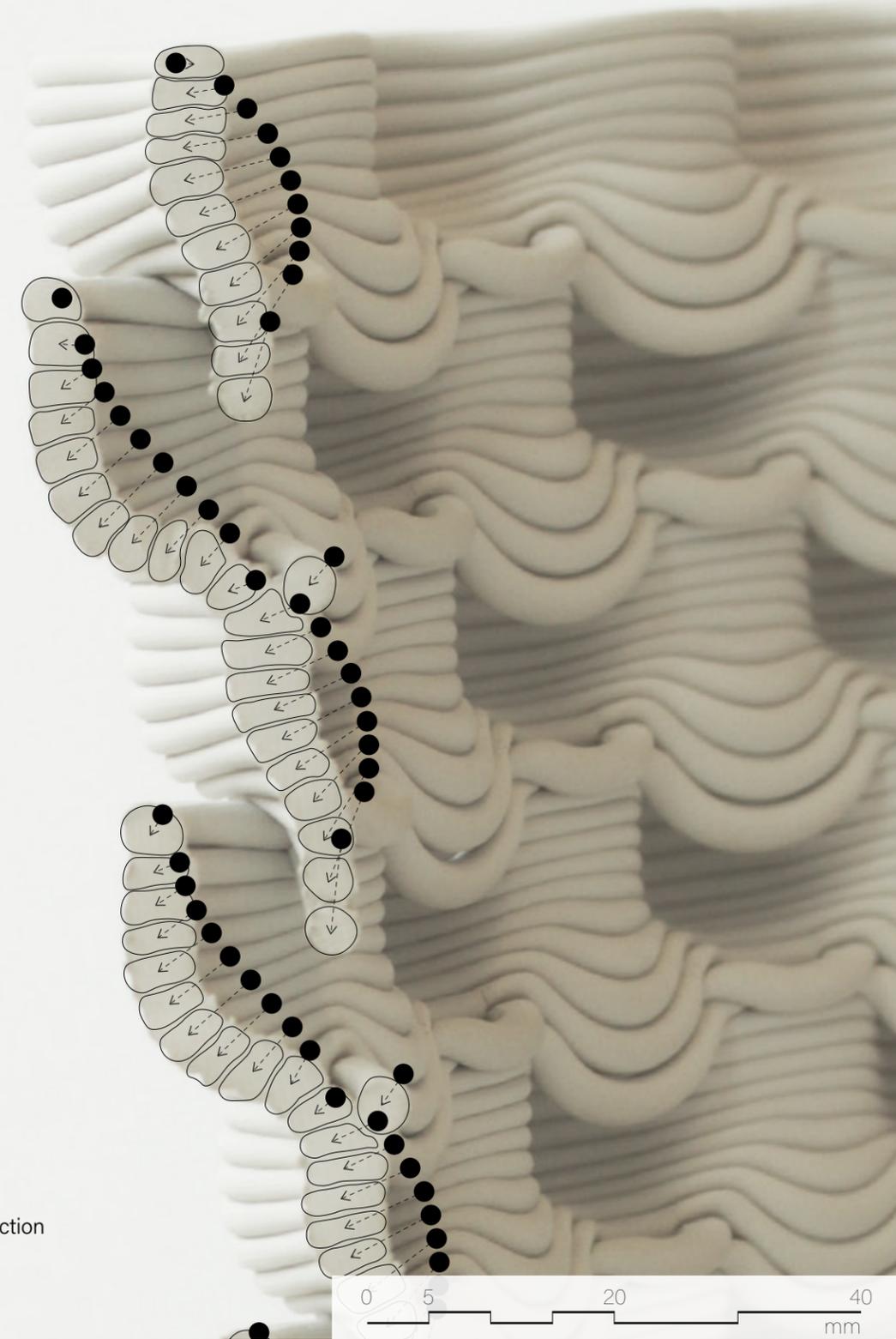
**Figure 4.5.6** Deformation of tool path mapped onto physical print.
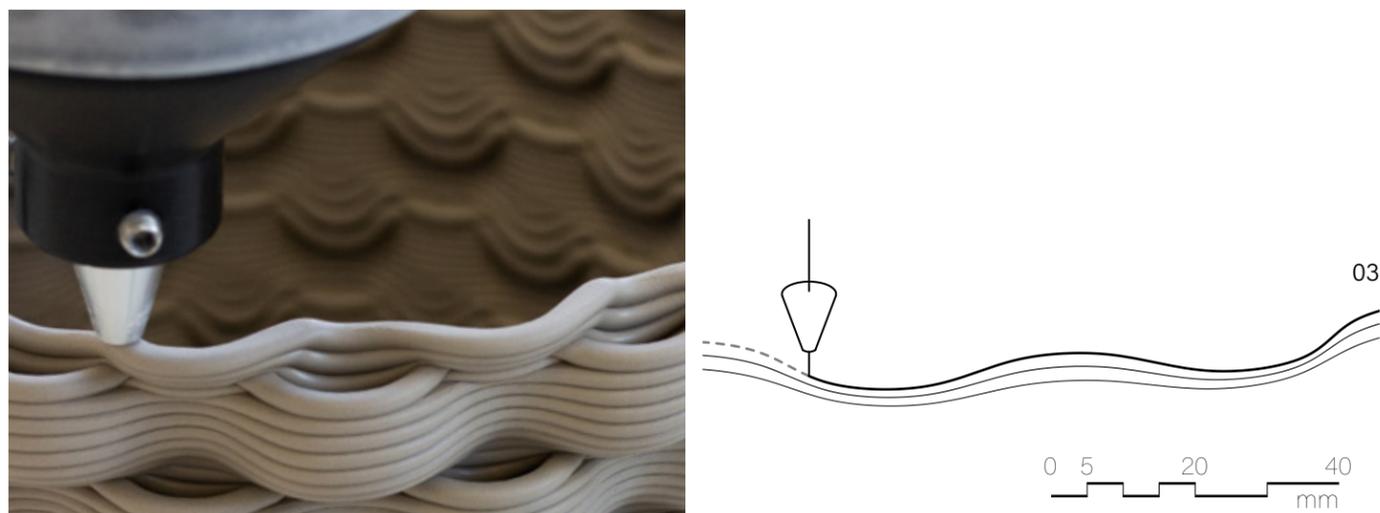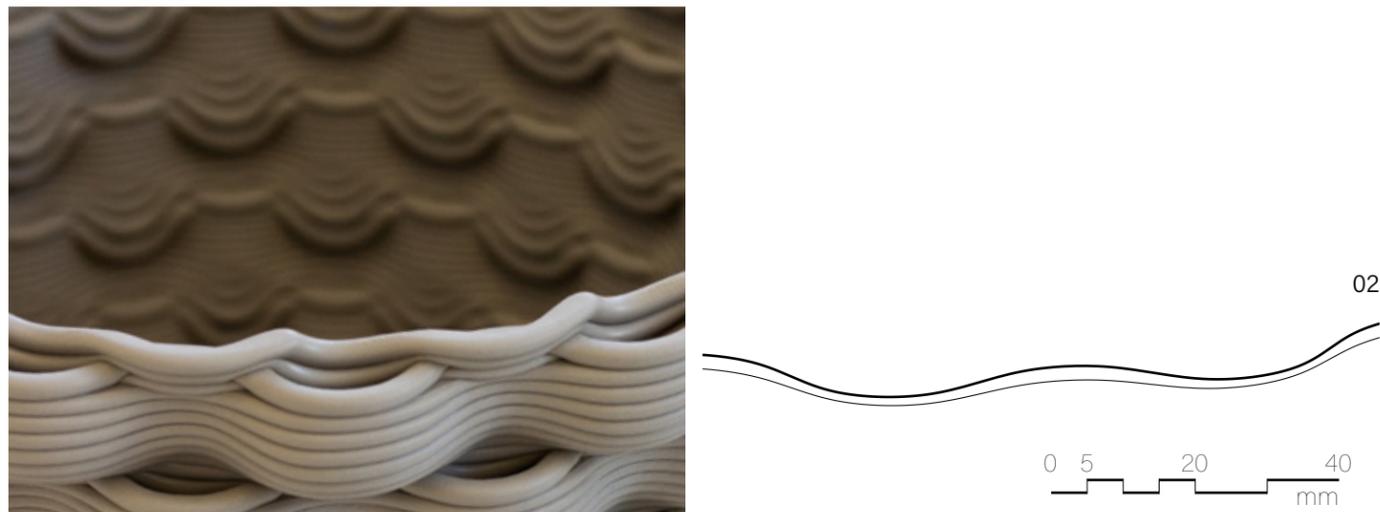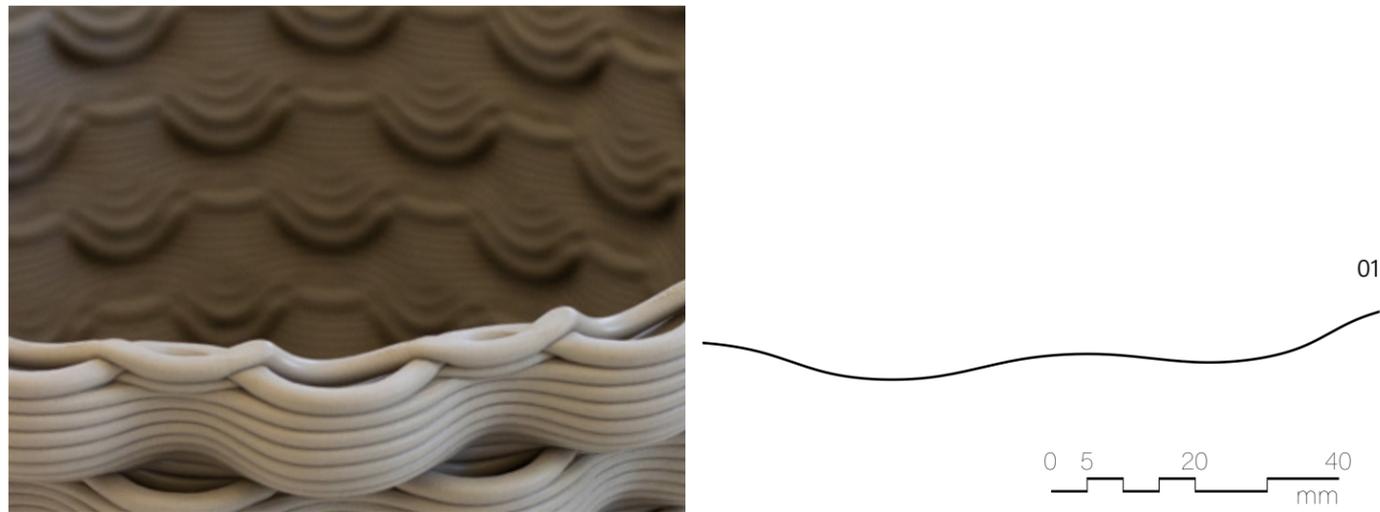
**Figure 4.5.7** Scoop sequence print layers 01, 02, 03.
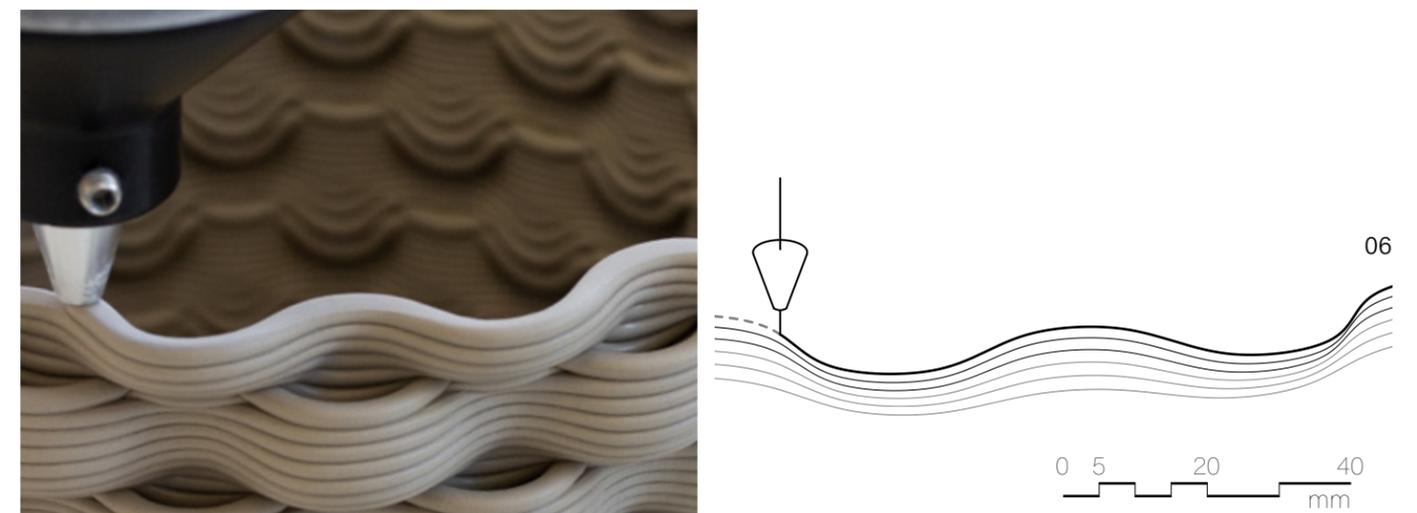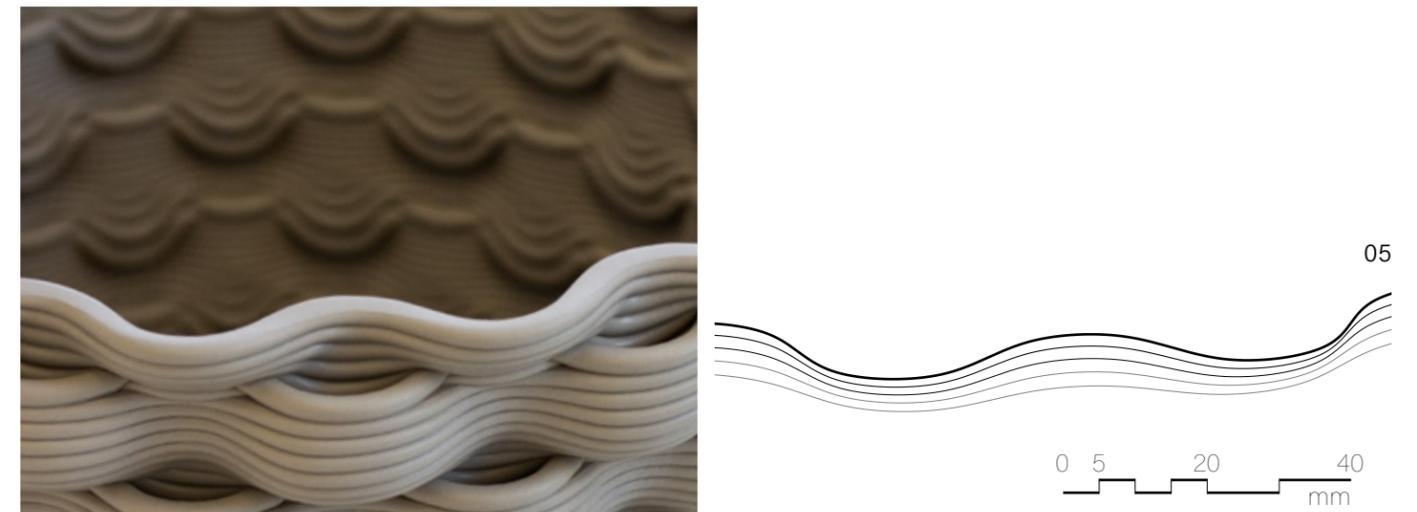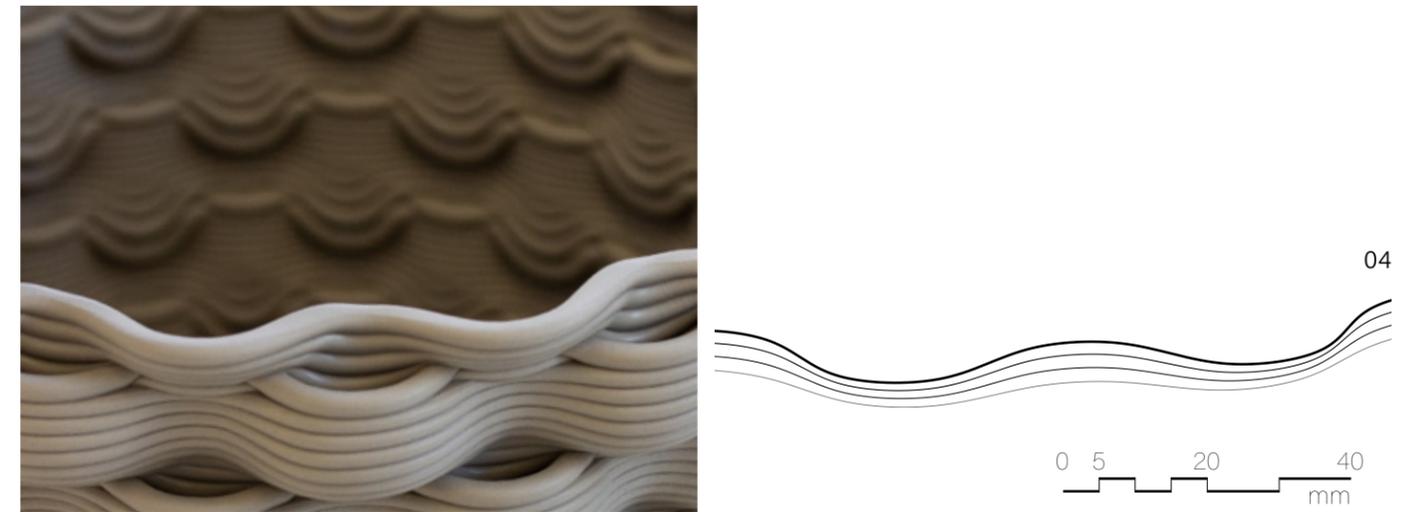


**Figure 4.5.8** Scoop sequence print layers 04, 05, 06.

07



08



09
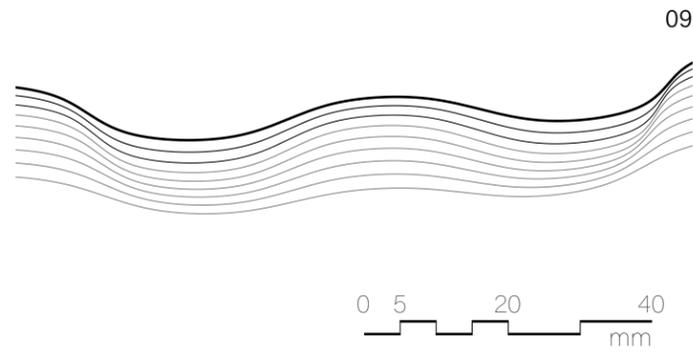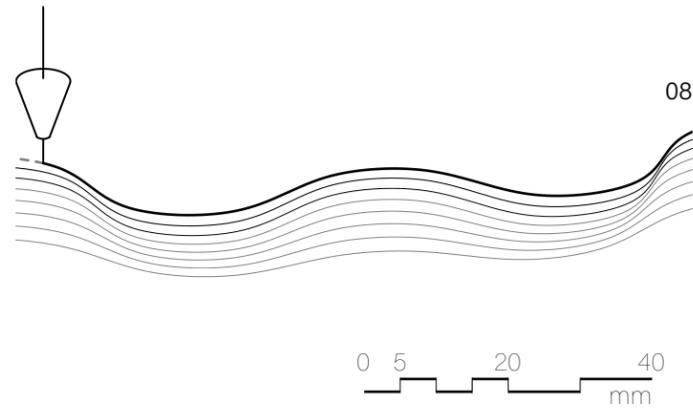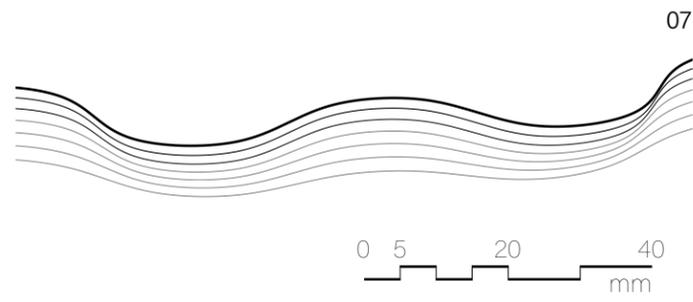
**Figure 4.5.9** Scoop sequence print layers 07, 08, 09.



10



11
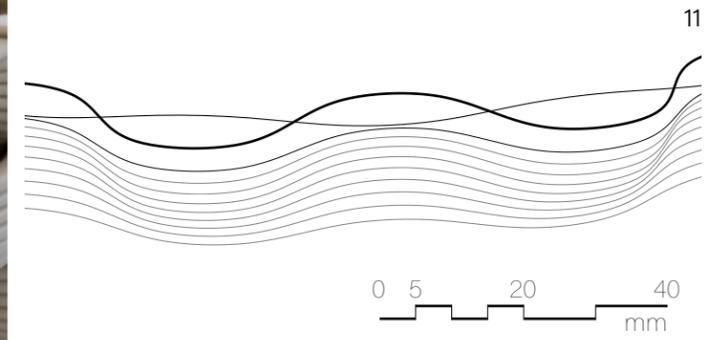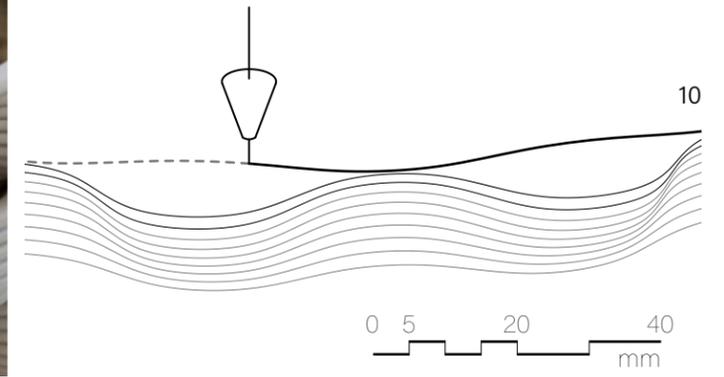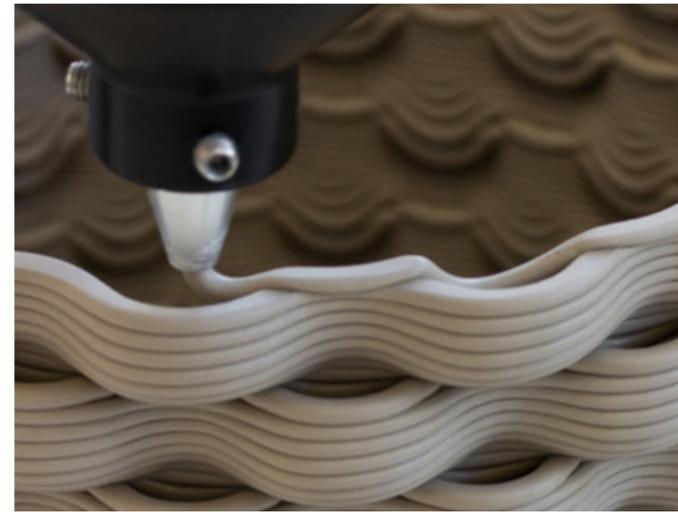
**Figure 4.5.10** Scoop sequence print layers 10, 11.
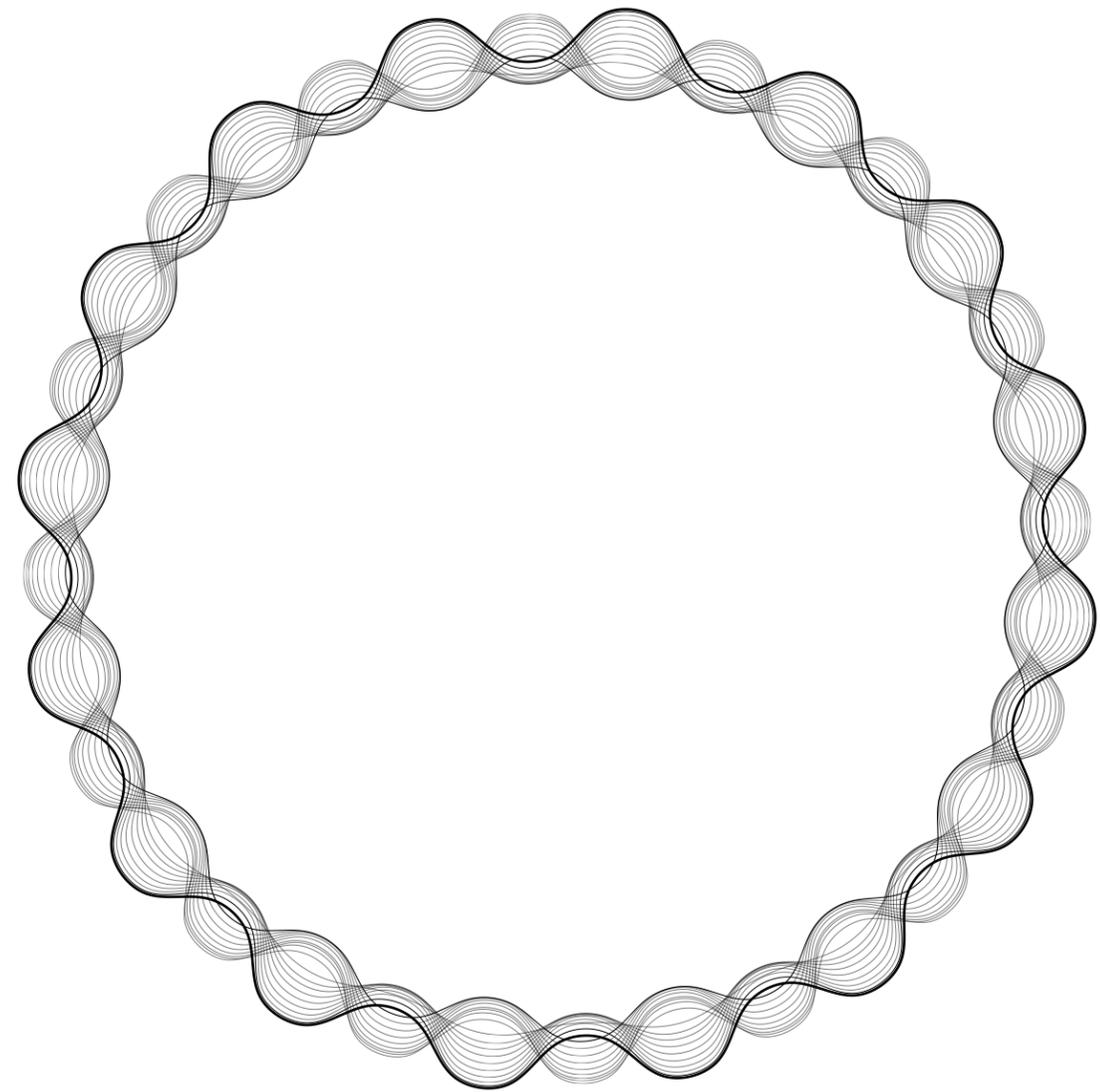
**Figure 4.5.11** 'L' typology tool path plan.

0    30    60    120
mm
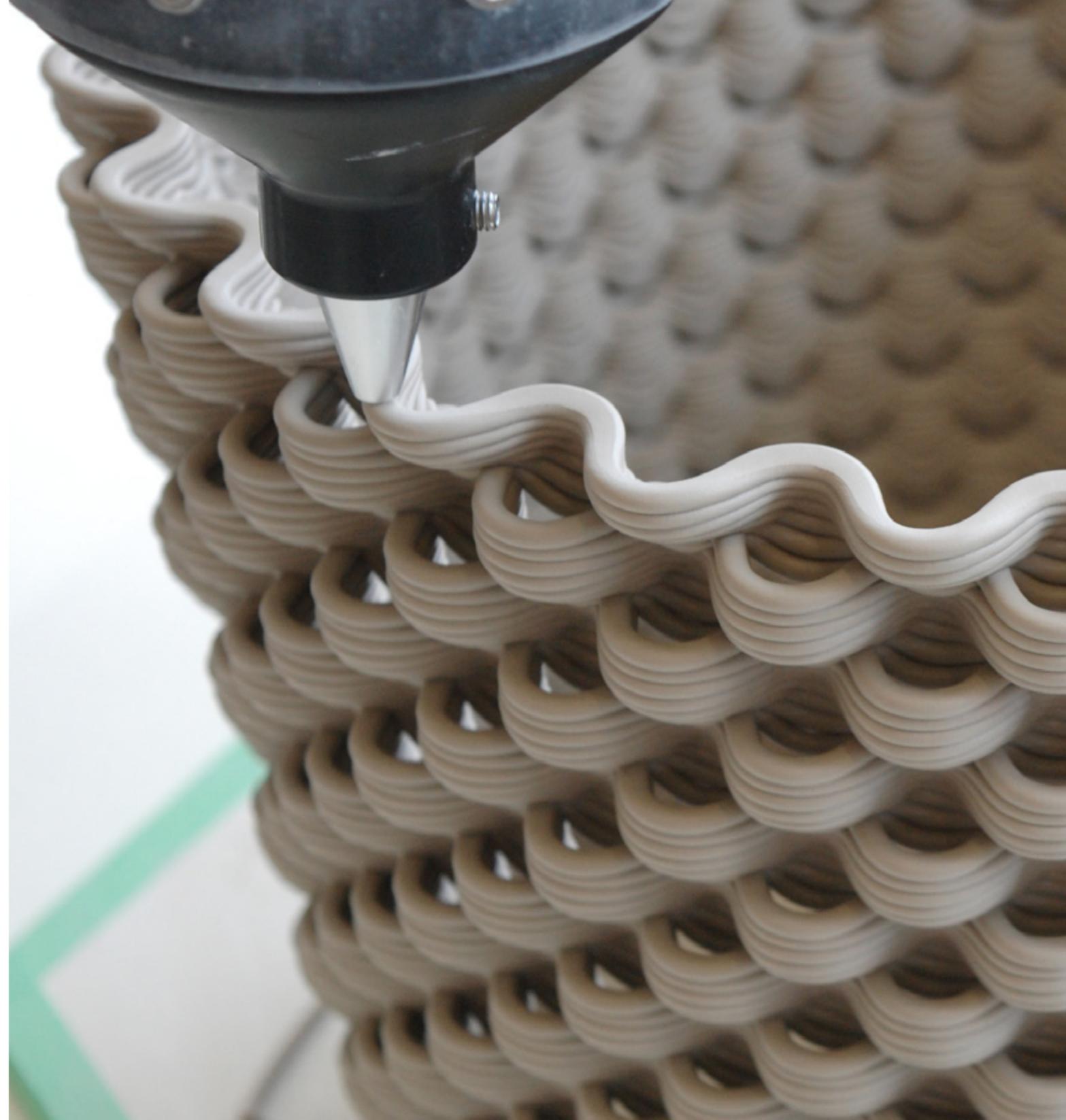


**Figure 4.5.12** 'L' prototype print in progress.

**Figure 4.5.13** 'L' prototype, front view.



**Figure 4.5.14** Illuminated 'L' prototype, front view.

**Figure 4.5.15** Illuminated 'L' prototype.
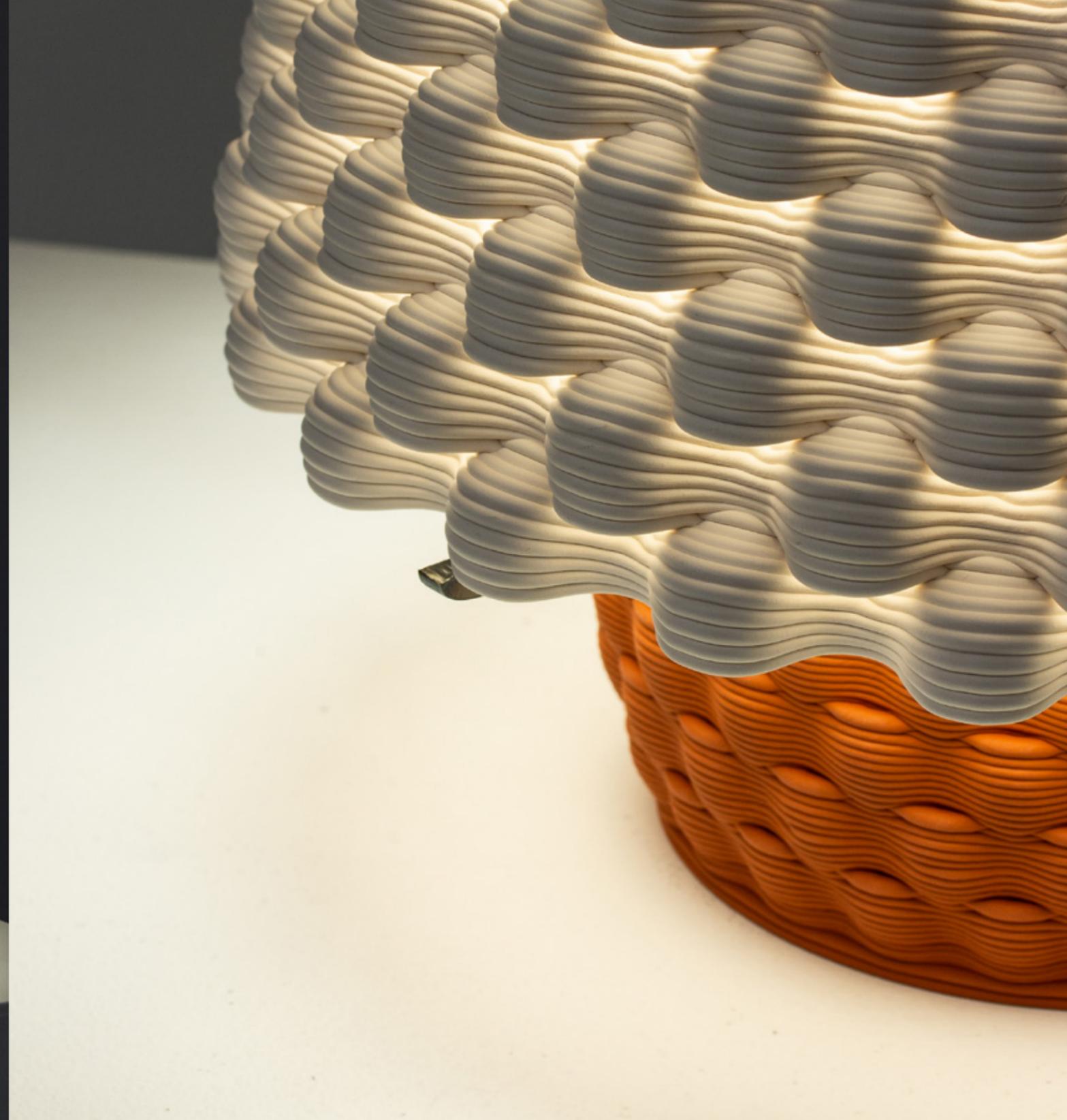
**Figure 4.5.16** Illuminated 'L' prototype, base detail.

**Figure 4.5.17** Illuminated 'L' prototype, base detail.
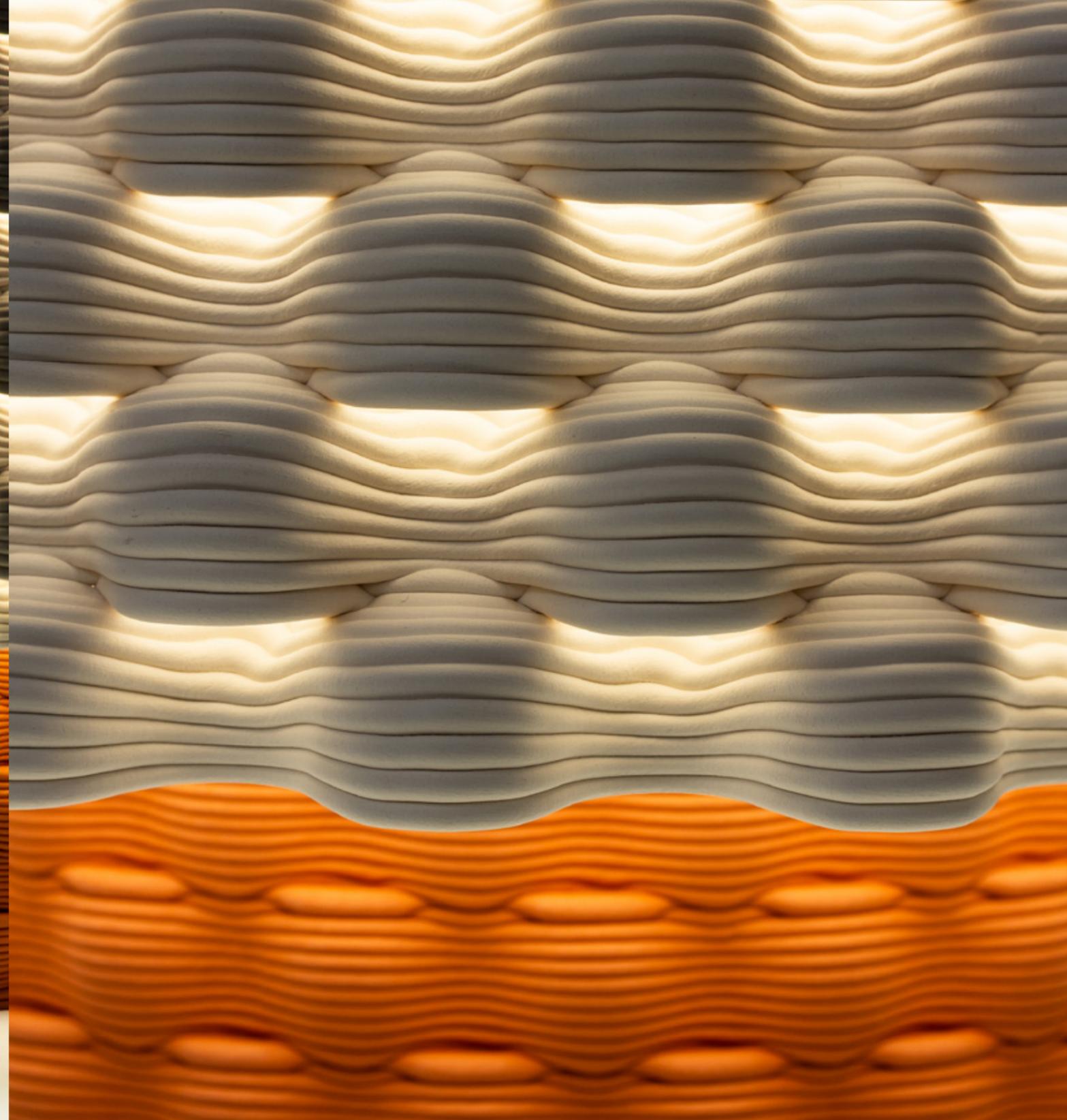


**Figure 4.5.18** Illuminated 'L' prototype, scoop detail.

## Directional Scoops

All prints within the 'L' typology utilize patterns comprised of six to twelve print layers. Two formal expressions of the print coil emerged from this series of experiments: inward-facing scoops and outward-facing scoops. Figure 4.5.22 displays two prints with identical wave patterns and print parameters. The two pieces are distinguished by having inverted domains that determine wave amplitude. The resulting light qualities and formal expressions are very different: outward-facing scoops provide directional light, while inward-facing scoops provide ambient illumination. These geometries cast patterns of dappled light and shadow on the surfaces below. These effects disappear when the screens are displaced approximately 100mm above these surfaces.



**Figure 4.5.19** 'L' prototype scoop, section detail.
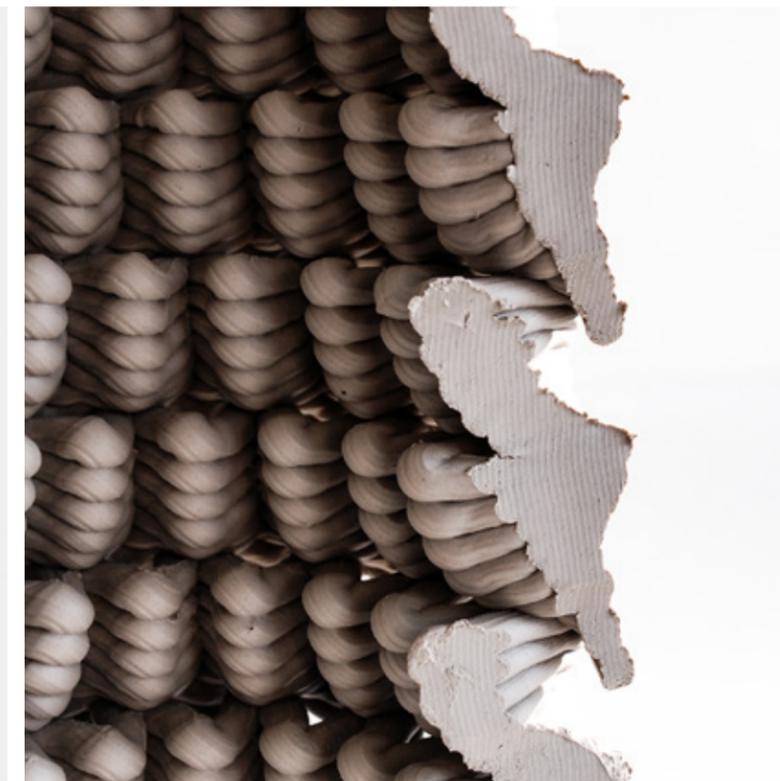
**Figure 4.5.20** Inverted light scoop study, section detail.

**Figure 4.5.21** Oversized light scoops, greenware.

**Figure 4.5.22** Two prints with identical print parameters, the only difference being the left print has inverted wave amplitudes.

**Figure 4.5.23** Rapid iteration of aperture sizes and scoop profiles. The final iteration in the sequence incorporates both inward and outward-facing scoops.
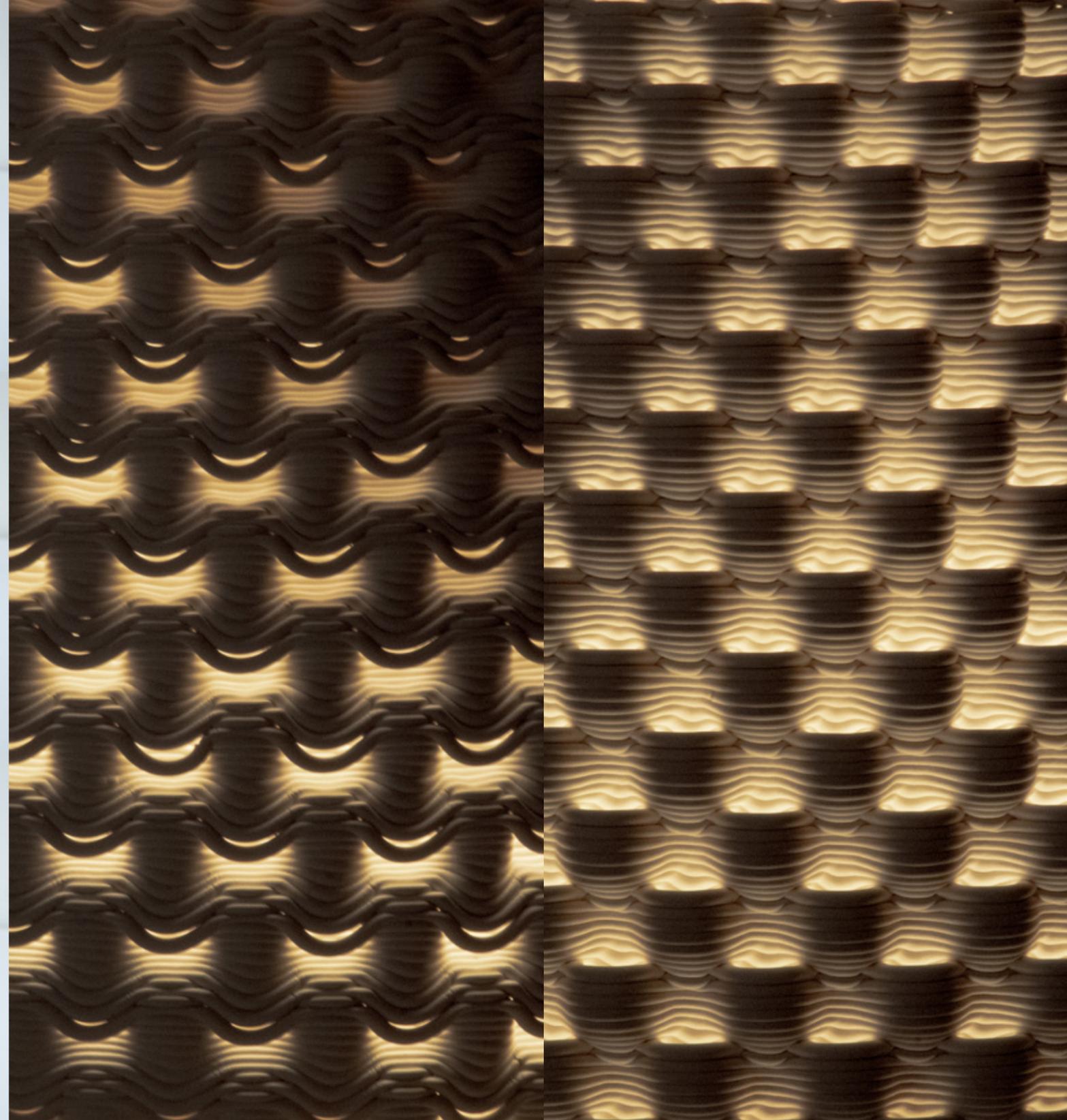
**Figure 4.5.24** Light gradients with both inward and outward facing scoops.

**Figure 4.5.25** Angular scoop pattern (above) produces triangular light dappling effect. Angular inverted scoop pattern (below) produces reversed triangular light dappling effect.
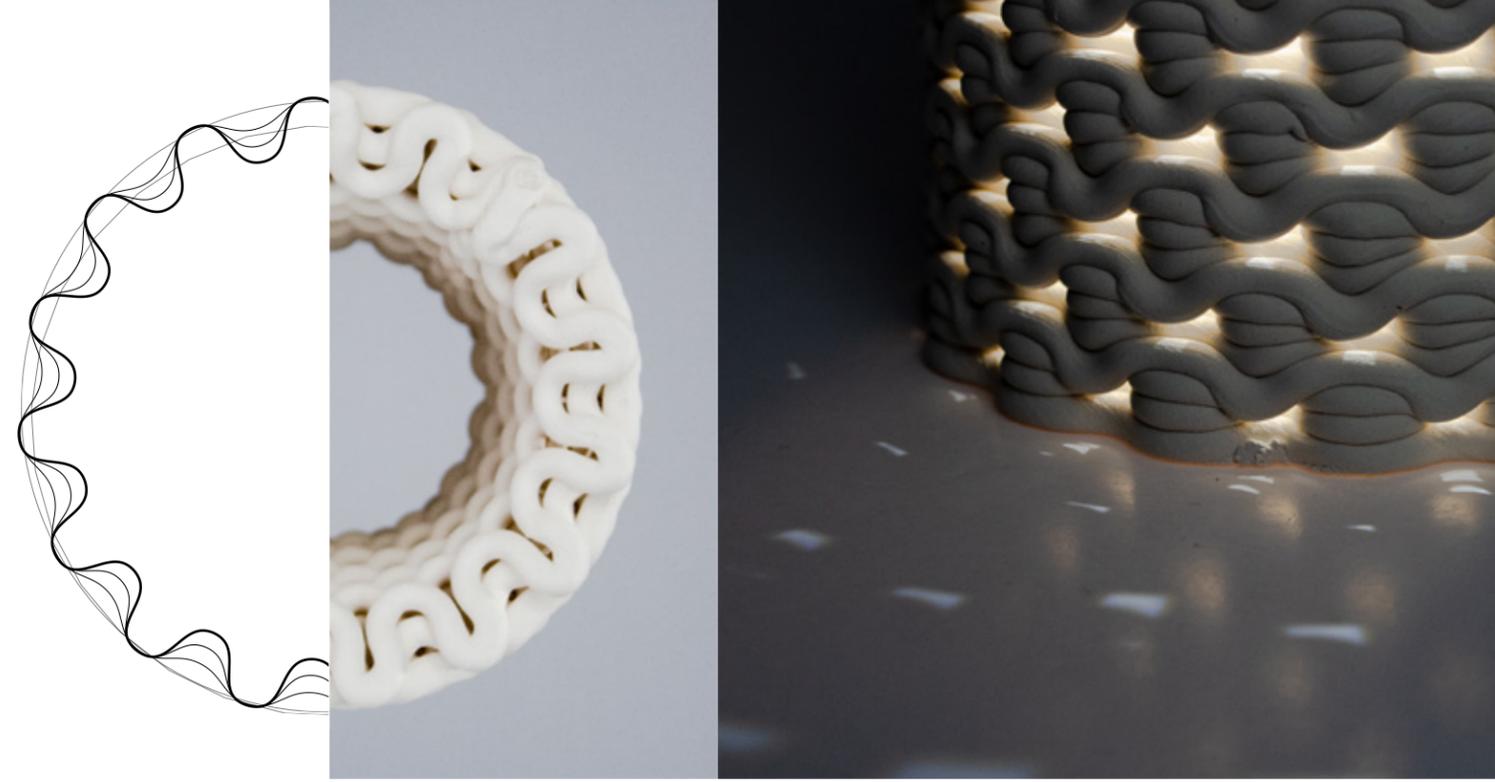


**Figure 4.5.26** The light dappling effect experiment (above) is diminished by the small scale of the light aperture.

## 'L' Index

This index consists of two sets of prototypes ordered chronologically. The first experiments are tool path/aperture studies applied to 100mm x 100mm x 200mm cylinders. These experiments display different print coil expressions and non-planar printing.

The second set consists of prototypes that maximize print cartridge capacity on the Potterbot XLS-1. These experiments focus on shaping the base surfaces to which tool paths are mapped and grading light effects across these surfaces.



**Figure 4.5.27** Unglazed PSH-515, fired to cone 04, 90mm x 90mm x 180mm, 4 layer sequence (x2).



**Figure 4.5.28** Unglazed PSH-515, fired to cone 04, 90mm x 90mm x 180mm, 4 layer sequence (x2).

**Figure 4.5.29** Unglazed PSH-515, fired to cone 04, 90mm x 90mm x 140mm, 13 layer sequence.



**Figure 4.5.31** Unglazed PSH-515, fired to cone 04, 90mm x 90mm x 180mm, 8 layer sequence (x3), spiral scoop pattern.



**Figure 4.5.30** Unglazed PSH-515, fired to cone 04, 90mm x 90mm x 180mm, 8 layer sequence (x2).
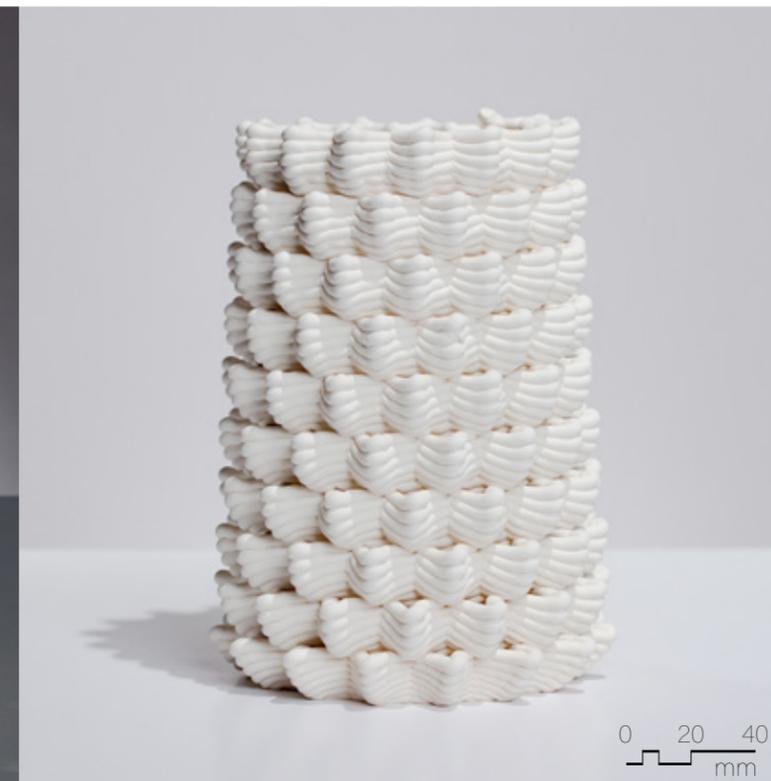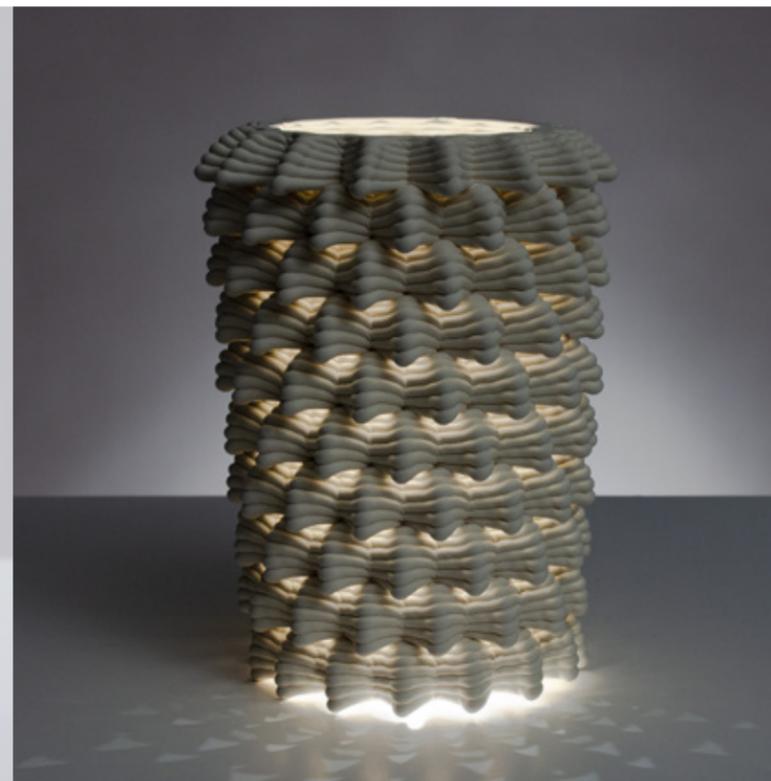


**Figure 4.5.32** Unglazed PSH-515, fired to cone 04, 110mm x 110mm x 180mm, 8 layer sequence (x2), inverted scoop pattern.

**Figure 4.5.33** Unglazed PSH-515, fired to cone 04, 90mm x 90mm x 180mm, 8 layer sequence (x2), non-planar pattern.

**Figure 4.5.35** Unglazed PSH-516, fired to cone 04, 230mm x 230mm x 340mm, 11 layer sequence (x2), inverted scoop pattern.

**Figure 4.5.34** Unglazed PSH-516, fired to cone 04, 230mm x 230mm x 340mm, 11 layer sequence (x2).

**Figure 4.5.36** Unglazed PSH-425, fired to cone 06, 300mm x 300mm x 420mm, 11 layer sequence (x2).

**Figure 4.5.37** Unglazed PSH-516, fired to cone 04, 300mm x 300mm x 420mm, 11 layer sequence (x2).

**Figure 4.5.39** Unglazed PSH-516, fired to cone 6, 300mm x 300mm x 420mm, 11 layer sequence (x2).

**Figure 4.5.38** Unglazed PSH-516, fired to cone 6, 300mm x 300mm x 420mm, 11 layer sequence (x2).

**Figure 4.5.40** Clear liner glaze on PSH-516, fired to cone 6, 300mm x 300mm x 420mm, 11 layer sequence (x2).

## 4.6 'XL' TYPOLOGY

Brightness and light scattering in the Extra-Large ('XL') typology are controlled by aperture size. The apertures in the final 'XL' prototype are vertically graded. Brightness and light scattering gradually increases towards the bottom of the screen. Graded light conditions are achieved using two digital tooling operations:

1. **Extrusion Variability**– Unique to the 'S' and 'XL' typologies.
2. **Waves**– Contours that expand and contract in amplitude to change the sectional distribution of material.

Extrusion variability is attached to a variable domain that controls material deposition relative to a given location on the prototype. The final 'XL' prototype has an extrusion domain of 9 to 20. Nine represents the least amount of material deposited at the top of the print, while twenty represents the greatest amount of clay deposited at the bottom. When extrusion increases, more material is being deposited at a given location along the tool path. If this occurs across a void in the geometry, unsupported material will sag, resulting in more significant plastic deformation. Greater extrusion results in more material distribution across the depth of the wall section, minimizing brightness.

The apertures in the 'XL' typology consist of sixteen vertically tessellated layers. Each layer is composed of a series of waves. Waves in every second layer of the final 'XL' prototype decrease in amplitude,



**Figure 4.6.1** Final XL' prototype with steel hardware.

creating two overlapping planes in section. Staggering the print layers in the X-Y axis gives the material additional room to deform in the Z-axis. Waves located on the interior of the geometry provide structural support to facilitate plastic deformation occurring on the exterior of the geometry. The 'interior' wall forms a shelf that reflects light off the stoneware and out through voids in the 'exterior' wall. Following the sixteen-layer sequence, the vector domain that controls wave amplitude is reset to zero. Five print coils are required to restabilize material situated above voids in the geometry and allow layers to adhere to one another completely. Waves are horizontally staggered in the following sixteen-layer sequence, creating rows of alternating light apertures.

The final 'XL' prototype is conceived of as a standing lamp. Steel supports taper upwards, mimicking the shape of the screen. The final 'XL' prototype is designed to utilize a full 3600cc cartridge of clay on the Potterbot XLS-1.



**Figure 4.6.2** 'XL' full scale prototypes in a variety of clay bodies.

## Plastic Deformation and Structural Collapse

Extrusion variability is the most significant contributor to plastic deformation in the 'XL' typology. The volume of clay deposited is reduced by over fifty percent across the print. Since most of the material is distributed at the bottom of the piece, this produces a very stable form. During prototyping, various non-linear variable extrusion domains were tested. These non-linear domains required a lot of fine-tuning to alter brightness and light scattering effects while maintaining structural stability. Linear domains were found to provide the most structural stability when vertically graded across the geometry.

In the 'XL' typology, structural stability also relies on the relationship between extrusion variability and aperture size. When extrusion variability is too high relative to aperture size, print coils deform and touch the layers below, minimizing porosity. However, increased plastic deformation in the final 'XL' prototype produces small openings between delaminated print layers. These small openings promote light scattering and reduce glare on the exterior of the geometry. The 'interior' wall of the geometry tapers to create an angled shelf that directs light down through the small delaminations on the 'exterior' wall. Alternatively, low extrusion variability at the top of the print prevents plastic deformation and maximizes brightness.
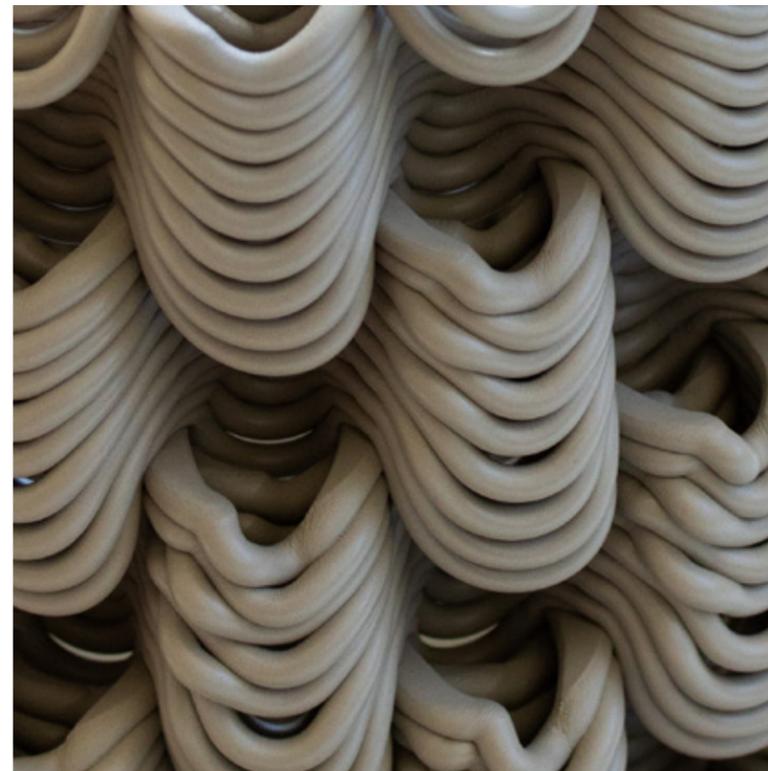


**Figure 4.6.3** Exterior shelf pattern.
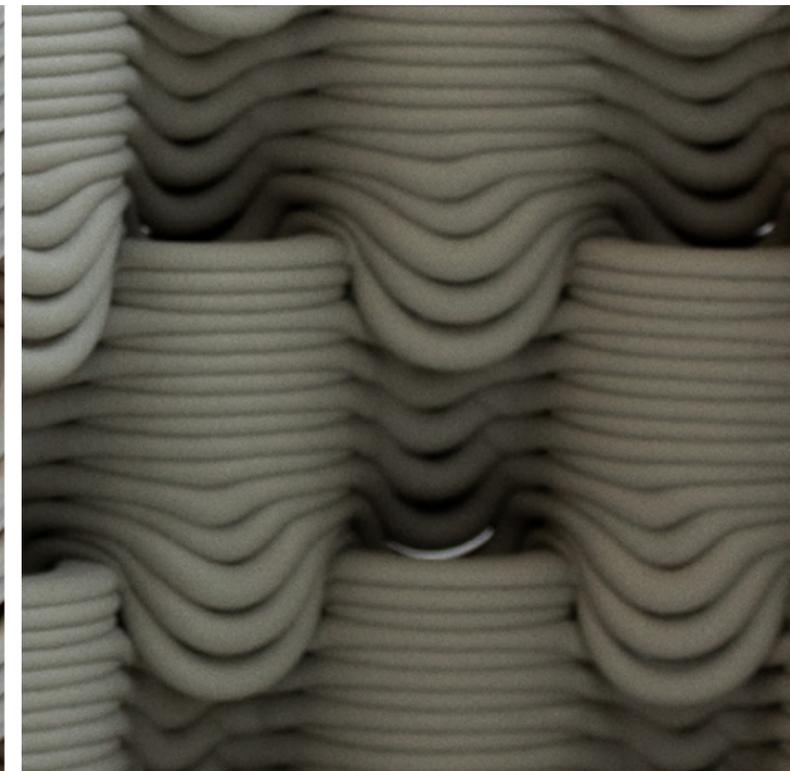
**Figure 4.6.4** Interior shelf pattern.
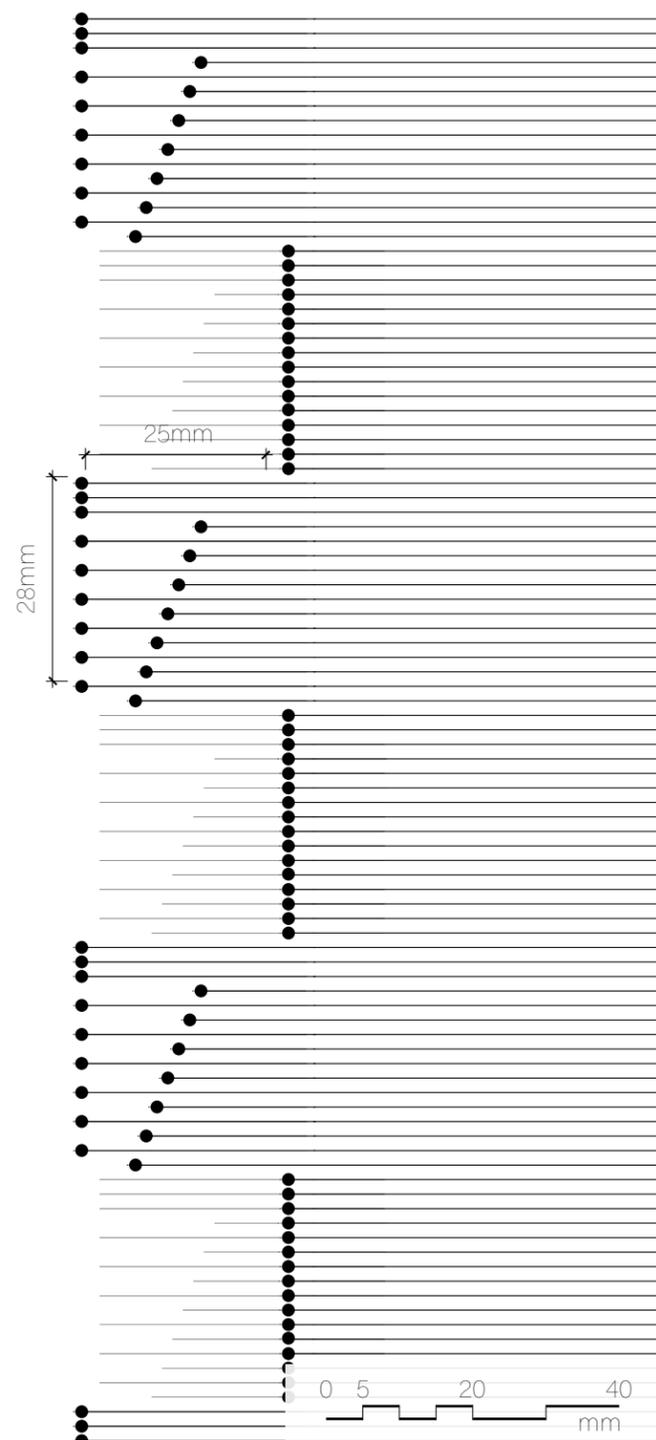
**Figure 4.6.5** Tool path section.
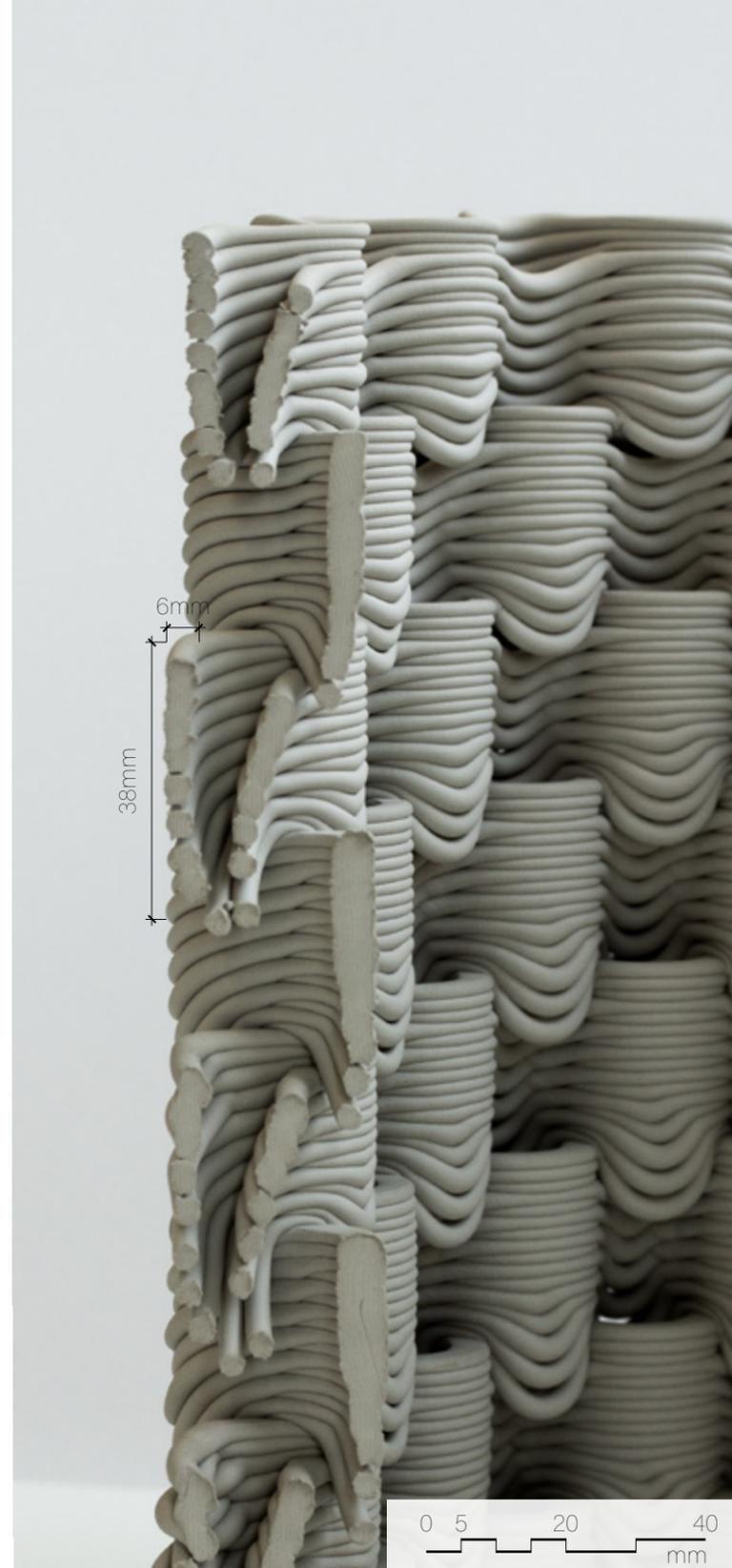


**Figure 4.6.6** Physical print section.



● Digital tool path section

○↓ Post-processed print layer section
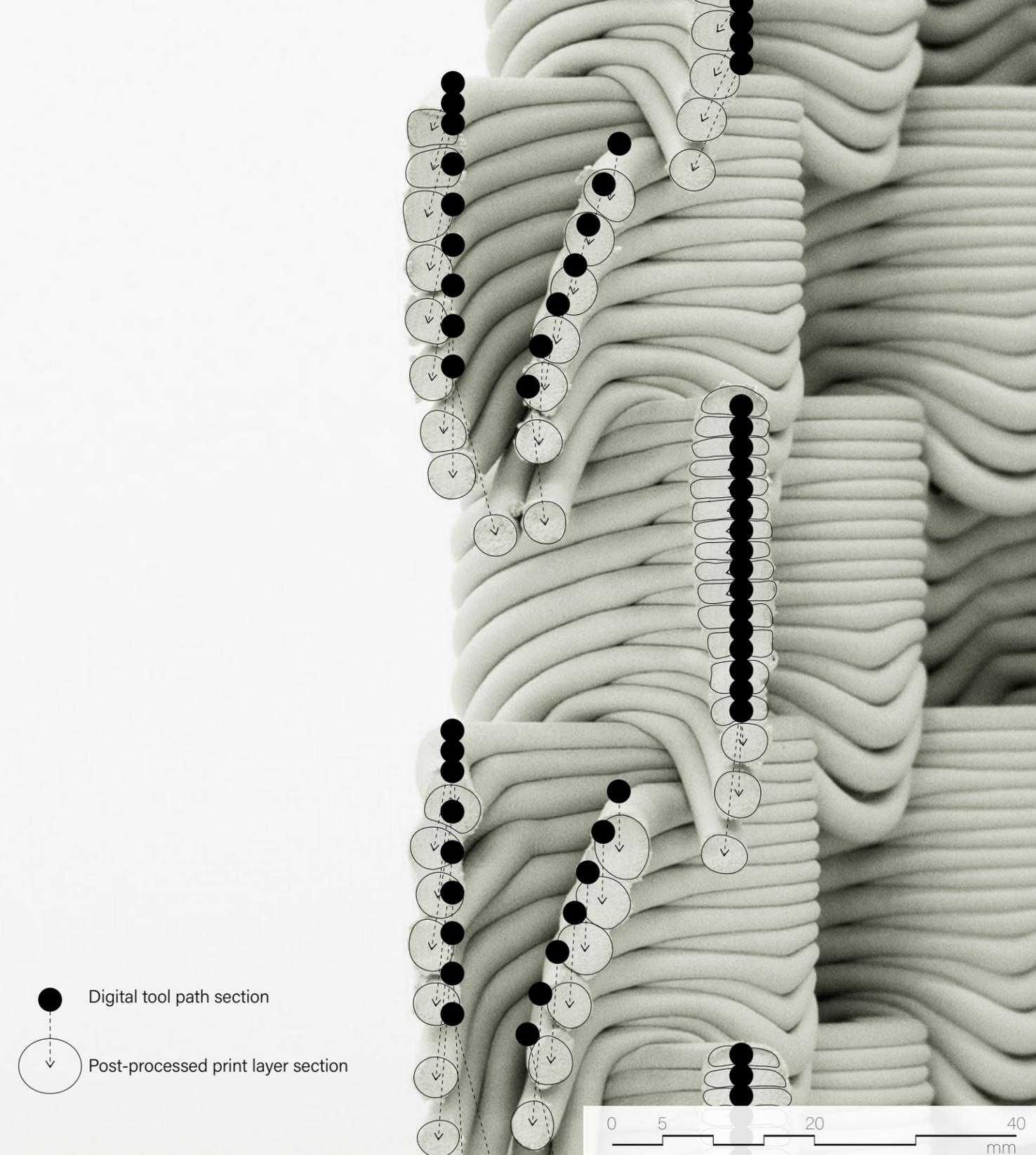
**Figure 4.6.7** Deformation of tool path mapped onto physical print.

01

0  5    20    40
mm

02

0  5    20    40
mm

03

0  5    20    40
mm
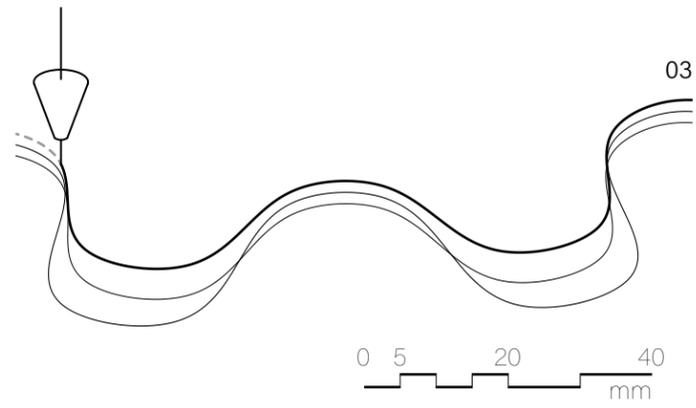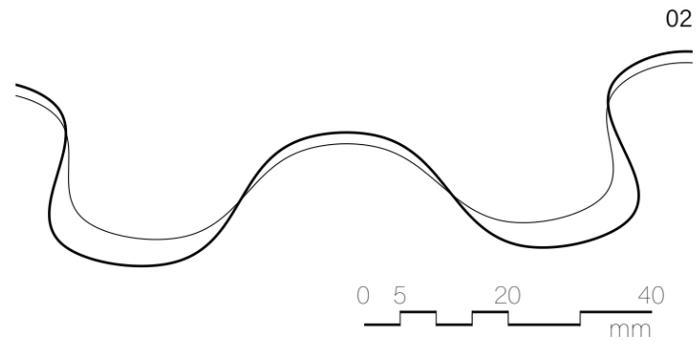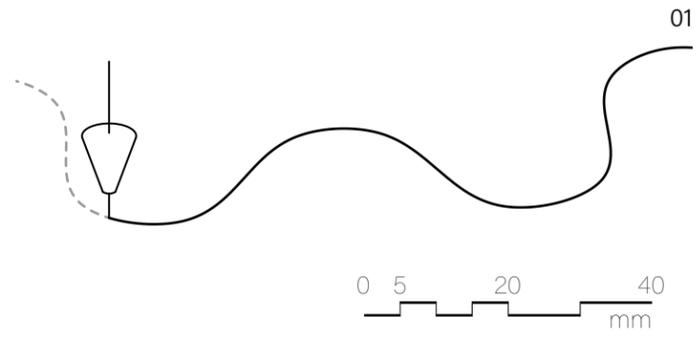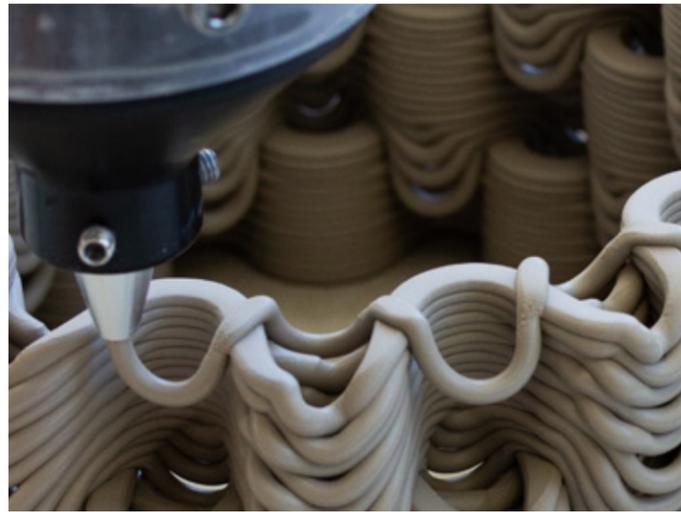
**Figure 4.6.8** Shelf print layers 01, 02, 03.

04

0  5    20    40
mm

05

0  5    20    40
mm

06

0  5    20    40
mm
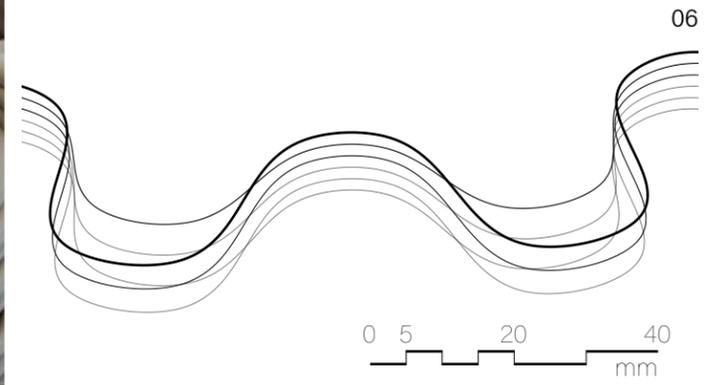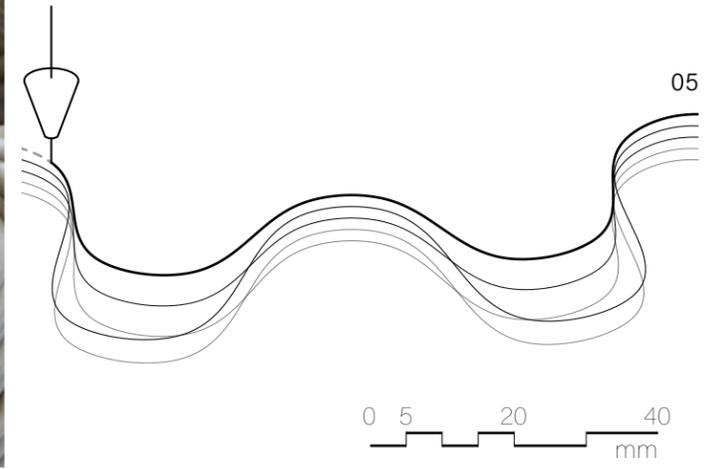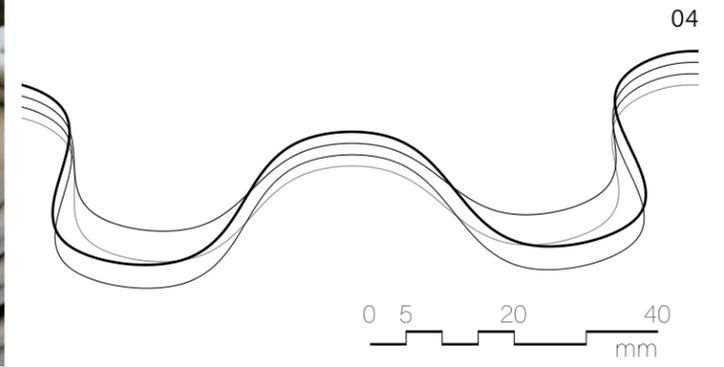
**Figure 4.6.9** Shelf print layers 04, 05, 06.
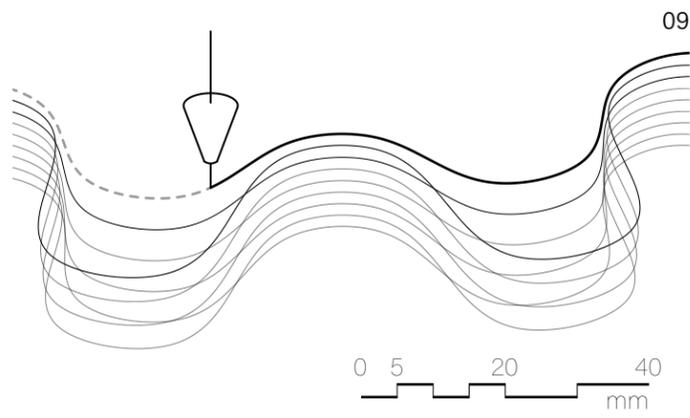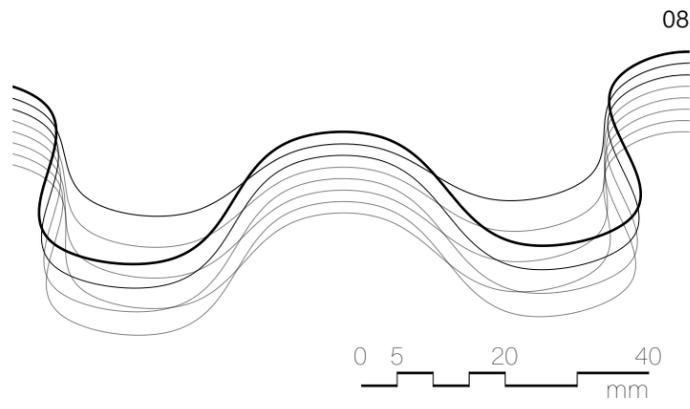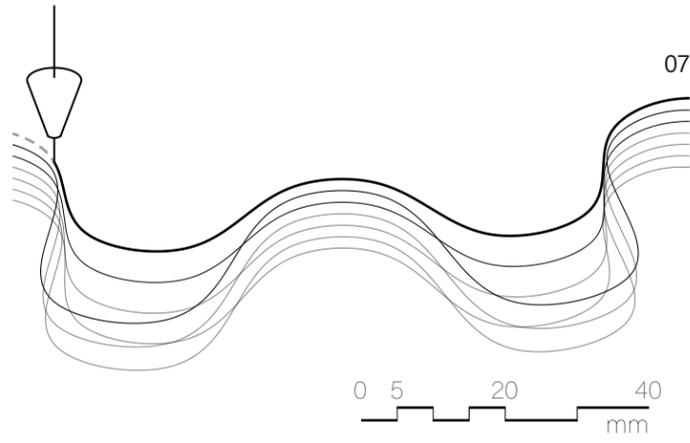
**Figure 4.6.10** Shelf print layers 07, 08, 09.
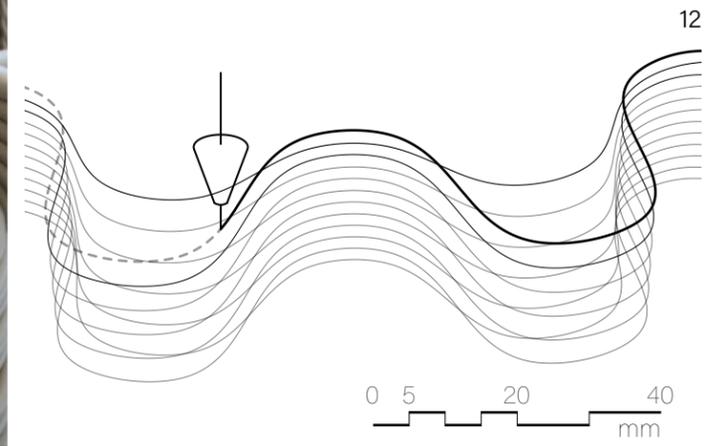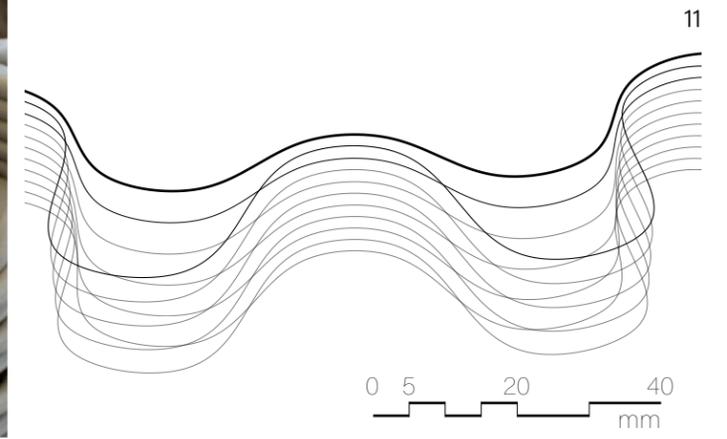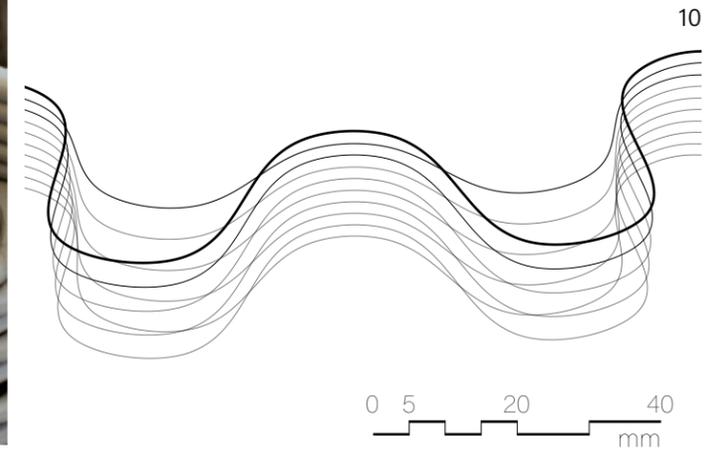


**Figure 4.6.11** Shelf print layers 10, 11, 12.

13

0  5      20      40
mm

14

0  5      20      40
mm

15

0  5      20      40
mm
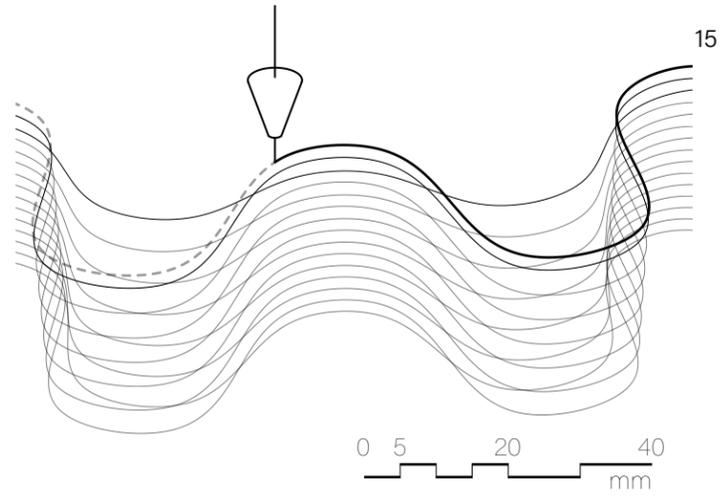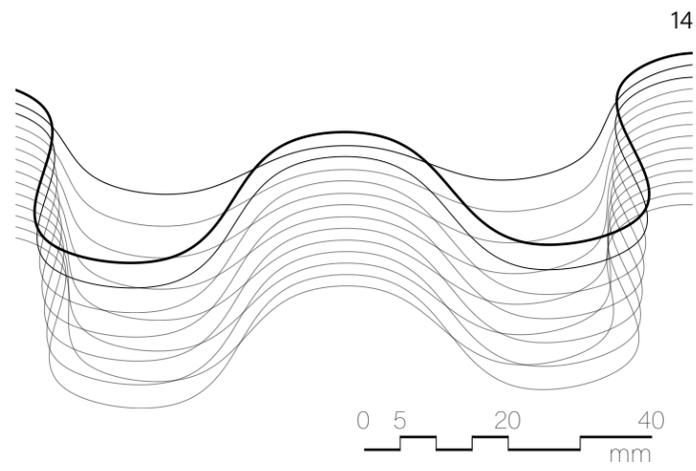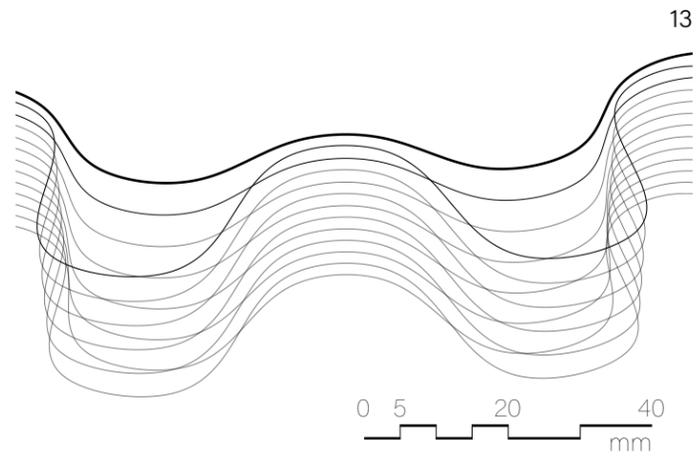
**Figure 4.6.12** Shelf print layers 13, 14, 15.



16

0  5      20      40
mm
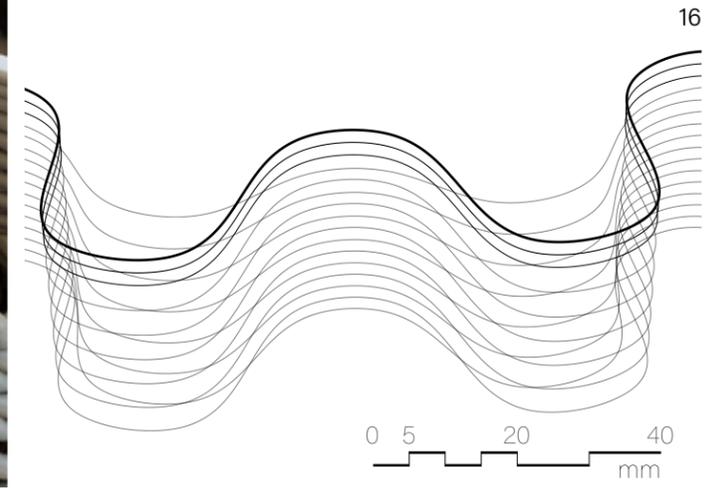
**Figure 4.6.13** Shelf print layer 16.
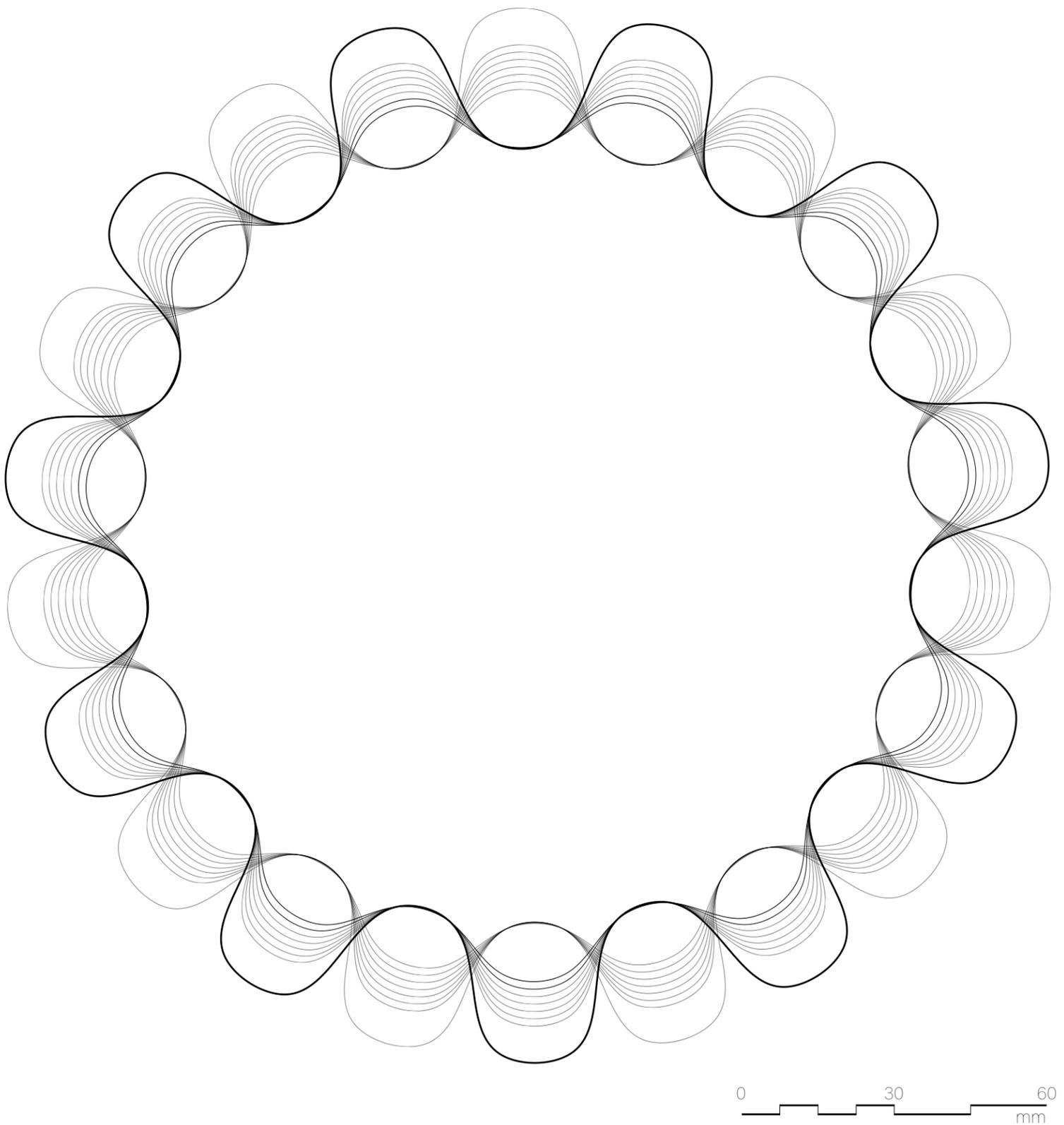
**Figure 4.6.14** 'XL' typology tool path plan.
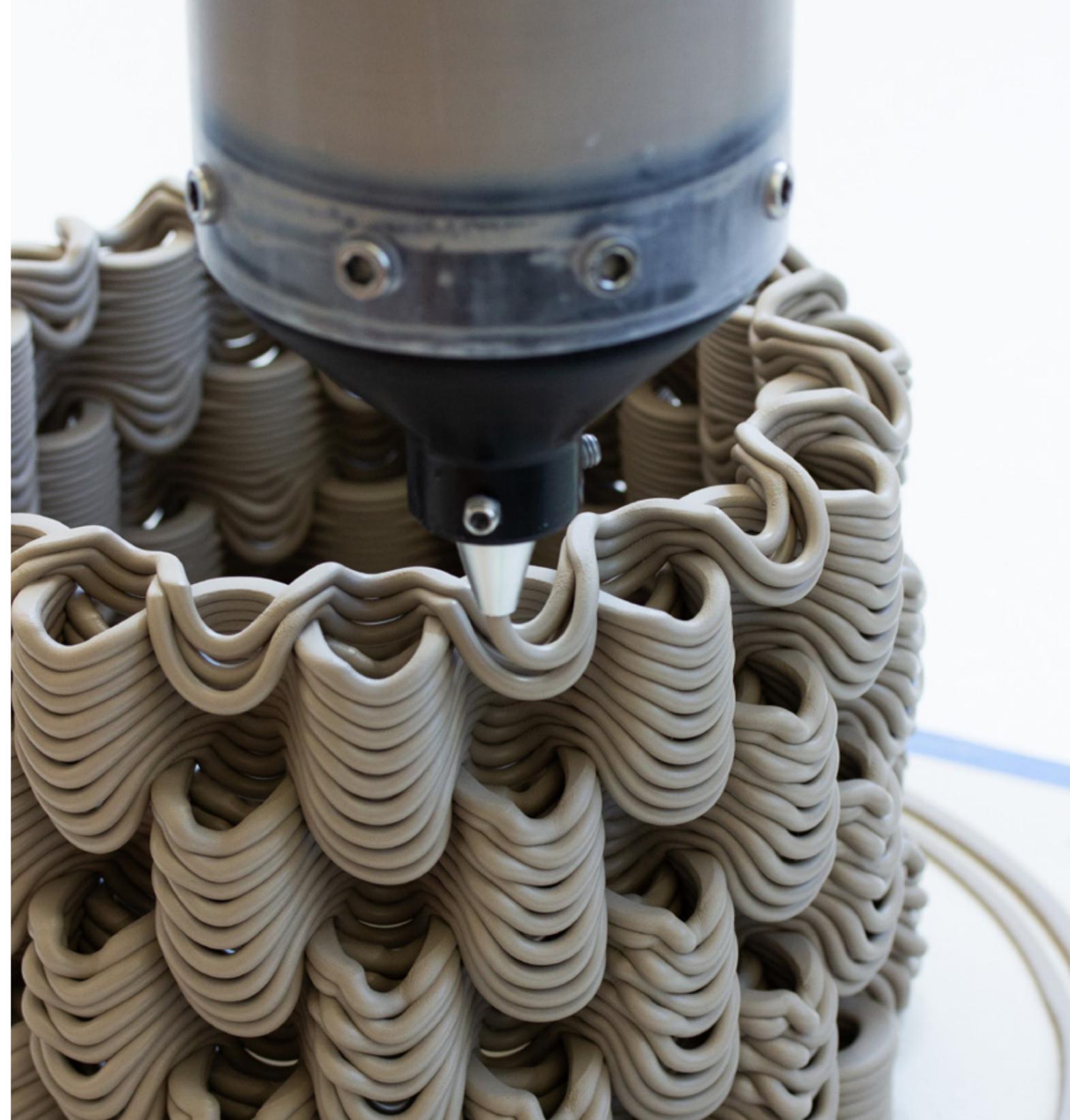


**Figure 4.6.15** 'XL' prototype print in progress.

0          30          60
mm

**Figure 4.6.16** 'XL' prototype, front view.

**Figure 4.6.17** Illuminated 'XL' prototype, front view.

**Figure 4.6.18** Illuminated 'XL' prototype, light shelf detail.



**Figure 4.6.19** Illuminated 'XL' prototype, base detail.

**Figure 4.6.20** Illuminated 'XL' prototype, light shelf detail.

**Figure 4.6.21** Illuminated 'XL' prototype, light shelf detail.

## Light Shelves

The tool path development in the 'XL' typology developed from the research outputs of the 'L' typology. Initial experiments consist of patterns that operate at the scale of twelve to eighteen layers. The delamination that occurs in the 'XL' typology when depositing material across large apertures diverges from the tool path principles explored in the 'L' typology. Scoops at the 'XL' scale tend to buckle and delaminate in ways that diminish brightness and cause structural collapse. Scoops in the 'L' typology were modified to 'shelves' as a product of structural constraints that emerged from experimenting with extra-large apertures. These shelves provide a structurally stable framework for testing extrusion variability and controlled delamination.



**Figure 4.6.22** Extrusion Multiplier (EM) ranging from 9 to 20 in the final 'XL' prototype.
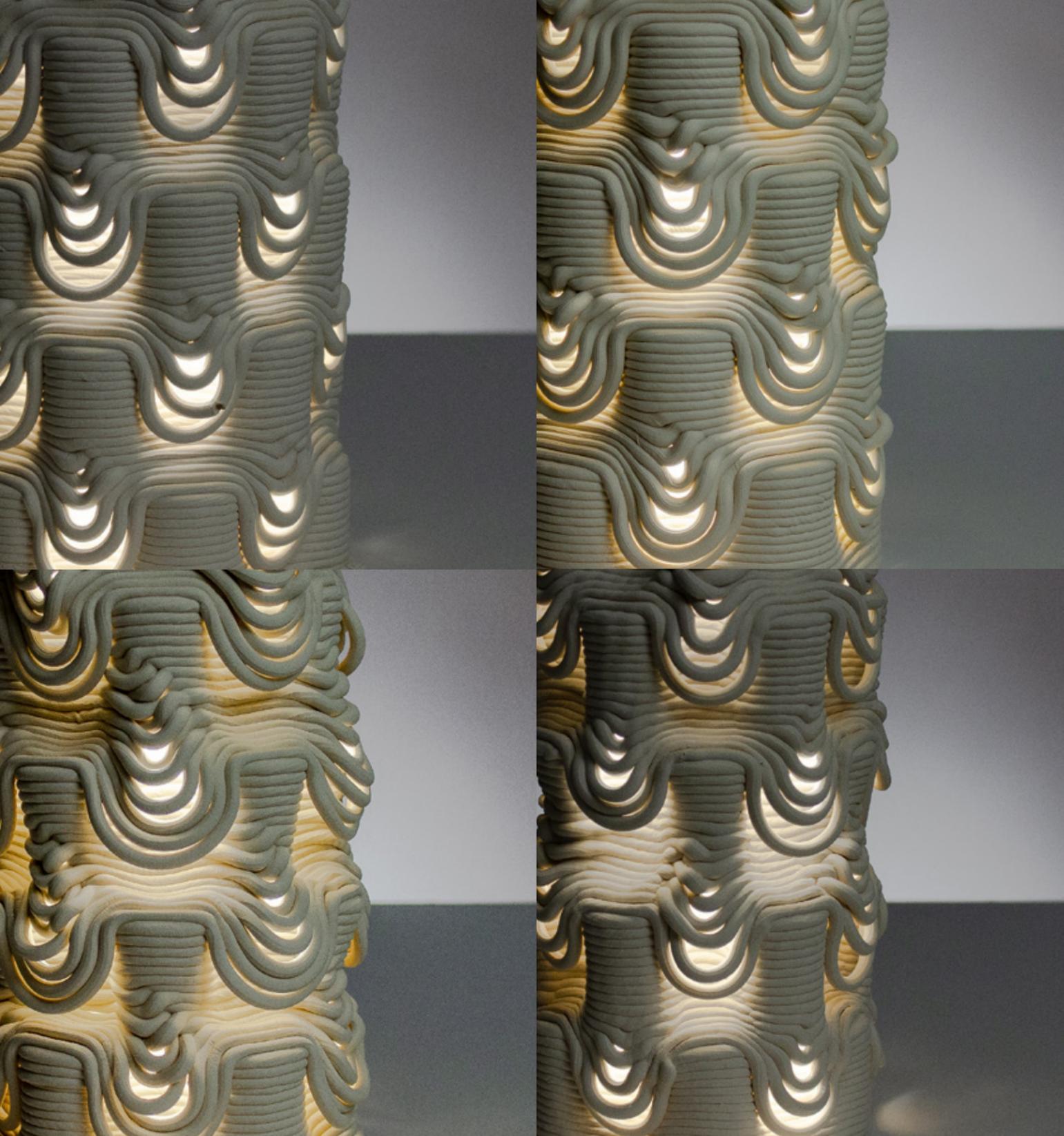
**Figure 4.6.23** Large scale scoop studies, precursors to the 'XL' prototype.

**Figure 4.6.24** The scoop pattern (above) is transformed into light shelves (below) by staggering wave print layers with circular print layers.

## 'XL' Index

This index consists of two sets of prototypes ordered chronologically. The first set of experiments are tool path/aperture studies applied to 100mm x 100mm x 200mm cylinders. These experiments display different print coil expressions and non-planar printing.

The second set consists of prototypes that maximize print cartridge capacity on the Potterbox XLS-1. These experiments focus on shaping the base surfaces to which tool paths are mapped as well as grading light effects across these surfaces.



**Figure 4.6.25** Clear Linear glaze on Polar Ice, fired to cone 6, 90mm x 90mm x 150mm, 21 layer sequence.



**Figure 4.6.26** Unglazed PSH-515, fired to cone 04, 80mm x 80mm x 160mm, 18 layer sequence.

**Figure 4.6.27** Unglazed PSH-515, fired to cone 04, 90mm x 90mm x 180mm, 22 layer sequence (x2).



**Figure 4.6.29** Unglazed PSH-515, fired to cone 04, 90mm x 90mm x 180mm, 20 layer sequence (x2).



**Figure 4.6.28** Unglazed PSH-515, fired to cone 04, 90mm x 90mm x 180mm, 16 layer sequence (x2).



**Figure 4.6.30** Unglazed PSH-515, fired to cone 04, 90mm x 90mm x 180mm, 16 layer sequence (x2).

**Figure 4.6.31** Unglazed PSH-515, fired to cone 04, 90mm x 90mm x 180mm, 20 layer sequence (x2).
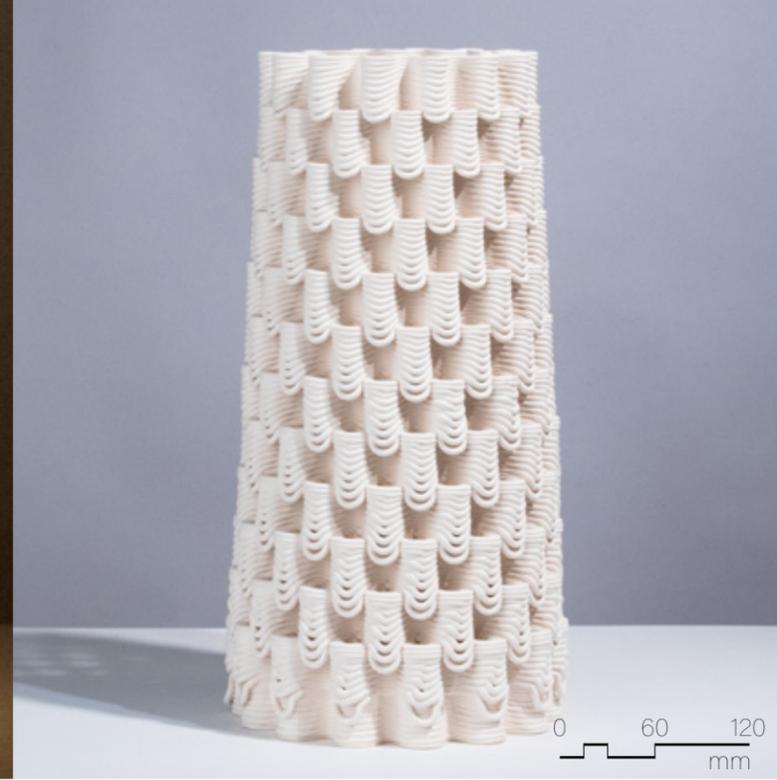
**Figure 4.6.33** Unglazed PSH-515, fired to cone 04, 200mm x 200mm x 400mm, 20 layer sequence (x2).
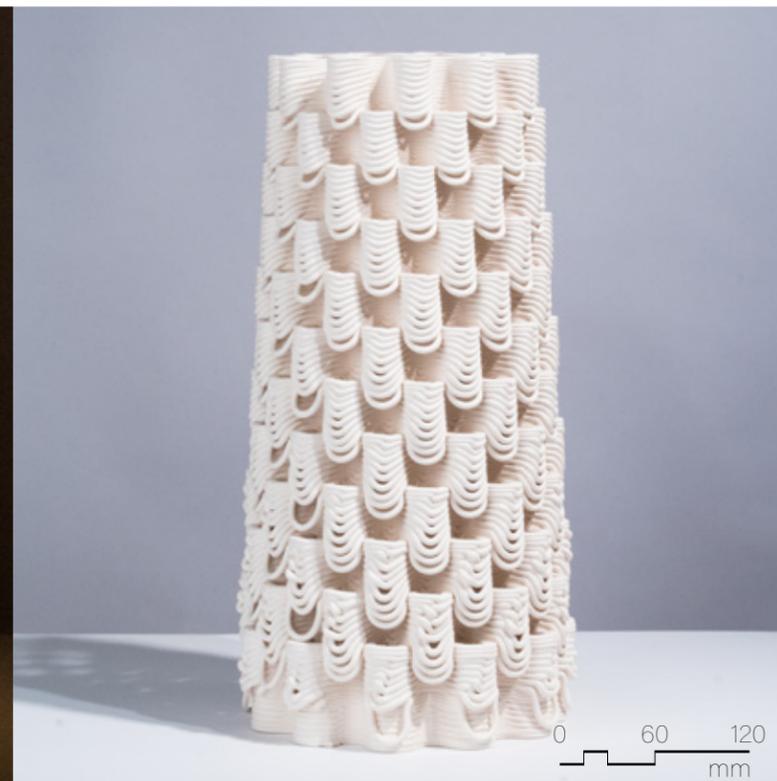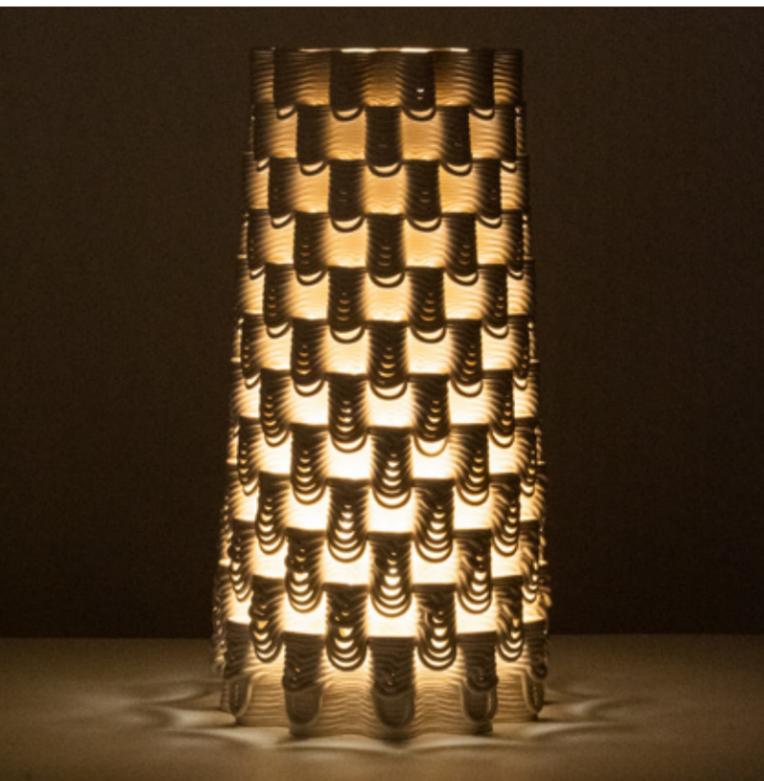
**Figure 4.6.32** Unglazed PSH-515, fired to cone 04, 200mm x 200mm x 400mm, 20 layer sequence (x2).
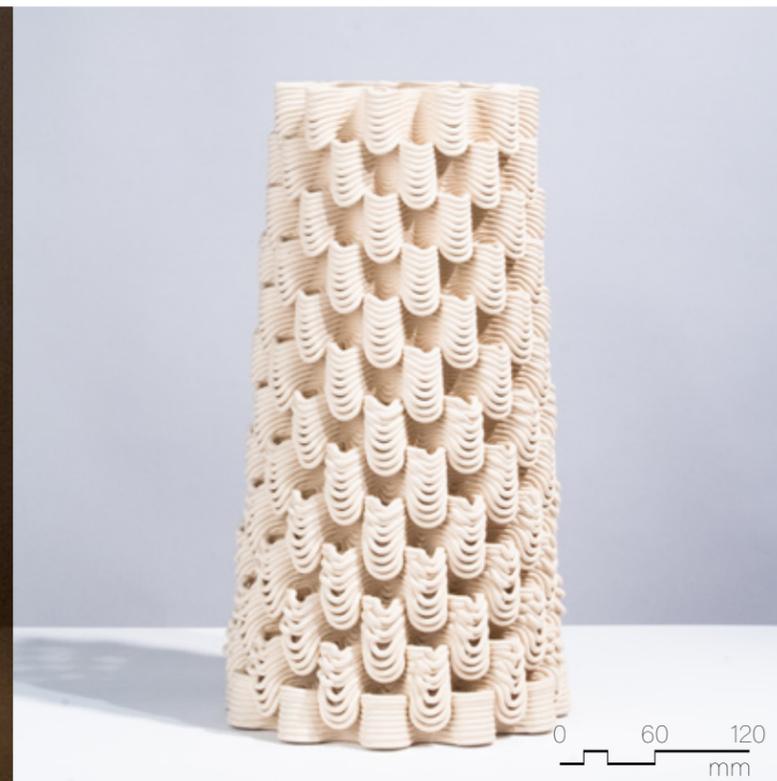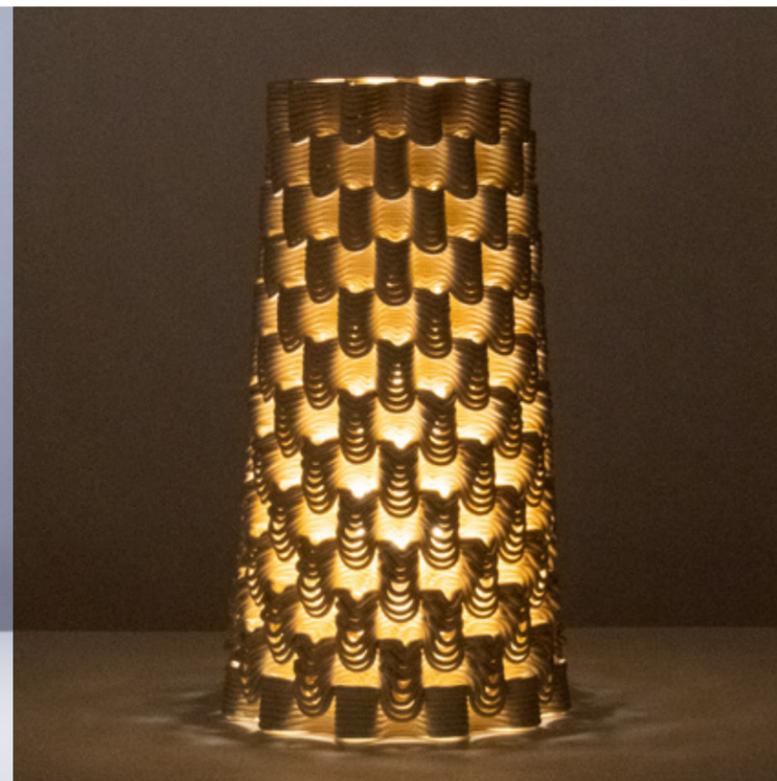
**Figure 4.6.34** Unglazed PSH-515, fired to cone 6, 200mm x 200mm x 380mm, 20 layer sequence (x2).

**Figure 4.6.35** Unglazed PSH Dark Granite, fired to cone 04, 200mm x 200mm x 340mm, 20 layer sequence (x2).
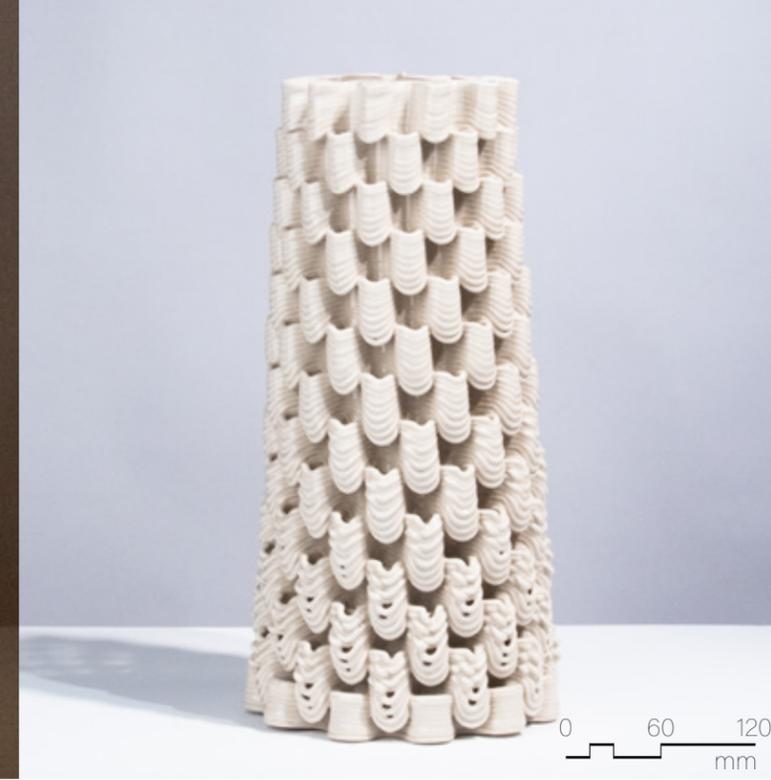


**Figure 4.6.37** Clear liner glaze on PSH-515, fired to cone 6, 200mm x 200mm x 380mm, 20 layer sequence (x2).
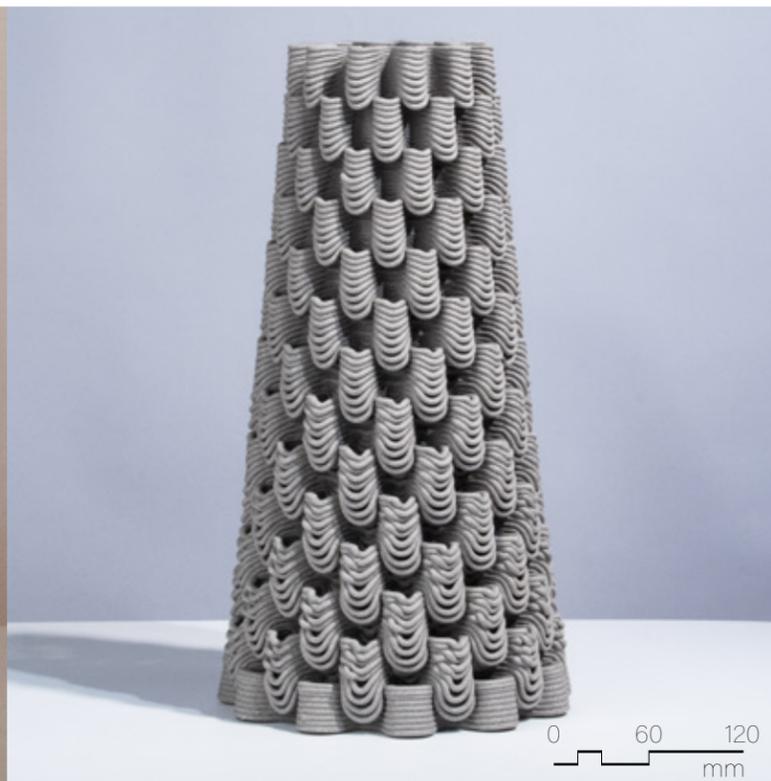


**Figure 4.6.36** Unglazed PSH Dark Granite, fired to cone 6, 200mm x 200mm x 380mm, 20 layer sequence (x2).

# PART 5

## CONCLUSION

## 5.1 DESIGN PROCESS MODEL

The flexibility and programmability of clay 3D printing enable us to better adapt our design methodologies to material behaviour. In this research, the most effective way of enhancing programmability was to remove slicer software from the material computation process. The first three months of research and development utilized a mesh to slicer workflow to translate digital geometries to physical outputs. While providing an accessible digital interface between the designer and the physical tools, most slicer software cannot simulate material performance. The suite of programmable materials this software can accurately process is largely limited to plastics and other quick-curing materials that yield high fidelity between digital models and physical outputs. We were prepared to work within the constraints of this design space for the duration of the project when the global COVID-19 pandemic resulted in the closure of all non-essential workplaces in March of 2020. Without any physical tools at our disposal, we shifted our focus from developing design products to developing a design process model. Through the 'Preliminary Studies of Plastic Deformation' conducted from January to March 2020, it became clear that conceiving of ceramic materials as digital meshes misrepresented how clay behaves during 3D printing. With only digital tools at our disposal from March to September 2020, we looked to create a new material computation strategy that would better represent the layer-by layer deposition of clay during 3D printing, rather than seek to pre-determine the process' physical outcomes. The result was a suite



**Figure 5.1.1** Stoneware undergoing plastic deformation during 3D printing.

of computational means to generate the 3D printer's tool path. This shift to tool path design represented a significant change in our approach from thinking about formal expression to how the role of tools could be defined and become integral to a design-and-make process.

## 5.2 RESEARCH OUTLOOK

This process-based approach to material computation allowed us the opportunity to expand the scope of this research beyond our thesis. Two projects form part of this extended project scope:

1. **HIVE**– a ceramic 3D printed installation, developed and fabricated at the University of Waterloo, under the supervision of Professor David Correa (Principal Investigator). The project was completed in collaboration with six fellow students: Isabel Ochoa (Graduate Researcher), James Clarke-Hicks (Graduate Researcher), Ye Sul Cho (Project Lead), Ji Shi (Scientific Development Lead), Meghan Taylor (Alumna) and Ben Ma (Student).

2. **Functionally Graded Performance in Terracotta Structures**– a course co-taught between myself and James Clarke-Hicks on computational workflows for digitally crafting ceramics. The course was taught through the Architectural Association Toronto Visiting School 'F^2: Morphological Experiments Between Force and Form' in partnership with Autodesk Technology Centers.



**Figure 5.2.1** Final installation of HIVE.

These two projects allowed us to investigate the following key questions:

1. How do we assess the constructibility of a design using the production workflows established in our research methods?
2. What are the impacts of representation and simulation in a design and fabrication process?

## 5.3 SCALABILITY AND CONSTRUCTIBILITY

From January to May of 2021, we joined the design and development team for HIVE, a 2.4-meter x 5-meter masonry screen consisting of 200 unique ceramic units. HIVE allowed us to test the structural limits of material performance and the efficacy of our design-to-production workflows on a large scale. The installation is conceived of as a traditional bonded masonry system- with units adhered together using mortar and grout. Our role in the design team was focused on re-conceiving the original design concept into a feasible system in terms of tooling, time, labour, and economic constraints. This involved process re-design at two scales:

1. **The micro-scale–** the individual unit.
2. **The macro-scale–** the installation and its assembly.



**Figure 5.3.1** Final units in HIVE showing apertures that selectively open and close along the wall.

**Figure 5.3.2** HIVE prototype assembly process.

## Micro-Scale

Stoneware units in HIVE form apertures that selectively expand and contract to allow for visual connections and enable the passage of light across spaces. Each unit formed a single aperture on the wall in its original conception, creating a matrix of 1200 units. By aggregating four apertures into a single unit and utilizing the maximum clay cartridge capacity per print on the Potterbot XLS-1, we reduced the number of units from 1200 to 200. This dramatically improved the feasibility of the project in terms of how we could allocate resources within the design process model of the entire installation. Fewer units meant we no longer had to purchase a second machine for production and improved economic constraints within the project budget.

## Macro-Scale

The decrease in the number of bricks also reduced the number of mortar joints across the full breadth of the installation, reduced labour costs, and improved dimensional tolerances produced by human error. The original conception of the installation also involved adhering units within our facilities to create modules. Each module would consist of approximately 30 units, which would then be mortared together on site. This proposal was problematic in terms of the weight of the modules and the labour it created on our end of production. Although our team was responsible for fabricating all the



**Figure 5.3.4** Detail of HIVE prototype highlighting dimensional inconsistencies across mortar joints.

units and producing a full-scale mock-up, a professional construction crew was hired to do the final build. Computationally aggregating units and maximizing their size allowed us not to adhere units together into modules, making transportation and assembly far more efficient.  However, the new form of the units redistributed material in a way that caused significant amounts of plastic deformation during the drying and firing process. Plastic deformation of the bricks caused serious challenges during assembly. Edge conditions warped, resulting in the need for mortar joints to vary in size. While typical masonry joints are approximately ½" wide, the final HIVE installation has mortar joints ranging from ¼" to 2" to accommodate dimensional tolerances. Techniques to slow down the drying process and mitigate warping were employed. Ultimately, a number of these issues remain unresolved and are visible in the final installation. When constructing the proof-of-concept prototype, we built a wood frame that allowed us to level each brick according to a series of datum lines. The assembly of the 21-unit prototype took our team seven days to complete. The final 200-unit installation relied on the expertise of a team of three masons to carry out the work in the same amount of time.

## 5.4 DISSEMINATING NEW TOOLS

In August of 2021, James and I had the opportunity to co-teach our working methodologies to a group of students as part of a course taught remotely with the Architectural Association. The two-week workshop asked students to think about how to harness terracotta's working properties and ceramic traits using a set of material computation tools. In preparation, we packaged our code into accessible computational tools for the students to use. We were excited to share with students a performance-based approach to digitally crafting ceramics. However, in our efforts to bridge the gap between conceptualization and production, the methods for designing the machine's tool path abstracted geometry. The impact of the lack of representation and simulation of material behaviour proved to be more difficult than we expected in the online learning environment. To mitigate this issue, the Autodesk team had helped us create a clay simulator  in Bifrost in preparation for the workshop. We were able to take the student's tool paths generated in Grasshopper and visualize them in Autodesk software. Although the simulator was not able to mimic structural performance, it could compute collisions between clay particles. The course was structured so that learning Grasshopper and Bifrost tools was front-loaded within three days, leaving the remaining eight days of the course for students to explore potential learning outcomes in the design of a functional artifact. We provided several lectures explaining how the material behaves and its impacts on the ceramic 3D printing process, providing examples from other contemporary technology uses. However, without being able to touch the clay and study plastic deformation, material performance became abstracted. It wasn't until the students were able to produce their first prototypes that they could grasp relationships between the production and material systems. At this point, harnessing unique types of material performance in the students' respective projects

took precedence over their adherence to the computational methods provided. Material computation became a way for students to take agency over their projects while they were in the process of learning to adapt to new design frameworks. As a result, approaches to the project were vastly different, prompting us to design custom computational tools for each group of students and, in one case, help them use analogue post-processing techniques as part of their workflow. Teaching became an exciting part of the feedback loop in our processes of production and materialization, pushing us to step outside our own design space and experiment with approaches we had never tried before. The course was an inspiring opportunity to help others create differently with new interfaces and conceive of new design-to-production systems.



**Figure 5.4.1** 3D print in progress by Hannah Ni and Yingying Zeng.

**Figure 5.4.2** Plastic deformation studies by Hannah Ni and Yingying Zeng.



**Figure 5.4.3** Bioinspired terracotta vessel for growing mushrooms, designed by Hannah Ni and Yingying Zeng.

**Figure 5.4.4** Print in progress, designed in collaboration with Randal Pope.

**Figure 5.4.5** Bioinspired terracotta structural lattices, designed in collaboration with Randal Pope.

# BIBLIOGRAPHY

AlOthman, Sulaiman, Hyeonji Claire Im, Francisco Jung, and Martin Bechthold. "Spatial Print Trajectory." In *Robotic Fabrication in Architecture, Art and Design 2018*, 167-180. Cham: Springer International Publishing, 2018.

Bechthold, Martin, Anthony Kane, and Nathan King. *Ceramic Material Systems.* Basel/Berlin/Boston: Walter de Gruyter GmbH, 2015.

Carlota, V. "Ceramic 3D Printing: A Revolution within Additive Manufacturing?" Accessed July 7, 2021. https://www.3dnatives.com/en/ceramic-3d-printing-170420194/#!.

Clampham, Christopher and James Nicholson. "Tessellation." In *The Concise Oxford Dictionary of Mathematics* (5th Ed.): Oxford University Press, 2014.

"Clay Laguna Frost." Accessed September 1, 2021. https://cdn.shopify.com/s/files/1/0326/8352/4229/files/CLAY_LAGUNA_FROST.pdf?v=1589456138.

"Clay PSH 516." Accessed September 1, 2021. https://cdn.shopify.com/s/files/1/0326/8352/4229/files/CLAY_PSH_516.pdf?v=1589440982.

DeLanda, Manuel. "The New Materiality." *Architectural Design* no. 85 (2015): 16-21.

García Cuevas, Diego and Gianluca Pugliese. *Advanced 3D Printing with Grasshopper*. 1st ed. Wrocław: Amazon, 2020.

Grabar, Oleg. "The Archeological and Historical Setting." In *The Alhambra*, 25-98. Cambridge: Harvard University Press, 1978.

Gürsoy, Benay. "From Control to Uncertainty in 3D Printing with Clay." *Fabrication - Virtual & Physical Prototyping* 2, no. Volume 2 (2018): 21-30.

Hauer, Erwin. *Continua: Architectural Screens and Walls.* New York: Princeton Architectural Press, 2004.

Keep, Jonathan. "Iceberg Series." Accessed July 7, 2021. http://www.keep-art.co.uk/digitial_icebergs.html.

Kluska, Ewelina, Piotr Gruda, and Natalia Majca-Nowak. "The Accuracy and the Printing Resolution Comparison of Different 3D Printing Technologies." *Transactions on Aerospace Research* 2018, no. 2 (Jun 1, 2018): 75-92.

Ko, Minjae, Donghan Shin, Hyunguk Ahn, and Hyungwoo Park. "InFormed Ceramics: Multi-Axis Clay 3D Printing on Freeform Molds." In *Robotic Fabrication in Architecture, Art and Design 2018*, 297-308. Cham: Springer International Publishing, 2018.

Linsey Hunt, Erin. "Seki." Accessed July 7, 2021. https://erinlhunt.com/seki.

Lloyd Thomas, Katie. "Introduction: Architecture and Material Practice." In *Material Matters: Architecture and Material Practice,* 1-12. New York: Routledge, 2007.

Mahamood, Rasheedat Modupe and Titilayo Esther Akinlabi. "Introduction." In *Functionally Graded Materials*, edited by Bergmann, Carlos, 1-8. Cham: Springer International Publishing, 2017.

Menges, Achim. "Computational Material Culture." *Architectural Design* 2, no. 86 (2016): 76-83.

Menges, Achim. "Fusing the Computational and the Physical: Towards a Novel Material Culture." *Architectural Design* 85, no. 0 (2015): 8-15.

Oxman, Neri, Steven Keating, and Elizabeth Tsai. "Functionally Graded Rapid Prototyping." In *Innovative Developments in Virtual and Physical Prototyping,* 483-489: Taylor & Francis Group, 2011.

Pei, Eujin, Giselle Hsiang Loh, David Harrison, Henrique de Amorim Almeida, Mario Domingo Monzón Verona, and Rubén Paz. "A Study of 4D Printing and Functionally Graded Additive Manufacturing." *Assembly Automation* 37, no. 2 (2017): 147-153.

"Polar Ice." Accessed September 1, 2021. https://plainsmanclays.com/data/index.php?product=12881.

"Potterbot XLS-1." Accessed July 7, 2021. https://emergingobjects.com/project/potterbot-xls-1/.

Rael, Ronald, Virginia San Fratello and Phirak Suon. "Bad Ombres V.2." Accessed July 7, 2021. http://emergingobjects.com/project/bad-ombres-v-2/.

Reiser, Jessie and Nanako Umemoto. "Intensive and Extensive." In *Atlas of Novel Tectonics,* 72-77. New York: Princeton Architectural Press, 2006.

Rhodes, Daniel. *Clay and Glazes for the Potter*. Pennsylvania: Chilton Co., Books, 1957.

Tedeschi, Arturo. *AAD Algorithms-Aided Design*. 1. ed. ed. Brienza: Le Penseur, 2014.

van Herpt, Olivier. "Colorful White." Accessed July 7, 2021. https://oliviervanherpt.com/colorful-white/.

Violatti, Cristian. "Pottery in Antiquity." Accessed July 17, 2021. https://www.worldhistory.org/pottery/.

Ward, Gerald. "Openwork." In *The Grove Encyclopedia of Materials and Techniques in Art*: Oxford University Press, 2008.

"What does Resolution Mean in 3D Printing?" . Accessed July 28, 2021. https://formlabs.com/blog/3d-printer-resolution-meaning/.

Winchip, Susan M. *Fundamentals of Lighting*. 2. ed. ed. New York, NY: Fairchild Books, 2011.